

DEFORMED PEBBLES

ANALYSIS OF STRAIN, SHAPE, AND ORIENTATION
OF THE DEFORMED PEBBLES IN THE
SEINE RIVER AREA, ONTARIO

By

MAO-YANG HSU, B.Sc., M.Sc.

A Thesis

Submitted to the School of Graduate Studies

in Partial Fulfilment of the Requirements

for the Degree

Doctor of Philosophy

McMaster University

February, 1971

DOCTOR OF PHILOSOPHY (1971)
(Geology)

McMASTER UNIVERSITY
Hamilton, Ontario.

TITLE: Analysis of Strain, Shape, and Orientation of the Deformed
Pebbles in the Seine River Area, Ontario

AUTHOR: Mao-Yang Hsu, B.Sc. (National Taiwan University)
M.Sc. (McMaster University)

SUPERVISOR: Professor P.M. Clifford

NUMBER OF PAGES: xvii, 179

SCOPE AND CONTENTS:

Detailed mapping was carried out to provide reliable data concerning the geologic structure which is relevant to the original pebble fabrics.

Mathematical determination of an ellipsoidal shape from any two cross-sections and its application to the study of deformed ellipsoidal particles are developed and discussed.

Final pebble fabric resulting from special coaxial superpositions of the tectonic strain ellipsoid upon the originally ellipsoidal pebbles, is employed to determine the strain ratio and the original pebble orientation and shape.

Some general techniques are outlined for different cases to determine the strain ellipsoid and the original shape of deformed pebbles. Weighted vector mean is introduced in the orientation analysis of de-

formed pebbles. The concept of average axial ratio in the case of unextractable pebbles is examined.

Pebble size, pebble ductility ratio, shortening strain, and strain rate are all calculated and discussed. Finally, selective veins developing in the less-deformed pebbles are subjected to detailed orientation and petrofabric analyses.

ACKNOWLEDGEMENTS

First of all, the writer wishes to express his sincere gratitude to Dr. Paul M. Clifford who suggested the map area for studying deformed pebbles, collaborated with the writer in the field for two weeks, continuously assisted and encouraged the writer throughout the whole period of the work, and, finally, critically read the manuscript.

The writer has benefited from many discussions with Drs. R. G. Walker and H. E. Hendry on the sedimentation problem, with Julian Coward on computer programming, and with Douglas Underhill on the stress concentration concept. Drs. R. G. Walker, R. H. McNutt and D. C. Ford, and Professor N. E. Wilson have also offered their advice and time at various phases of the project.

Many thanks are extended to Wayne Alexander and David MacLean who acted as field assistants in 1968 and 1969, respectively; to H. D. and L. J. Falkiner for thin section preparation; to John Whorwood for reducing the diagrams; to Joyce Barrett for typewriting the final manuscript, and to all the other persons who have assisted the writer in the study in one way or another.

Financial assistance towards this study was provided by the National Research Council of Canada, the Geological Survey of Canada, the Ontario Department of Mines and Northern Affairs, the Ontario Department of University Affairs, the J. P. Bickell Foundation, and McMaster University.

TABLE OF CONTENTS

	Page
Acknowledgements	iv
Table of Contents	vi
List of Figures	ix
List of Plates	xii
List of Tables	xiv
Abstract	xv
Chapter I. Introduction	1
Chapter II. Geological Setting	10
1. Stratigraphic Sequence	10
2. Shoal Lake Conglomerate	20
3. Geological Structure	22
4. Paleocurrent Direction	24
Chapter III. Deformation Plot	28
1. Deformation Path	29
2. Contours of X_f/d , Y_f/d , and Z_f/d	34
3. Volume Change	37
Chapter IV. Mathematical Determination Of An Ellipsoid From Its Two Cross-sections	40

Chapter V. Determination Of The Original Orientation Of Deformed Pebbles On Identical And Parallel Principal Planes	49
1. Pebble Fabrics In Sedimentary Deposits	49
2. Mathematical Relationship Between The Original And The Final Orientations of Deformed Pebbles	51
3. Deformation Of Ellipses With Various Orientations	61
4. Concept Of Mean Orientation Of Ellipsoidal Pebbles	70
5. Simultaneous Determination Of The Tectonic Strain Ratio And The Original Orientation And Shape Of Deformed Pebbles	76
Chapter VI. Determination Of The Strain Ellipsoid And The Original Shape Of Deformed Pebbles	82
1. Extractable Individual Pebbles	83
Original Pebbles With Random Fabric	83
Original Pebbles With A Planar Fabric	87
2. Unextractable Pebbles	92
Concept of Average Axial Ratio	92
Original Pebbles With Random Orientations	96

	Page
Original Pebbles With A Planar Fabric	102
Deformed Pebbles With Unknown Final Fabric	
On The Foliation Plane	103
(A) Construction Of The Imaginary	
Ellipsoid	104
(B) Computation For a_o , b_o , and a_t , b_t	118
Chapter VII. Pebble Size	126
Chapter VIII. Pebble Ductility	135
Chapter IX. Selective Veining In Pebbles	140
1. Vein Orientation	142
2. Crystallographic Fabrics of Quartz	146
3. Interpretation	151
Chapter X. Conclusion	157
Bibliography	163
Appendix	
A. Derivation of Equations Representing The Contours	
of X_f/d , Y_f/d , and Z_f/d	168
B. Proof of Identical Shape For Parallel Cross-Sections	
Through An Ellipsoid	169
C. Calculation of a_o , b_o , a_t , and b_t For The Granitic And	
Quartzose Pebbles	174

LIST OF FIGURES

		Page
1.	Location map	8
2.	Stratigraphic sequence	13
3.	Trough cross-lamination directions	26
4.	Example of the logarithmic deformation plot showing the relationship of the original ellipsoid, the final deformed ellipsoid, the tectonic strain ratios, and the simplest deformation path in an ir-rotational coaxial deformation	32
5.	Contours of X_f/d , X_f/d , and Z_f/d in a logarithmic deformation plot	35
6.	Homogeneously volume-reduced deformation of an originally spherical particle with a diameter of unit length \underline{l}	38
7.	Relationship between an ellipsoid and its cross-sectional ellipse	42
8.	Homogeneous deformation of an $X_o Y_o$ ellipse in a coordinate system with axes taken parallel to the principal strain directions	55

9. Orientation plot of deformed ellipses during progressive deformation ($a_t = 1.40$) 63
10. Orientation plot of deformed ellipses during progressive deformation ($a_t = 1.60$) 64
11. Orientation plot of deformed ellipses during progressive deformation ($a_t = 2.00$) 65
12. General feature of the final pebble-fabrics in the map area 71
13. Determination of the mean X_f -orientation of deformed pebbles 75
14. Construction of the bounding isostrain curves from the final pebble-fabric of Figure 12(C) 78
15. Expanded diagram showing the complex relationship among a_o , a_f , θ , and \emptyset , from the final pebble-fabric of locality 144 80
16. Deformation field of extractable deformed pebbles in the case of originally random orientation 85
17. Deformation field of extractable deformed pebbles in the case of coaxial superposition of $Z_f || Z_t || Z_o$ 89
18. Deformation field of extractable deformed pebbles with different ductilities in the case of $Z_f || Z_t || Z_o$ 91
19. Deformation field of extractable deformed pebbles in the case of coaxial deformation of $X_f || X_t || X_o$ 93

	Page
20. Orientation plots on sections parallel to a principal plane of the tectonic strain ellipsoid in the case of original randomly-oriented pebbles	97
21. Construction of imaginary ellipsoids when $\bar{\phi} = 30^\circ$	105
22. Construction of imaginary ellipsoids when $\bar{\phi} = 60^\circ$	107
23. Construction of imaginary ellipsoids when $\bar{\phi} = 45^\circ$	111
24. Logarithmic deformation plot of the imaginary ellipsoids constructed from the deformed pebbles in the Seine River area, Ontario	117
25. Determination of the tectonic strain ellipsoid and the original pebble shape on the logarithmic deforma- tion plot of the final deformed pebbles in the map area	120
26. Pebble size <u>versus</u> spatial distribution	133
27. Orientation of eight pebbles with veins of the extensional- fracture type at locality 297	145
28. Quartz c-axis fabrics	150

LIST OF PLATES

	Page
1. Geologic Map	11
2. (A). Cross-lamination in arenites	16
(B). Cross-section of trough cross-lamination	16
3. (A). Load casts beneath arenite beds	17
(B). Normal graded bedding in the arenite on top of conglomerate bed	17
4. (A). Pillowed lavas preserved in greenstones	18
(B). Vesicular texture on top of lava flow	18
5. (A). Foliation refraction on bedding	19
(B). Local unconformity	19
6. (A). Dextral kink band developed in rocks containing pebbles already deformed	72
(B). Three-dimensional view of the deformed pebbles	72
7. (A). Vein in a granitic pebble extending into the matrix	141
(B). Offset along the shear-fracture trace	141
8. (A). Veins of the extensional-fracture type perpendicular to the foliation trace	143
(B). A transverse vein of the extensional-fracture type cut off by an oblique vein of the shear-fracture type	143

9.(A). Rod-like, columnar vein quartz	147
(B). Cross-section of columnar vein quartz	147
10.(A). Quartz pseudomorph of plagioclase in host pebble	149
(B). Petrofabric of a quartzite pebble	149

LIST OF TABLES

	Page
1. Comparison of average axial ratios	95
2. Axial ratios of the imaginary ellipsoids constructed from different sections on Figure 21	110
3. Axial ratios of the imaginary ellipsoids constructed from different sections on Figure 23	112
4. Axial ratios and Z/d ratios of the constructed ellipsoids of the deformed granitic pebbles	114
5. Axial ratios and Z/d ratios of the constructed ellipsoids of the deformed quartzose pebbles	115
6. Axial ratios and Z/d ratios of the constructed ellipsoids of the deformed volcanic pebbles	116
7. Calculated size of the granitic pebbles	130
8. Calculated size of the quartzose pebbles	131
9. Calculated size of the volcanic pebbles	132
10. Shortening strain of the deformed pebbles in the Seine River area	138

ABSTRACT

The long-time controversy of the Couthiching problem has been solved at least in the map area. The general stratigraphic sequence is that the thick greenstones of the Keewatin series overlies the thick fine sediments of the Couthiching series with the Shoal Lake conglomerate and local greenstones belonging to the upper part of the Couthiching.

Mathematical equations are derived to represent the contours of X/d , Y/d , and Z/d for constant-volume ellipsoids with three principal axes of $X > Y > Z$ and a nominal diameter of d . These contours are useful in the determination of the special coaxially deformed pebbles which yield data for calculation of the axial ratios of both the strain ellipsoid and the original pebble.

Final pebble fabric resulting from coaxial superposition of the tectonic strain ellipsoid upon the originally ellipsoidal pebbles is illustrated on an orientation plot, which facilitates the simultaneous determination of the strain ratio and the original pebble orientation and shape. The complex relationships of orientation and shape among the original undeformed ellipse, the tectonic strain ellipse, and the final

deformed ellipse, are shown by both mathematical equations and a graphical expression.

From extractable pebbles resulting from deformation of original, randomly-oriented pebbles, adequate equations can be sought to determine the strain ellipsoid and the original pebble shape. For unextractable pebbles, Ramsay's (1967, p. 209-211) technique is found to be unsuitable for determining the original shape of deformed pebbles in the case of originally random fabric.

Pebbles in the Shoal Lake conglomerate of Archean age show distinct deformation. The strain ellipsoid and the original shape of the deformed pebbles in the map area are calculated from the coordinates of coaxially deformed pebbles on the logarithmic deformation plot. The deformation path of the deformed pebbles has a slope of a calculated K-value of 2.74 and so the strain ellipsoid belongs to the flattening type, which is conformable with the regionally poor development of mineral lineation in the strongly-foliated rocks.

The calculated original shape is equant for the granitic pebbles and oblate for the quartzose pebbles; the volcanic pebbles have their original shape between equant and oblate. The average shortening strain of the volcanic pebbles is 60%, the quartzose pebbles, 37%, and the

granitic pebbles, 7%. Most of the granitic and volcanic pebbles lie in the size range of cobbles with some of the former reaching the boulder size, whereas the quartzose pebbles generally are smaller than 100 mm.

Selective cross-veins are found to have developed mainly in extensional fractures of the less-deformed granitic pebbles. Quartz is the major constituent mineral of the veins and is likely to have grown the columnar grain shape in pace with the dilation of fracture, because some of the columnar quartz grains show crystallographic continuity across the vein from side to side. Double elliptical girdles of quartz c-axes around the direction of the principal tectonic shortening are reported for the first time in coaxially deformed quartzite pebbles.

The only plausible explanation for the ductile deformation of the granitic pebbles under the P-T conditions of low-grade metamorphism is the hypothesis of a very low strain rate, which probably is of the order of 10^{-15} to 10^{-16} sec^{-1} if 2 to 10 m. y. is assumed to be the duration of the deformation episode.

CHAPTER I

INTRODUCTION

Strain is a quantitative measure of the amount of deformation. Determination of strain in deformed rocks is a difficult undertaking for geologists. The difficulty stems primarily from the fact that both original features and fabrics of deformed rocks in which strain is to be determined are commonly unknown.

Deformed fossils can be a good tool for the strain calculation, because their original features may be known precisely. However, occurrences of deformed fossils having easily measurable shapes in three-dimensional space are very limited. This is not a possible technique in the Precambrian rocks, such as those investigated by the writer, because recognizable fossils are absent.

Deformed pebbles and ooids have been used in many places for the determination of strain. Both elements were assumed to have been originally spherical in shape before deformation, an assumption whose validity is now open to question.

The first geological application of the strain concept was made by Sorby (1853) who studied the deformed reduction spots in the Cambrian slates of North Wales. He concluded that the spots have been compressed along a line perpendicular to the cleavage plane. A couple of years later, Haughton (1856) was the first to compute the ratios of three principal strains by comparing deformed brachiopods to undeformed ones, assuming that two principal strains lay in the cleavage plane with one of them parallel to the intersection of cleavage and bedding.

Cloos (1947) gives a very good review of all the earlier work on deformed objects. He himself computed the magnitudes of principal strains from distorted ooids in the Paleozoic limestones on the western side of the Appalachian fold belt. However, his otherwise valuable results now need a modified interpretation, in which his original assumptions that ooids had no volume changes and were originally spherical before tectonic deformation, may not be valid.

Flinn (1956), in his study of the deformed pebbles of the Funzie conglomerate in northeastern Shetland, presented a graph, later called the deformation plot (Flinn, 1962), in which he plotted the ratio Y/Z against the ratio X/Y , where $X > Y > Z$ are the principal axes of an ellipsoidal pebble. This method was originally employed by Zingg (1935, p. 54) for describing the shape of pebbles in sedimentary rocks.

Flinn also showed the contours of X/d , Y/d , and Z/d in the plot, where d is the diameter of the equivalent sphere with the same volume as the ellipsoidal pebbles. Although these contours have not received attention since then, they turn out to be very useful in the strain analysis developed in Chapter VI of this thesis.

More than 110 years after Sorby (1853) studied the deformed reduction spots, Ramsay (1967) was the first to point out the effect of original shape and original fabric of objects on their finite strained state. Ramsay also presented a graphical method of determining the tectonic strain ratio and the original shape of the deformed objects. Though some problems exist in his descriptions, there is no doubt that his work is the most stimulating and most valuable reference thus far published in this field of study.

Assuming that rock behaves as a viscous fluid during deformation and that deformation is caused by pure shear or simple shear, Gay (1968) developed some mathematical equations to demonstrate the relationships among original shape, original orientation, final shape, and final orientation of deformed ellipses according to different strains. He also showed that the viscosity ratio (competence difference) between pebble and matrix under conditions of different pebble concentration in the rock, plays a prime role in relating tectonic strain to both the final shape and the final orientation of deformed pebbles. Though the assump-

tions involved are open to question, the general relationship may be useful. Gay's (1969) subsequent work, however, is misleading and confused in many respects. Beginning from the determination of vector mean orientation of pebbles, Gay plotted the mean cleavage plane (this means that cleavage planes are not all parallel to one another) on a stereogram, and then plotted the angles of rake of the major pebble axes in that plane (op. cit., p. 381). The vector mean orientation thus obtained will be in great error if the major axes are measured on a plane which makes an angle (say, greater than 10°) with the mean cleavage plane. Secondly, Gay mixed up the measured lengths of extracted-pebble axes with those made on planar sections. Therefore, some of the calculated standard deviations do not make any sense. Thirdly, the technique described by Ramsay (1967, pp. 209-211) was used improperly to compute the initial pebble shape by Gay (see pp.96-102 of this thesis for details). In addition, Gay's (1969, p. 383) Equations (2a) and (2b), unfortunately, are wrong; they should be

$$\sqrt{\lambda_1/\lambda_2} = \left[(X/Y)_{\max} \cdot (X/Y)_{\min} \right]^{1/2} \quad (1-1)$$

and

$$\frac{X_i}{Y_i} = \left[\frac{(X/Y)_{\max}}{(X/Y)_{\min}} \right]^{1/2} \quad (1-2)$$

but not

$$\sqrt{\lambda_1/\lambda_2} = (X/Y)_{\max} \cdot (X/Y)_{\min} \quad (\text{Gay's (1969) Eq. (2a)})$$

$$X_i/Y_i = (X/Y)_{\max} / (X/Y)_{\min} \quad (\text{Gay's (1969) Eq. (2b)})$$

where $X > Y > Z$ are the lengths of the three principal axes of a deformed pebble, a subscript i refers to that of an initial pebble; $\lambda_1 > \lambda_2 > \lambda_3$ are the principal quadratic elongations of strain. Moreover, it should be noted that Eqs. (1-1) and (1-2) exist only if the initial pebbles had a planar fabric with all their $X_i Y_i$ planes parallel to the $\sqrt{\lambda_1 \lambda_2}$ plane, and also if $\sqrt{\lambda_1/\lambda_2} > (X_i/Y_i)$. Given the former condition occurs, the latter does not always hold, because the range of rake over 90° , as shown in Gay's Figures 3A and 3D, is good evidence to indicate that $(X_i/Y_i) > \sqrt{\lambda_1/\lambda_2}$ (see Chapter V, pp. 67-69 in particular, of this thesis) at some localities, where $(X/Y)_{\min} = (X_i/Y_i) / \sqrt{\lambda_1/\lambda_2}$.

Consequently, the equations to determine the strain ratio and the initial pebble shape in the case of $\sqrt{\lambda_1/\lambda_2} < (X_i/Y_i)$, should be

$$\sqrt{\lambda_1/\lambda_2} = \left[\frac{(X/Y)_{\max}}{(X/Y)_{\min}} \right]^{1/2} \quad (1-3)$$

$$\text{and } X_i/Y_i = \left[(X/Y)_{\max} \cdot (X/Y)_{\min} \right]^{1/2} \quad (1-4)$$

if the X_i -axis of the initial pebbles had a random orientation on sections parallel to the $\sqrt{\lambda_1 \lambda_2}$ plane and all the $X_i Y_i$ planes. The above argument

is based on the assumptions that Gay had obtained all the axial ratios from extracted individual pebbles and that all the pebbles had an identical initial shape. Otherwise, the above relationships will become more complex and even indeterminate (see pp. 96-102). The initial pebble shapes calculated by Gay from those false equations probably are all wrong. Fourthly, Gay's equation 4 was given to calculate the viscosity ratio between pebble and conglomerate, which is based on the assumption that a deformed pebble had its axes parallel to the strain axes during deformation. If the measurements of the deformed pebbles were made on a section parallel to, say, the $\sqrt{\lambda_1 \lambda_3}$ plane, then those deformed pebble ellipses aligned parallel to the strain axes on that section would predominantly contain only one principal axis of the initial pebbles because of the original orientation. Therefore, most axial ratios of the initial pebble ellipses calculated from that section are not the real ones. By using any of the apparent axial ratios to compute the viscosity ratios, the errors are likely to be very large.

Equations derived by Dunnet (1969) enabled him to determine simultaneously the initial elliptical form and the "magnitude" and orientation of the finite strain from the final elliptical ratio and orientation of deformed particles. However, these equations must be applied with great caution. They will be discussed later (pp. 51-52).

From the above brief review of previous work on ellipsoidal particles, we can summarize the major problems involved in the study of deformed pebbles, which may include:

- (1) the shape, orientation, and size of deformed pebbles;
- (2) the deformation path which deformed pebbles have taken;
- (3) the volume change of pebbles;
- (4) the original pebble shape and orientation before deformation;
- (5) the finite strain ellipsoid and strain magnitude;
- (6) the ductility difference between pebble and matrix as well as between pebbles of different lithologies;
- (7) the strain rate of deformation.

As outlined above, some of these problems have been partially solved, but most solutions are not entirely satisfactory. The purpose of this study is to explore possible methods to solve these problems without dubious assumptions or at least to determine systematically the minimum number of assumptions required to make the solutions acceptable.

The Archean Shoal Lake conglomerate, which occurs between Mine Centre and Flanders, Ontario (Figure 1), was chosen for this study of pebble deformation. Scattered exposures on the roadcuts along Ontario Highway 11 provide excellent outcrops for measurement of deformed pebbles.

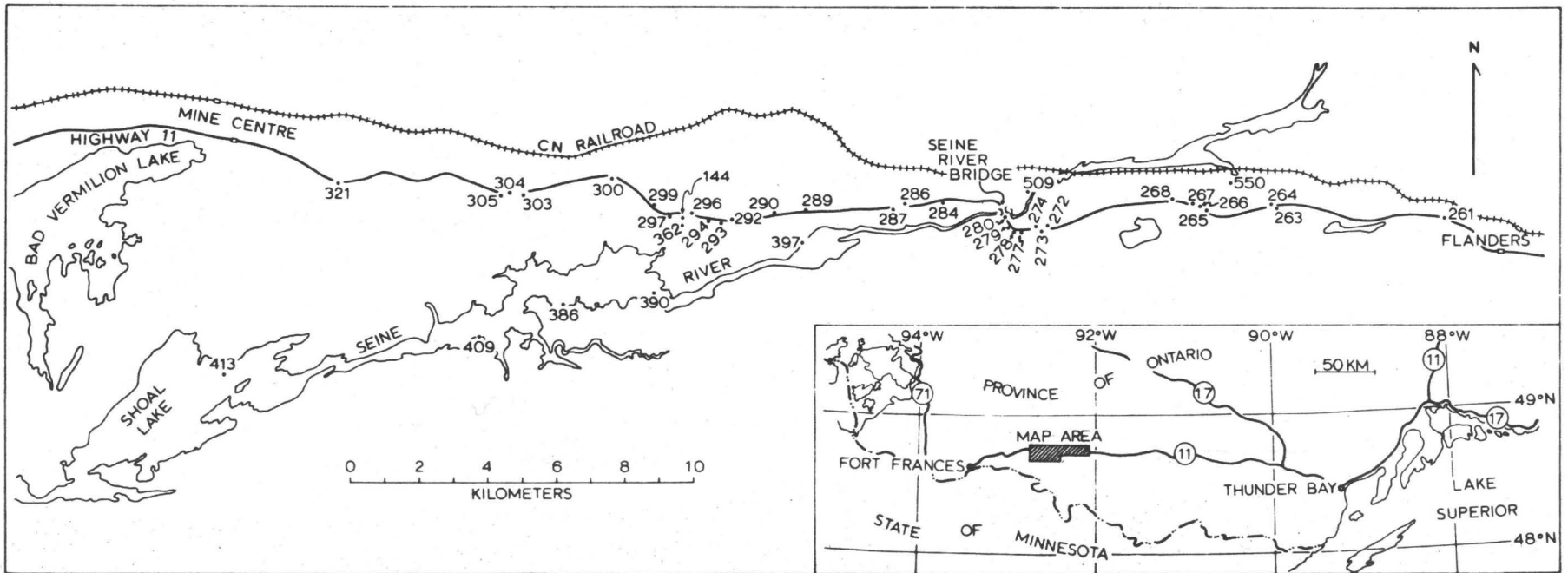


Figure 1. Location Map

Field work was first carried out in August, 1968. A two-week general reconnaissance of the regional geology in the map area suggested to the writer that the conventional method could not be applied to the study of the deformed pebbles there, because among all the outcrops observed there were only two foliation planes on which distinguishable pebbles can be measured and only one cross-section which is perpendicular ($\pm 5^{\circ}$) to the mineral lineation. The disappointing sections compelled the writer to derive most of the mathematical equations developed in this thesis during the academic year 1968-1969.

The second field season was started in early July, 1969. Nearly five weeks were spent in the field. More than half of this time was used in geological mapping, since the gross structure of the conglomerate bed is not correctly shown in any of the previously published geological maps (Lawson, 1888; Lawson, 1913; Merritt, 1934) covering the map area.

CHAPTER II

GEOLOGICAL SETTING

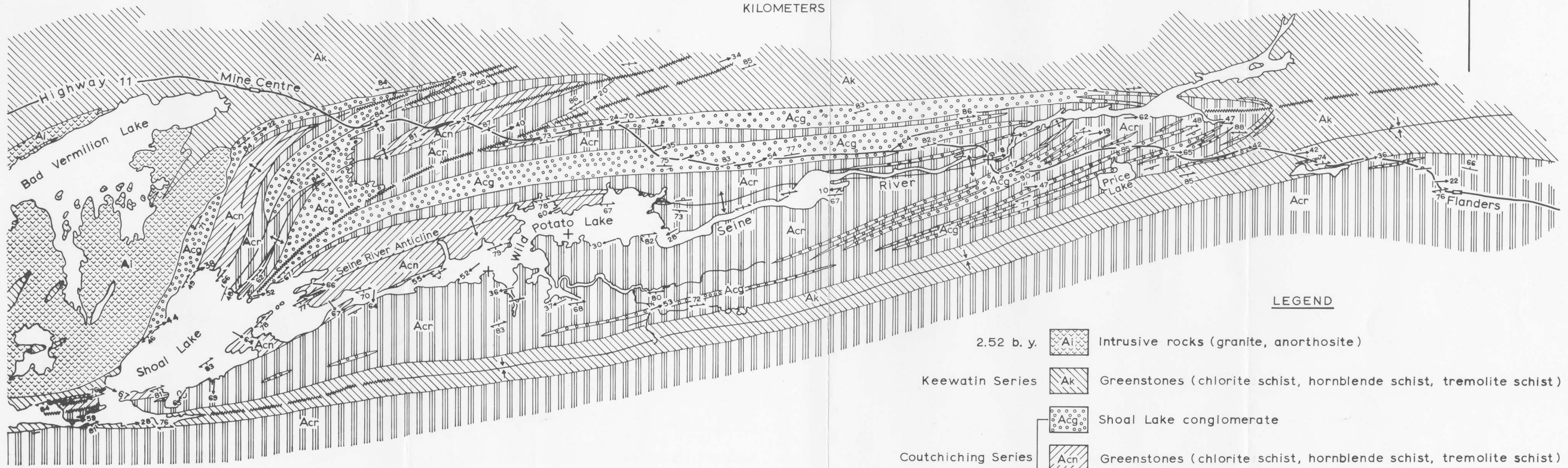
The rocks exposed in the map area are of Archean age. They are believed to have been subjected to a low-grade regional metamorphism about 2.75 b. y. ago (Hart and Davis, 1969). Many sedimentary structures are still preserved in arenaceous rocks; pillowed lavas and vesicular texture on top of lava flows are still recognizable. For geological mapping in the field, the terms arenite and greenstone have been widely used. Arenites refer to all the arenaceous rocks which under the microscope may turn out to be quartzite, biotite schist, sericite schist, or calcite schist; whereas greenstones refer to all the greenish rocks which may be petrographically chlorite schist, hornblende schist, tremolite schist, or their mixture.

1. STRATIGRAPHIC SEQUENCE

Lawson (1888, see particularly pp. 21-22, p. 105, and p. 139), in mapping the geology of the Rainy Lake region, designated the arenite and slate in the southernmost part of the present map area (Plate 1) as

GEOLOGIC MAP OF THE SEINE RIVER AREA, ONTARIO

GEOLOGY BY MAO-YANG HSU (1971)



LEGEND

- 2.52 b. y. Intrusive rocks (granite, anorthosite)
- Keewatin Series Greenstones (chlorite schist, hornblende schist, tremolite schist)
- Shoal Lake conglomerate
- Coutchiching Series Greenstones (chlorite schist, hornblende schist, tremolite schist)
- Arenites (quartzite, biotite schist, sericite schist, calcite schist)

- Bedding, tops known (horizontal, inclined, overturned, dip unknown)
- Foliation (inclined, vertical)

- Shear zone
- Mineral lineation
- Anticline
- Syncline

the Couthiching series. This series lies unconformably beneath the Keewatin series, which includes the greenstones and the conglomerates on Shoal Lake. The oldest division of the Archean complex considered by Lawson is the Laurentian orthogneisses, upon which the Couthiching and the Keewatin rocks were originally deposited.

In 1904 a visit to the area "along one line of section at the east end of Shoal Lake" was made by a special international committee composed of members of the Canadian and the United States geological surveys (see Van Hise et al., 1905). The committee concluded that "The Couthiching schists form the highest formation. These are a series of highly micaceous schists graduating downward into green hornblende and chloritic schists, here mapped by Lawson as Keewatin, which pass into a conglomerate known as the Shoal Lake conglomerate. This conglomerate lies upon an area of green schists and granites known as the Bad Vermilion granites ". Unfortunately, this is exactly the reverse of the sequence as it is understood now (see Figure 2).

Lawson's (1913) re-study of the area affirmed his earlier convictions about the relative positions of the Keewatin and the Couthiching rocks. He retained the name Couthiching for the rocks of the pre-Keewatin series and applied a new term Seine to those of the "younger post-Keewatin" series including the Shoal Lake conglomerate. In

2.52 b. y. PLUTONIC INTRUSION on Bad Vermilion Lake
2.75 b. y. REGIONAL METAMORPHISM

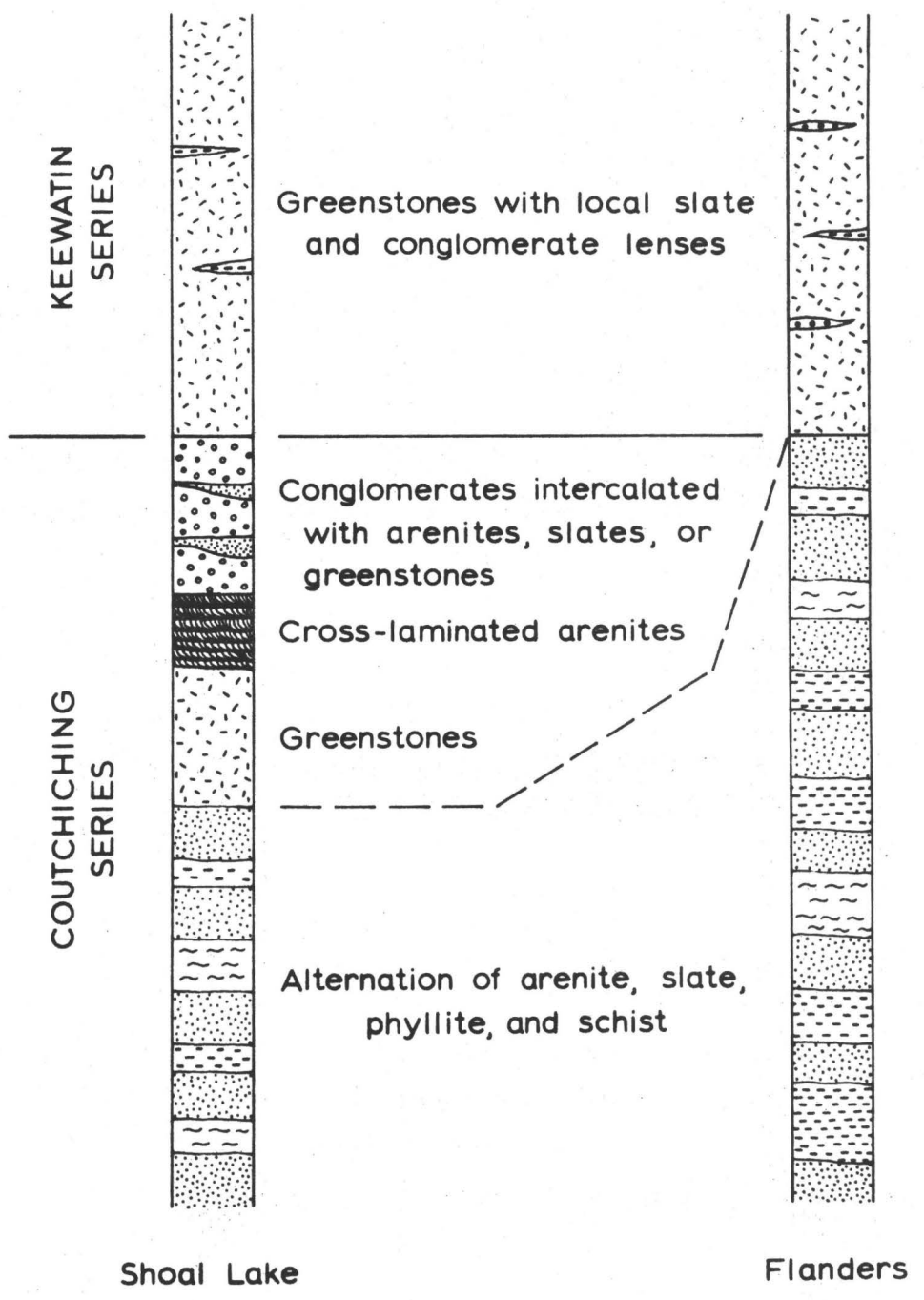


Figure 2. Stratigraphic Sequence

addition to the mistake of assigning the Shoal Lake conglomerate to the post-Keewatin, Lawson regarded the foliated rocks of the "Seine" series as deposited on a basement of granitic rocks which are not foliated near Shoal Lake.

After having mapped the Archean metamorphosed sedimentary rocks extending from Rainy Lake eastwards for about 240 kilometers to the vicinity of Lac des Mille Lacs, Merritt (1934) concluded that the sedimentary belt in the southern part of that area, equivalent to Lawson's Couthiching series, appears to lie unconformably on the Keewatin series. Consequently he put the rocks of Lawson's Couthiching series together with the Shoal Lake conglomerate into the "Seine" series. The conglomerate, according to Merritt, lies unconformably on the Laurentian rocks which in turn are intrusive into the Keewatin greenstones. Again, this is the reverse of the sequence as it is presently realized (Figure 2).

The latest investigation carried out by the present writer has uncovered a great deal of new field data, previously overlooked or previously inaccessible, which warrant a new interpretation concerning the structural relations of the sediments with the adjoining formations. Because of the absence of fossiliferous strata and the scarcity of reliable horizon markers, the geological structures have been determined by means of field tracing of the stratigraphic horizons and the use of minor

structural criteria including cross-lamination, graded bedding, load-cast, vesicular texture on top of lava flow, and foliation refraction on bedding (Plates 2-5(A)). The general stratigraphic sequence, then, is that the thick greenstones overlie the thick fine sediments (arenite, slate, etc.) with conglomerate lying in between (Figure 2). In places, such as the western portion of the map area, greenstones also lie be-
neath arenite, a fact that has unfortunately misled Merritt and the international committee mentioned above to regard Lawson's Coutchiching and the Shoal Lake conglomerate as lying on the Keewatin greenstones. Locally, conglomerate, arenite, and greenstone may be interbedded without any recognized break, although one single small-scale local unconformity (Plate 5(B)) has been observed. In the whole area, no basement has been found. Thus, in the map area, we may retain the term "Keewatin series" for the thick greenstones lying on the thick meta-sediments, but redefine the Coutchiching to include all the rocks underlying the Keewatin. The Coutchiching series thus defined includes Lawson's Coutchiching as well as the Shoal Lake conglomerate and the greenstones on Shoal Lake.

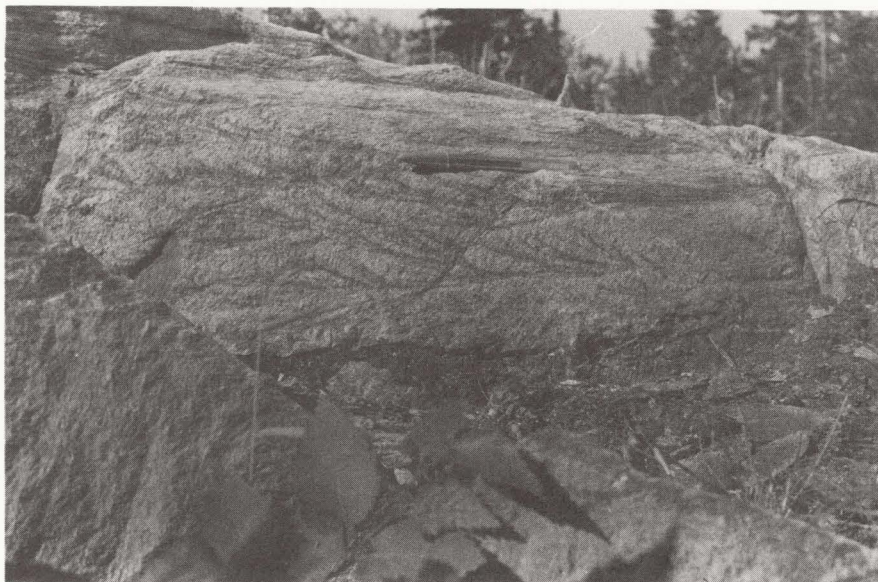
All these rocks probably were first folded and then subjected to a low-grade regional metamorphism. During metamorphism, the pebbles in the Shoal Lake conglomerate were deformed, and penetrative

Plate 2

(A) Cross-lamination in medium- to coarse-grained arenites.

Here, one coset consists of more than 5 single sets of cross-lamination, all showing a consistent flow direction. The section is parallel to the general trough direction of cross-lamination but is roughly perpendicular to the truncating surface. Note that some of the foreset laminations are inclined at angles greater than 35° to the truncating surface, due to tectonic deformation.

(B) Cross-section of trough cross-lamination.



(A)



(B)

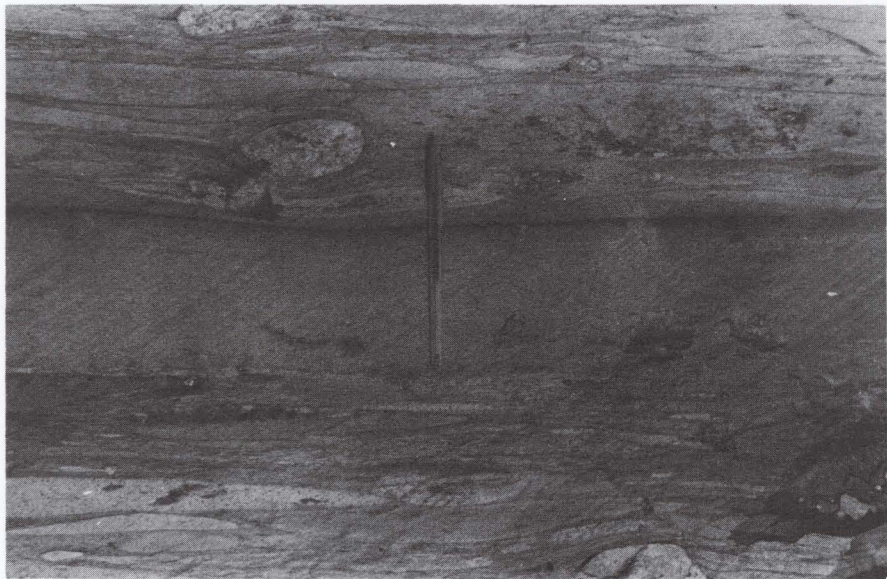
Plate 3

(A) Load casts beneath arenite beds. The underlying turbidites show repetition of graded bed followed by parallel lamination.

(B) Normally graded bedding in the arenite on top of a conglomerate bed.



(A)



(B)

Plate 4

(A) Pillowed lavas preserved in greenstones. Top on the left-hand side.

(B) Vesicular texture on top of lava flow indicating stratigraphic way-up to the right-hand side. Note that the foliation is not parallel to the bedding here.



(A)



(B)

Plate 5

(A) Foliation refraction on bedding.

(B) Local unconformity. Laminated greenstone lies on locally-deformed siltstone beds. A piece of siltstone was squeezed into the overlying greenstone, probably due to extreme loading.



(A)



(B)

foliation and mineral lineation were formed in all the rocks. The detrital Couthiching zircons are believed by the present writer to have been derived from an older sialic source, just like the granitic pebbles in the Shoal Lake conglomerate. Therefore, the zircon age of 2.75 b. y. (Hart and Davis, 1969) from the Couthiching rocks, which is indistinguishable in age from that of the Laurentian intrusive rocks (not exposed in the map area), probably was the result of metamorphic resetting. All the foliated rocks in the map area were subsequently intruded by the anorthosite and granite on Bad Vermilion Lake (see Plate 1). Both later intrusive rocks show no penetrative foliation and give a whole-rock Rb-Sr isochron age of 2.52 b. y. (Hart and Davis, 1969).

2. SHOAL LAKE CONGLOMERATE

The Shoal Lake conglomerate consists of numerous conglomerate beds with thicknesses varying from 40 centimeters up to more than 10 meters. Stratigraphically above each conglomerate bed lies a bed of arenite, or slate, or greenstone of varying thickness, each of which has composition similar to that of the matrix in the underlying conglomerate bed. The arenite commonly shows normally graded bedding, but in a few places reversed graded bedding was also observed. Slate, greenstone, and conglomerate, on the other hand, do not show appreciable graded bedding. However, slate and greenstone may locally show

content grading with pebbles being more abundant towards their bases.

Only one outcrop (locality No. 550, Figure 1) has been observed to show cross-lamination in the intercalated arenite within the conglomerate sequence, although cross-lamination is very common in the arenite beds stratigraphically beneath the Shoal Lake conglomerate.

The above features might suggest that the conglomerate beds are products of resedimentation*, similar to the mass movements which result from disturbance by overloading, earthquakes, and hydraulic pressures (Dott, 1963). If this is true, then the conglomerate beds should be called "paraconglomerate", although the predominant constituent of well-rounded pebbles of different lithology, mostly showing intact framework, may favor the term "polymictic conglomerate" (Pettijohn, 1957, pp. 254-255). The fine sediment beds lying on each conglomerate bed were probably deposited from suspended materials accompanying the mass movement of pebble clasts.

* This view seems to be generally true for all Archean clastic sediments coarser than pebble size (4-64 mm), found in the Canadian Shield (R.G. Walker, 1970, personal communication).

At any one outcrop, it is very difficult to determine the lithology of all pebbles, and also it is hard to distinguish those strongly-deformed pebbles from the matrix with the same color. So measurement of pebble content in the rock was hindered and only those pebbles distinguishable in the field were studied. Generally, the most abundant pebbles came from volcanic rocks, followed by granitic and quartzose rocks, respectively. Hence, in the field only those pebbles belonging to the above three rock types were measured. Volcanic pebbles may have compositions ranging from rhyolite to andesite; many pebbles of slate and silty quartzite also were mistakenly included in this category. Granitic pebbles refer to various plutonic rocks from alkaline granite to quartz diorite; whereas quartzose pebbles may be vein quartz, chert, or those derived from previous quartzite or quartz-rich sandstone.

3. GEOLOGICAL STRUCTURE

Mapping has revealed a number of folds; among them only the largest one, here called the Seine River anticline, is of interest in this study, because of the 34 outcrops where pebble measurements were made, only two are not within this anticline.

Refolding appears to have occurred in the central-west portion of the area (presumably caused by the plutonic intrusions on Bad Vermilion Lake) after the rocks had been foliated. Except for this part of the map area, penetrative foliation shows consistent orientation throughout the area. It strikes east-northeasterly and dips nearly vertically, and approximately parallels the axial traces of major folds (Plate 1).

Mineral lineations, however, are not so regularly oriented and are not so prominent, although they are always found lying on the foliation plane. Starting at Shoal Lake, mineral lineations plunge to the southeast at moderate angles; then they become increasingly steeper (i. e. , change clockwise on the foliation plane which dips steeply to the south-southeast) at the east end of the Lake, from where mineral lineations begin to plunge southwesterly with angles of decreasing order moving eastwards along the Seine River. Near the Seine River Bridge, mineral lineations are nearly horizontal, but they soon plunge southeasterly towards the east. On the other side, along Highway 11 where measurements of pebbles were made, most mineral lineations plunge moderately to the east-northeast on steeply-dipping foliation planes except in the vicinity of the Seine River Bridge where mineral lineations are found to be parallel to the fold axis of the Seine River anticline, which is nearly horizontal there.

Penetrative foliations commonly intersect the bedding at angles smaller than 10° . The north limb of the Seine River anticline dips to the north at angles about five degrees less than that of foliation whereas the south limb stands almost vertically or dips steeply to the south. Hence, the attitude of bedding with respect to that of foliation is useful in determining the fold structure.

Because the axial traces of major folds are parallel to the penetrative foliation, and the fold axes are parallel to the mineral lineations as well as the maximum elongation of deformed pebbles, it is considered that buckling was prior to the major flow deformation which might have caused the further closing-up of the buckled beds to form tight folds.

4. PALEOCURRENT DIRECTION

It has been noted before (p. 21) that there is abundant cross-lamination preserved in the arenite beds stratigraphically beneath the Shoal Lake conglomerate, though these arenites, petrographically, might be better called schists of various components (p. 10). The cross-lamination commonly forms a scooplike plunging-trough structure with a tangential basal contact (Plate 2). It may be called trough cross-lamination.

There seems to be no doubt that cross-lamination is an excellent criterion for identifying flow directions and stratigraphic sequence, although it gives no guidance concerning depositional environment. The cross-lamination observed at any one outcrop in the map area commonly has a consistent flow pattern, even though one coset might consist of five or more single sets of cross-lamination on a section parallel to the general trough direction but normal to the truncating surface. The consistency of flow pattern in a thick vertical sequence possibly indicates the downslope direction.

As the sedimentary rocks in the map area have been folded, the paleocurrent directions measured in the field must be rotated with respect to the corresponding fold axis in order to ascertain their original attitude. Unfortunately, only the plunge angle of the Seine River anticline in the vicinity of the Seine River Bridge, is known. It follows that the original attitude of most paleocurrent directions in the map area cannot be determined with certainty. However, the hinge zone on the southern side of the anticline extends broadly along the Seine River, where most bedding is nearly horizontal and so needs no rotation to show the original attitude. A total of 9 trough directions of cross-lamination measured in the hinge zone is shown in Figure 3. Yet because the cross-lamination has been subjected to a tectonic strain, the trough directions must have been distorted also. The distortion

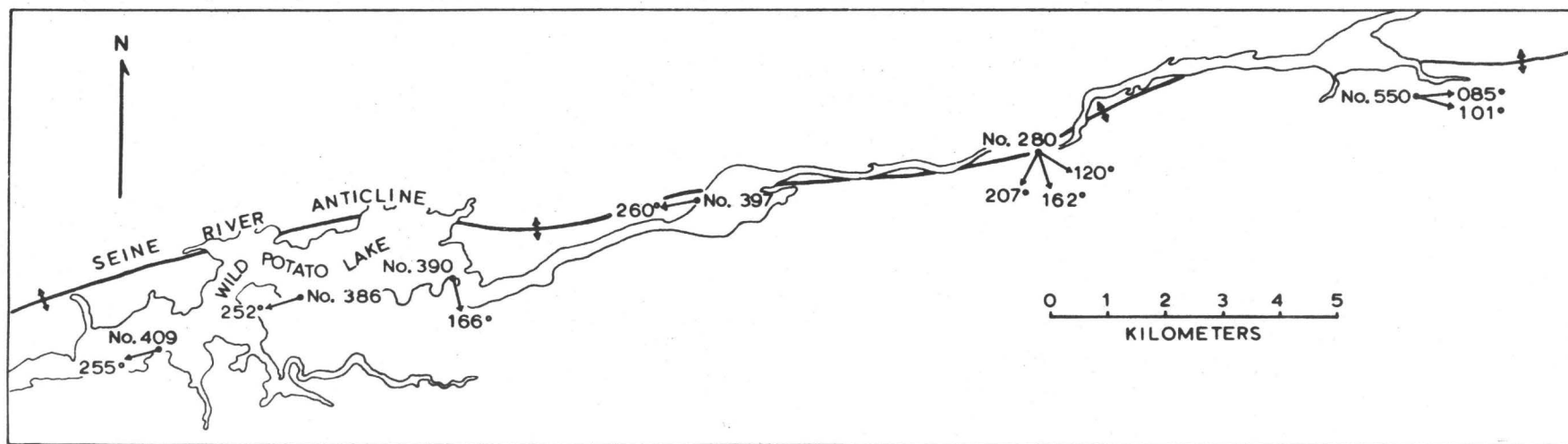


Figure 3. Trough cross-lamination directions measured in nearly horizontal beds.

of trough direction is believed to be similar to the change in the longest-axis orientation of ductile pebble during homogeneous deformation, which will be discussed in some detail in Chapter V of this thesis. Here we can only conclude that at the time of the deposition of the Archean arenites in the map area, the paleocurrent generally flowed towards the present south or southwest. In fact, no cross-lamination indicating an apparent paleocurrent direction in the clockwise azimuthal range of 340° - 080° , has ever been observed in the hinge zone of the Seine River anticline.

CHAPTER III

DEFORMATION PLOT

The tectonic strain considered throughout this thesis, is the constant-volume irrotational finite homogeneous strain belonging to the type of flow, either plastic or viscous, beyond the elastic limit of the rocks.

The finite homogeneous strain which a rock has suffered is most conveniently represented by the shape and orientation of the deformation ellipsoid - an ellipsoid resulting from deformation of an originally spherical portion of the rock being deformed (Flinn, 1962, p. 386).

In the study of pebble deformation, because the original pebble shape generally is not spherical, the final deformed pebble will not necessarily be the same in shape as the strain ellipsoid. Thus the symbols to represent different ellipsoids should be clarified as follows before further discussion is given:

X, Y, Z : Principal axes of an unspecified ellipsoid, where $X > Y > Z$.

X_f, Y_f, Z_f : Principal axes of a final deformed (or strained) pebble, where
 $X_f > Y_f > Z_f$.

X_t, Y_t, Z_t : Principal axes of the tectonic strain ellipsoid, where
 $X_t > Y_t > Z_t$; assuming that X_t is parallel to mineral lineation, Z_t is perpendicular to foliation, and Y_t lies on foliation plane but is normal to mineral lineation (Donath, 1963, p. 95; Ramsay, 1967, p. 436).

X_o, Y_o, Z_o : Principal axes of an original undeformed (or unstrained) pebble, where $X_o > Y_o > Z_o$.

X', Z' : Major and minor axes, respectively, of the exposed ellipse
(or X'', Z'') of a final deformed pebble on section 1 (or 2).

Since usually only the final shape of deformed pebbles can be measured, it is adequate to plot their axial ratios $b_f = Y_f/Z_f$ against $a_f = X_f/Y_f$ in a graphical plot so that different points in the plot represent different shapes of ellipsoid. Such a plot is called the deformation plot (Flinn, 1962, p. 386), whose ordinate and abscissa have an origin of unity and are of the same scale.

1. DEFORMATION PATH

When a rock is being deformed, an original sphere within it changes progressively through a series of ellipsoids varying increasingly

in eccentricity until the deformation ceases at a given finite strain.

The locus on the deformation plot of the ellipsoids of such continuously varying shape is called the deformation path (Flinn, 1962, p. 388).

Ramsay (1964; 1967, pp. 322-332) gives various equations to represent the states of finite strain of progressive deformation, in which the simplest deformation path has an equation of $a_t = b_t^K$ (where $a_t = X_t / Y_t$ and $b_t = Y_t / Z_t$; K is a constant, referring to the same path) on the deformation plot under conditions of constant irrotational stress and constant plastic proportionality factor.

It is clear from the equation $a_t = b_t^K$ that

$$K = (\ln a_t) / (\ln b_t) \quad (3-1)$$

where $\ln a_t = \ln X_t - \ln Y_t = 2(\epsilon_x - \epsilon_y)$

and $\ln b_t = \ln Y_t - \ln Z_t = 2(\epsilon_y - \epsilon_z)$;

ϵ_x , ϵ_y , and ϵ_z are the true strains of the three principal semiaxes of the tectonic strain ellipsoid (Ramsay, 1967, pp. 52-53). Moreover, as will be shown in Chapter V, in the case of coaxial deformation of $X_f \parallel X_t \parallel X_o$ and $Y_f \parallel Y_t \parallel Y_o$ (see p. 66),

$$a_f = a_t a_o \quad (5-19)$$

where a_o is the axial ratio X_o / Y_o .

Hence,

$$\ln a_f = \ln a_t + \ln a_o \quad (3-2A)$$

or

$$\ln a_t = \ln a_f - \ln a_o \quad (3-3A)$$

Similarly, in the case of coaxial deformation of $Y_f || Y_t || Y_o$ and $Z_f || Z_t || Z_o$,

$$\ln b_f = \ln b_t + \ln b_o \quad (3-2B)$$

or

$$\ln b_t = \ln b_f - \ln b_o \quad (3-3B)$$

where b_o is the axial ratio Y_o/Z_o .

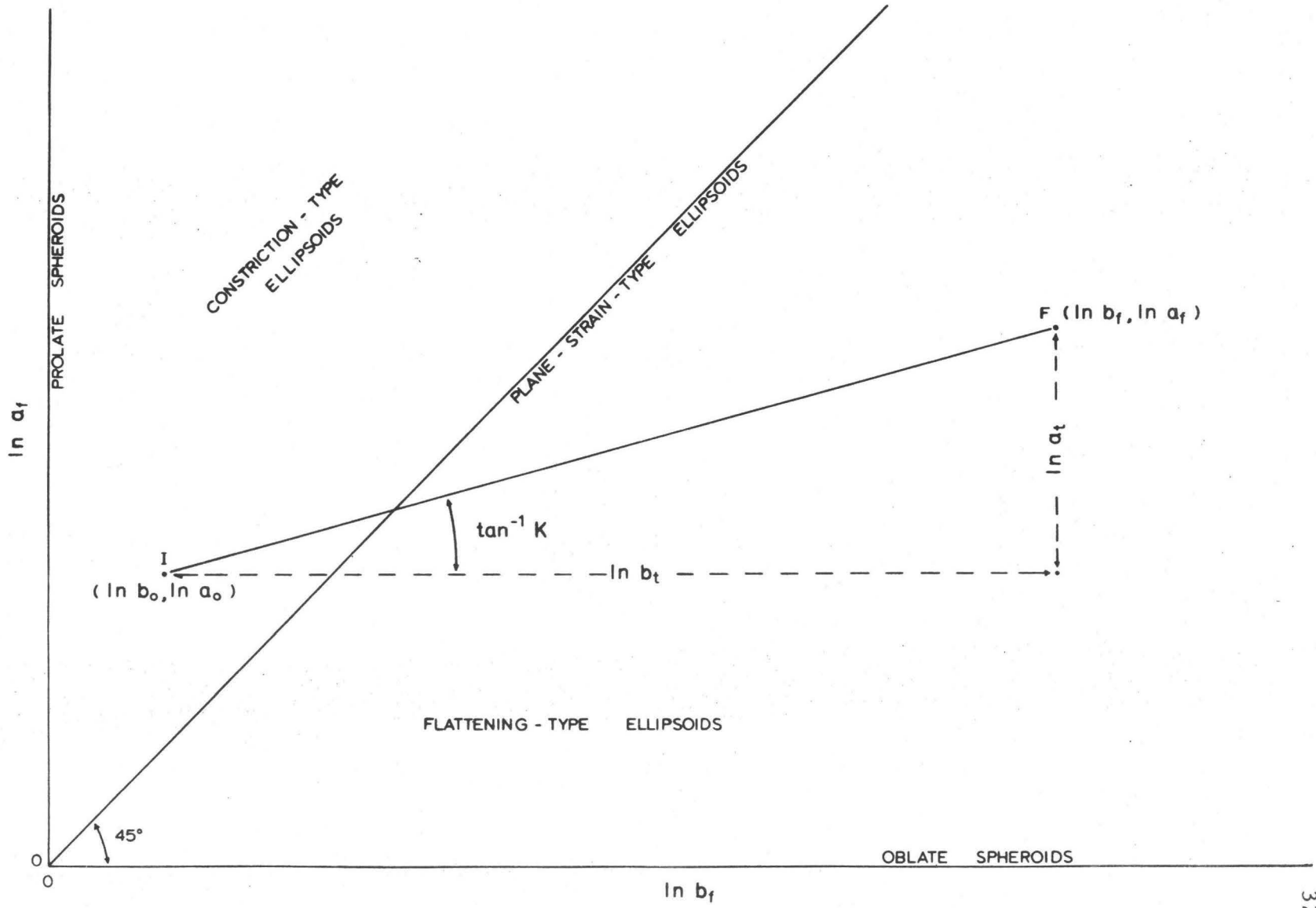
Substituting Equations (3-3A&B) in Equation (3-1), we have

$$K = (\ln a_f - \ln a_o) / (\ln b_f - \ln b_o) \quad (3-4)$$

From the simple relationship shown by Equation (3-4), it is, therefore, more convenient to construct a logarithmic deformation plot, using logarithmic axial-ratios as coordinates. In such a plot, the simplest deformation paths become straight lines for all possible K-values.

If the original shape is known, it can be plotted as point I ($\ln b_o, \ln a_o$) in Figure 4. Then the simplest deformation path is the straight line connecting point I and the final deformed shape shown by point F ($\ln b_f, \ln a_f$). The slope of this straight line in the logarithmic deformation

Figure 4. Example of the logarithmic deformation plot, showing the relationship of the original ellipsoid (I), the final deformed ellipsoid (F), the tectonic strain ratios, and the simplest deformation path (line IF) with a slope of $K = (\ln a_t)/(\ln b_t)$, in an irrotational coaxial deformation.



plot is simply the K-value computed from Equation (3-4). It must be noted again that the straight path in the above case holds only if the successive strain increments are added coaxially with respect to the originally ellipsoidal pebble (i. e. $X_t \parallel X_o$, etc.) and if the ratios of the strain increments (i. e. $d\varepsilon_x / d\varepsilon_y$ and $d\varepsilon_y / d\varepsilon_z$) remain constant throughout the deformation; otherwise, the deformation path can have any kind of route between points I and F.

In nature, it is virtually impossible to trace the deformation path correctly from geological strain, since the latter simply shows the final state of strained objects and gives no clue about the path the strained objects have ever taken to reach the final stage. However, deformed rocks in an area commonly show different strains in different components or at different parts. Therefore, a collection of strain data might reveal a trend of different strains similar to a deformation path, though the finite strain of each component or that at different parts might have taken a completely different path to arrive at its final state. If there are no better data available, this trend of different strains sometimes may be envisaged as a deformation path.

2. CONTOURS OF X_f/d , Y_f/d , AND Z_f/d

It was noted on page 3 that Flinn (1956) showed the contours of X_f/d , Y_f/d , and Z_f/d in the deformation plot, where d is the diameter of an equivalent sphere with the same volume as a final deformed pebble which has an ellipsoidal shape with three principal axes of $X_f > Y_f > Z_f$. Under certain circumstances, these contours can be used in determination of the original shape of deformed pebbles and the tectonic strain ellipsoid as will be discussed in Chapter VI.

The Z_f/d contours can be represented by the following equation (see Appendix A):

$$\ln a_f = -2 \ln b_f - 3 \ln (Z_f/d) \quad (3-5)$$

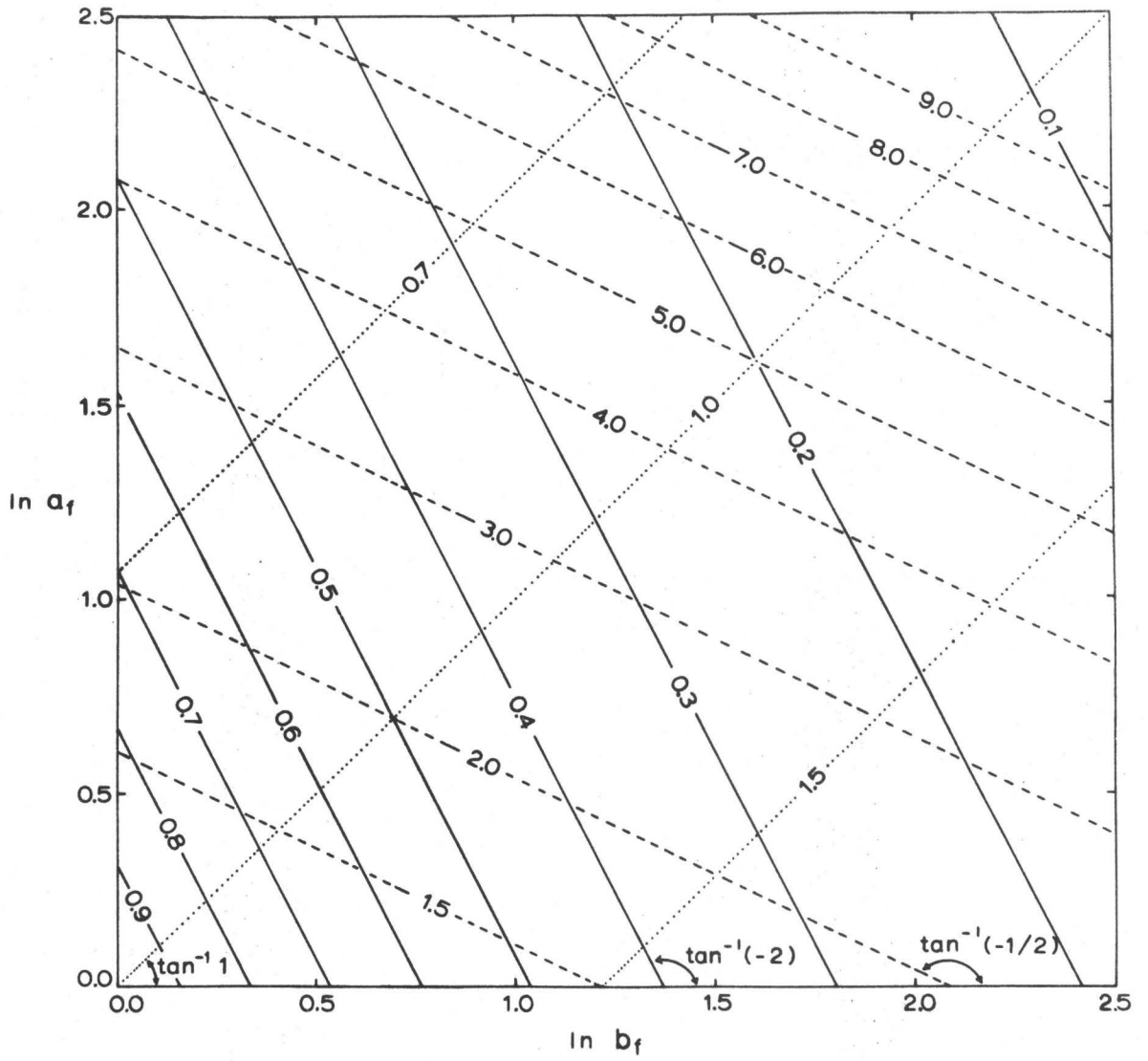
This is a straight line with a slope of -2 in the logarithmic deformation plot (Figure 5), indicating that all the Z_f/d contours are parallel to one another and make an angle of $\tan^{-1} (-2) = 116.5^\circ$ with the $\ln b_f$ axis.

By definition, $d > Z_f$, so $\ln (Z_f/d)$ always is negative and the intersection of a Z_f/d contour with the $\ln a_f$ axis always has a positive $\ln a_f$ value, i. e., $(-3 \ln (Z_f/d)) > 0$.

The equation representing the X_f/d contours (see Appendix A) is:

$$\ln a_f = -\frac{1}{2} \ln b_f + \frac{3}{2} \ln (X_f/d) \quad (3-6)$$

Figure 5. Contours of X_f/d , Y_f/d , and Z_f/d in a logarithmic deformation plot. Solid lines, Z_f/d contours; dashed lines, X_f/d contours (contours of $X_f/d > 9.0$ are not shown); dotted lines, Y_f/d contours (for simplicity, only 1.5, 1.0, and 0.7 contours are shown).



Again, they are all straight lines with an identical slope of $-\frac{1}{2}$ in the logarithmic deformation plot. These contours make an angle of $\tan^{-1}(-\frac{1}{2}) = 153.5^\circ$ with the $\ln b_f$ axis (Figure 5). Since $X_f > d$, $\frac{3}{2} \ln(X_f/d)$ must be positive.

The Y_f/d contours are represented by the following equation (see Appendix A):

$$\ln a_f = \ln b_f - 3 \ln(Y_f/d) \quad (3-7)$$

Clearly, the straight contours have a constant slope of 1, parallel to the deformation path of $K = (\ln a_t)/(\ln b_t) = 1$, suggesting that any deformation field (Ramsay, 1967, p. 141) parallel to the Y_f/d contours belongs to the deformation of plain strain. In the same case, if $Y_f > d$, $\ln(Y_f/d) > 0$, then $\ln b_f > \ln a_f$ (check Equation (3-7)), the Y_f/d contours fall in the deformation field of the flattening type, implying that the originally ellipsoidal shape falls in this field; whereas if $Y_f < d$, $\ln(Y_f/d) < 0$, then $\ln a_f > \ln b_f$ (check Equation (3-7)), and the Y_f/d contours lie in the field of the constriction type, indicating that the originally ellipsoidal shape lies on this side. When $Y_f = d$, $\ln(Y_f/d) = 0$, so $\ln a_f = \ln b_f$; i. e., the Y_f/d contour is identical with the diagonal of the deformation plot and the original shape may be either a perfect sphere or an ellipsoid with axial relationship of $X_o Z_o = Y_o^2$.

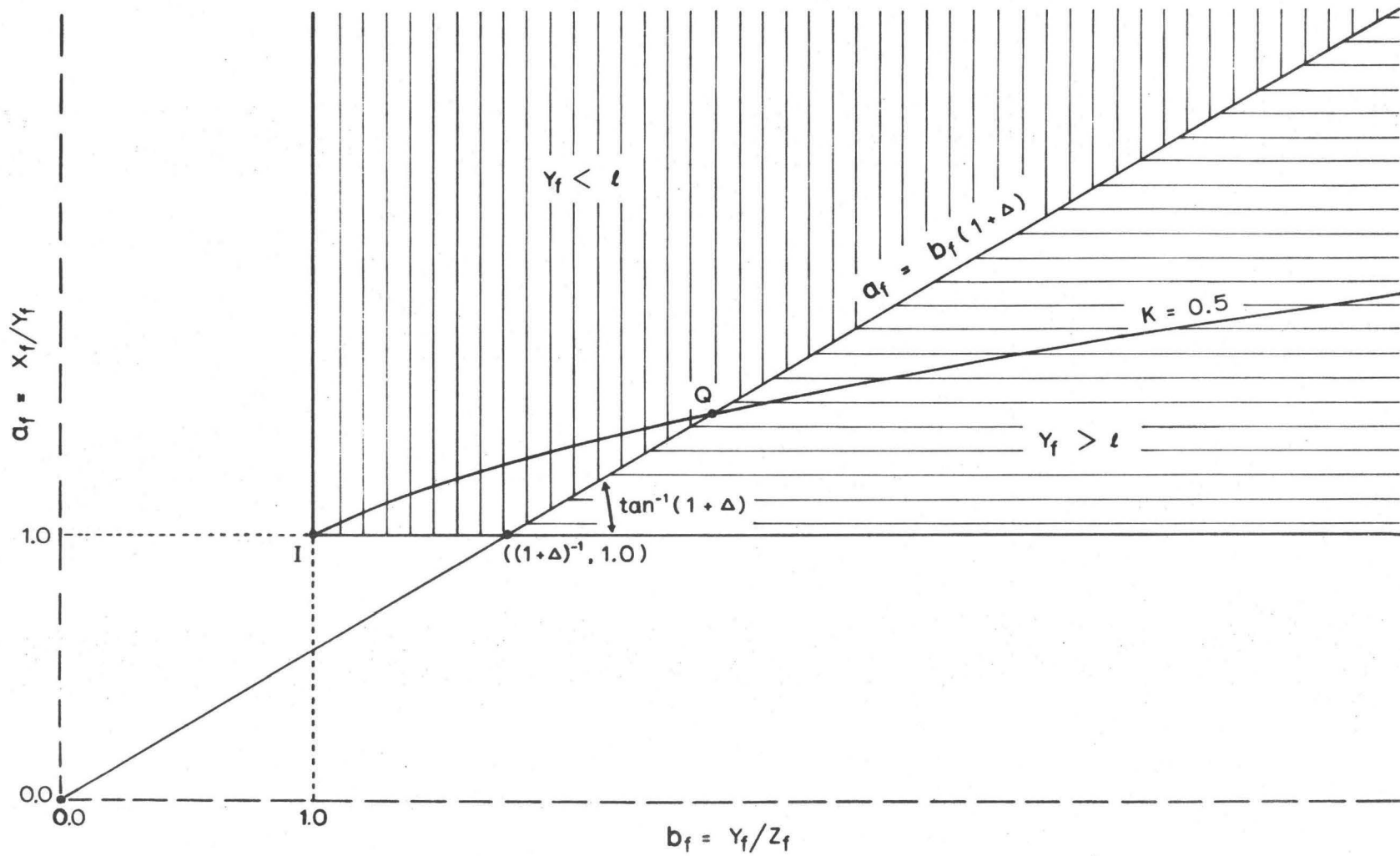
3. VOLUME CHANGE

Confusion of relating deformation field to volume change during deformation may possibly be caused by Ramsay's (1967, p. 162) explanation of his Figure 4-27 and also by his statement that "the prevalence of 'flattening type' ($1 > K > 0$) strain ellipsoids in slates may be explained by loss of volume during deformation, and not necessarily by actual expansion along the intermediate axis of the strain ellipsoid" (op. cit., p. 186). The reasons are given below:

(1) The shape of a deformation field is not represented by the line of the equation $a_f = b_f(1 + \Delta)$ at all (where Δ is the unit volume change), because the latter always makes an angle of $\tan^{-1}(1 + \Delta)$ with the b_f -axis and passes through the imaginary origin $a_f = b_f = 0$ (Figure 6), a feature not pointed out by Ramsay; whereas the shape of deformation field can be of any kind depending upon the shape and orientation of the originally ellipsoidal object as well as the shape and orientation of the finite strain ellipsoid.

(2) The line of the equation $a_f = b_f(1 + \Delta)$ simply shows the boundary along which the intermediate axis of a final ellipsoid, resulting from a homogeneously volume-reduced deformation of an original sphere, has been expanded from the reduced diameter due to volume reduction to reach a length equal to the original diameter of the sphere, by a

Figure 6. Homogeneously volume-reduced deformation of an originally spherical particle with a diameter of unit length l . The deformation path has a K-value of 0.5. Δ is the unit volume change (negative value for reduction).



flattening-type deformation. For example, an original sphere, with a diameter of unit length $\underline{1}$, is subjected to a volume-reduced homogeneous deformation of the type $K = 0.5$. Suppose the unit volume change is Δ , then the volume-reduced sphere (shown by point I in Figure 6) with a diameter shorter than $\underline{1}$ will be deformed into continuously-varying ellipsoids along the deformation path $K = 0.5$ during progressive irrotational deformation. The deformation path intersects the line of the equation $a_f = b_f(1 + \Delta)$ at point Q (Figure 6). If the final deformed ellipsoid falls in the field between points I and Q, then $Y_f < \underline{1}$; if the final ellipsoid is situated at point Q, then $Y_f = \underline{1}$. When the deformation intensifies further, the final deformed ellipsoid will reach beyond the point Q, then $Y_f > \underline{1}$.

Obviously, the problem of volume change during deformation has not been solved completely, and still needs further investigations.

CHAPTER IV

MATHEMATICAL DETERMINATION OF AN ELLIPSOID FROM ITS TWO CROSS-SECTIONS

Usually, determination of the shape of an ellipsoid relies heavily upon measurements of principal axes in principal planes. However, principal planes may not be obtained very often, especially when one studies deformed pebbles in the field where individual pebbles cannot be extracted from the rocks.

In order to cope with this problem, the writer has developed a mathematical method to determine the shape of an ellipsoid from any two cross-sections provided that the directions of three principal axes are known. The theory of the method is simple, which involves translation and rotation of two plane-ellipses to a three-dimensional space.

For simplicity, let us first examine only one of the two cross-sections of the ellipsoid to be sought. The cross-section is an ellipse in shape (two circular sections of an ellipsoid are special ellipses with equal axes), which can be expressed in the $x'z'$ plane of a cartesian $x'y'z'$ -coordinate system, with the ellipse center coincident with the origin of

the system. By translation and rotation, the ellipse of the $x'y'z'$ system can be expressed in a new xyz -system referred to the directions of the principal axes of the ellipsoid to be sought. The general equation of the translation is shown in a matrix form as

$$\begin{pmatrix} x \\ y \\ z \end{pmatrix} = \begin{pmatrix} \gamma'_{11} & \gamma'_{21} & \gamma'_{31} \\ \gamma'_{12} & \gamma'_{22} & \gamma'_{32} \\ \gamma'_{13} & \gamma'_{23} & \gamma'_{33} \end{pmatrix} \begin{pmatrix} x' + h' \\ y' + k' \\ z' + l' \end{pmatrix} \quad (4-1)$$

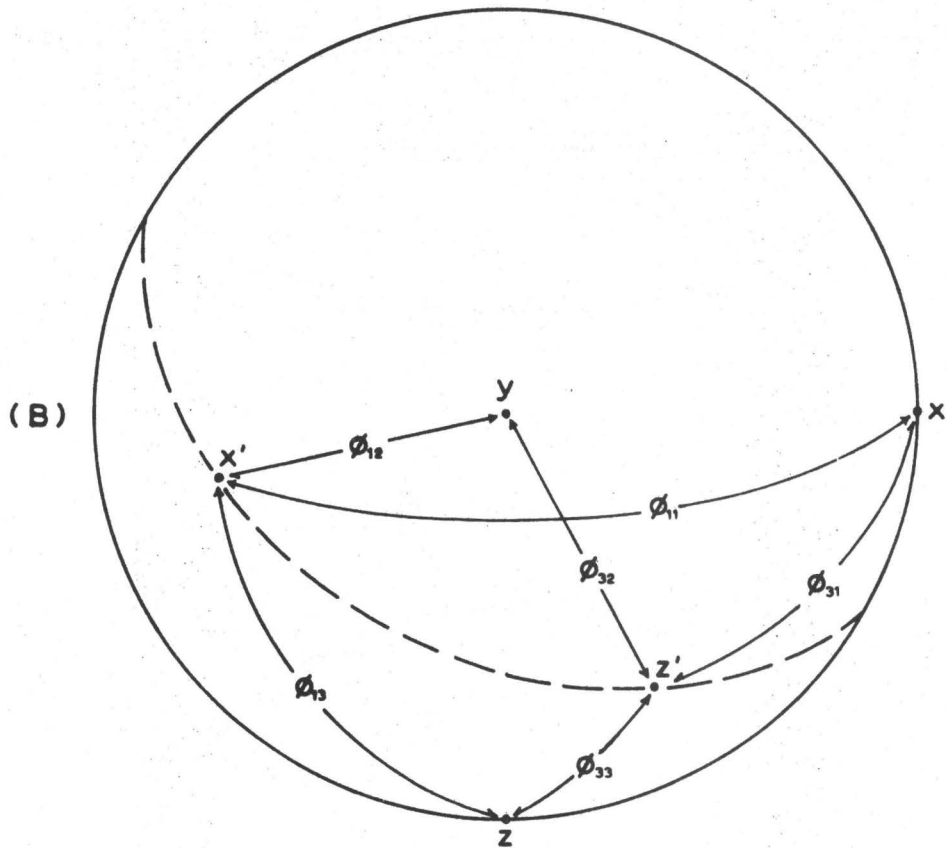
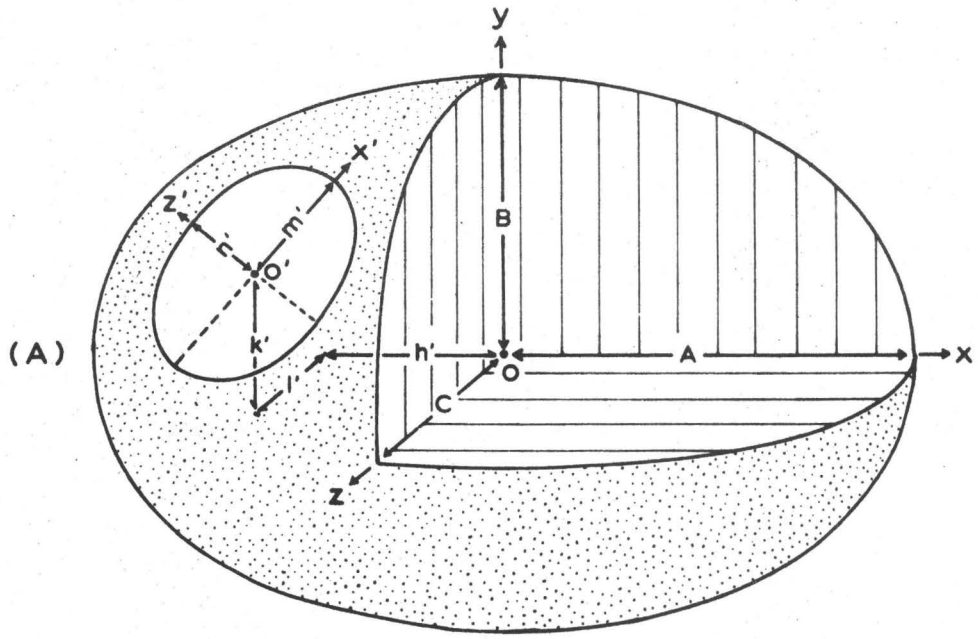
where γ'_{12} is the direction cosine of the x' -axis with respect to the y -axis, while γ'_{31} represents the direction cosine of the z' -axis with respect to the x -axis (notice the order of the subscript numbers, i. e. 1, 2, 3 refer to x, y, z , respectively; first number for that of the cross-sectional ellipse and second number for that of the ellipsoid being sought), etc.; (h', k', l') are the coordinates of the center of the cross-sectional ellipse in the xyz -system (Figure 7).

The general equation of the ellipsoid to be sought in the xyz -system is

$$\frac{x^2}{A^2} + \frac{y^2}{B^2} + \frac{z^2}{C^2} = 1 \quad (4-2)$$

where $A > B > C$ are the lengths of three principal semiaxes (the use of A, B, C here instead of customary a, b, c avoids confusion with the symbols $a = X/Y$ and $b = Y/Z$). Substituting Equation (4-1) in Equation (4-2), we get

Figure 7. Relationship between an ellipsoid and its cross-sectional ellipse. (A), the ellipse expressed in an $x'y'z'$ -system with its center coincident with the origin (point o') and its major and minor axes parallel to the x' and z' axes, respectively. This ellipse center has coordinates (h', k', l') in an xyz -system which refers to the principal directions of the ellipsoid. (B), angle relationship between the major and minor axes of the cross-sectional ellipse and the principal directions of the ellipsoid. Note that $\cos \phi'_{12} = \gamma'_{12}$, etc.



$$\begin{aligned}
& \frac{(\gamma'_{11} (x' + h') + \gamma'_{21} (y' + k') + \gamma'_{31} (z' + l'))^2}{A^2} \\
& + \frac{(\gamma'_{12} (x' + h') + \gamma'_{22} (y' + k') + \gamma'_{32} (z' + l'))^2}{B^2} \\
& + \frac{(\gamma'_{13} (x' + h') + \gamma'_{23} (y' + k') + \gamma'_{33} (z' + l'))^2}{C^2} = 1 \quad (4-3)
\end{aligned}$$

Under any circumstances the solution of this equation is time-consuming and tedious; but by setting D to represent all the terms containing h'^2 , k'^2 , l'^2 , $h'k'$, $k'l'$, or $l'h'$, and E to represent all the terms containing one of h' , k' , l' and one of x' , y' , z' , Equation (4-3) will become simpler as

$$\begin{aligned}
& B^2 C^2 (\gamma'^2_{11} x'^2 + \gamma'^2_{21} y'^2 + \gamma'^2_{31} z'^2 + 2(\gamma'_{11} \gamma'_{21} x' y' + \\
& \gamma'_{21} \gamma'_{31} y' z' + \gamma'_{31} \gamma'_{11} z' x')) + C^2 A^2 (\gamma'^2_{12} x'^2 + \gamma'^2_{22} y'^2 + \gamma'^2_{32} z'^2 \\
& 2(\gamma'_{12} \gamma'_{22} x' y' + \gamma'_{22} \gamma'_{32} y' z' + \gamma'_{32} \gamma'_{12} z' x')) \\
& + A^2 B^2 (\gamma'^2_{13} x'^2 + \gamma'^2_{23} y'^2 + \gamma'^2_{33} z'^2 + 2(\gamma'_{13} \gamma'_{23} x' y' \\
& + \gamma'_{23} \gamma'_{33} y' z' + \gamma'_{33} \gamma'_{13} z' x')) + D + E = A^2 B^2 C^2 \quad (4-4)
\end{aligned}$$

Suppose the cross-sectional ellipse intersects the $x'y'z'$ -axes in four points $(m', 0, 0)$, $(-m', 0, 0)$, $(0, 0, n')$, and $(0, 0, -n')$, then if we substitute the coordinates $(m', 0, 0)$ and $(-m', 0, 0)$, respectively, in Equation (4-4), we will get, by adding the two equations first and then dividing them by 2,

$$B^2 C^2 \gamma_{11}'^2 m'^2 + C^2 A^2 \gamma_{12}'^2 m'^2 + A^2 B^2 \gamma_{13}'^2 m'^2 + D = A^2 B^2 C^2 \quad (4-5)$$

Similarly, for points $(0, 0, n')$ and $(0, 0, -n')$, we have

$$B^2 C^2 \gamma_{31}'^2 n'^2 + C^2 A^2 \gamma_{32}'^2 n'^2 + A^2 B^2 \gamma_{33}'^2 n'^2 + D = A^2 B^2 C^2 \quad (4-6)$$

Equating Equations (4-5) and (4-6), we obtain

$$\begin{aligned} B^2 C^2 (\gamma_{11}'^2 m'^2 - \gamma_{31}'^2 n'^2) + C^2 A^2 (\gamma_{12}'^2 m'^2 - \gamma_{32}'^2 n'^2) \\ + A^2 B^2 (\gamma_{13}'^2 m'^2 - \gamma_{33}'^2 n'^2) = 0 \end{aligned} \quad (4-7)$$

It is interesting to note that all the terms containing h' , k' , or l' are eliminated in the above equation, indicating that the position of the cross-section center with respect to the ellipsoid center is not important in this method. It follows that only the shape and orientation of the elliptical cross-section are significant. In Appendix B, it is shown that any parallel planes cut through an ellipsoid, have elliptical cross-sections with an identical axial ratio.

Because m' and n' are the semimajor and semiminor axes, respectively, of the cross-sectional ellipse, their axial ratio can be expressed by $R' = m'/n'$. Thus, Equation (4-7) reduces to a simpler form as

$$\begin{aligned} B^2 C^2 (\gamma'_{11} R'^2 - \gamma'_{31}) + C^2 A^2 (\gamma'_{12} R'^2 - \gamma'_{32}) \\ + A^2 B^2 (\gamma'_{13} R'^2 - \gamma'_{33}) = 0 \end{aligned} \quad (4-8)$$

Now let us set

$$S_1 = \gamma'_{11} R'^2 - \gamma'_{31}$$

$$T_1 = \gamma'_{12} R'^2 - \gamma'_{32}$$

$$U_1 = \gamma'_{13} R'^2 - \gamma'_{33}$$

Then Equation (4-8) becomes

$$B^2 C^2 S_1 + C^2 A^2 T_1 + A^2 B^2 U_1 = 0 \quad (4-9)$$

The above equation is derived from one cross-section only. Similarly, from another cross-section based on the $x''z''$ plane of an $x''y''z''$ -system, we can obtain

$$B^2 C^2 S_2 + C^2 A^2 T_2 + A^2 B^2 U_2 = 0 \quad (4-10)$$

where

$$S_2 = \gamma_{11}''^2 R''^2 - \gamma_{31}''^2$$

$$T_2 = \gamma_{12}''^2 R''^2 - \gamma_{32}''^2$$

$$U_2 = \gamma_{13}''^2 R''^2 - \gamma_{33}''^2$$

in which R'' is the axial ratio of the second cross-sectional ellipse, while γ_{31}'' represents the direction cosine of the z'' -axis of the $x''y''z''$ -system with respect to the x -axis of the xyz -system (notice the order of the subscript numbers), etc.

Solving the simultaneous equations (4-9) and (4-10), we get

$$\frac{A^2}{B^2} = \frac{S_2 U_1 - S_1 U_2}{T_1 U_2 - T_2 U_1} \quad (4-11A)$$

and

$$\frac{B^2}{C^2} = \frac{S_1 T_2 - S_2 T_1}{S_2 U_1 - S_1 U_2} \quad (4-11B)$$

Adopting Flinn's (1962) terminology of axial ratios of deformation ellipsoid, we have $a = 2A/2B$ and $b = 2B/2C$. Hence,

$$a = \left[\frac{S_2 U_1 - S_1 U_2}{T_1 U_2 - T_2 U_1} \right]^{1/2} \quad (4-12A)$$

and

$$b = \left[\frac{S_1 T_2 - S_2 T_1}{S_2 U_1 - S_1 U_2} \right]^{1/2} \quad (4-12B)$$

Recovering the corresponding substitutions, we obtain

$$a = \left[\frac{(\gamma''_{11} R''^2 - \gamma''_{31}) (\gamma'_{13} R'^2 - \gamma'_{33}) - (\gamma'_{11} R'^2 - \gamma'_{31}) (\gamma''_{13} R''^2 - \gamma''_{33})}{(\gamma'_{12} R'^2 - \gamma'_{32}) (\gamma''_{13} R''^2 - \gamma''_{33}) - (\gamma''_{12} R''^2 - \gamma''_{32}) (\gamma'_{13} R'^2 - \gamma'_{33})} \right]^{1/2} \quad (4-13A)$$

and

$$b = \left[\frac{(\gamma'_{11} R'^2 - \gamma'_{31}) (\gamma''_{12} R''^2 - \gamma''_{32}) - (\gamma''_{11} R''^2 - \gamma''_{31}) (\gamma'_{12} R'^2 - \gamma'_{32})}{(\gamma''_{11} R''^2 - \gamma''_{31}) (\gamma'_{13} R'^2 - \gamma'_{33}) - (\gamma'_{11} R'^2 - \gamma'_{31}) (\gamma''_{13} R''^2 - \gamma''_{33})} \right]^{1/2} \quad (4-13B)$$

Equations (4-13) can be used for determining the axial ratios of a final deformed ellipsoid resulting from deformation of an originally spherical object, from any two cross-sections of the final ellipsoid, providing the directions of principal axes of the ellipsoid are known. If the original shape was ellipsoidal but with a random fabric, then the directions of the three principal axes of the strain ellipsoid can be taken as those of the representative final deformed ellipsoid, and

so Equations (4-13) can also be applied to determine the final shape of the representative ellipsoid from any two cross-sections.

Sometimes, the directions of maximum tectonic elongation and shortening are known, but only apparent strain ratios can be obtained on exposed sections which are not parallel to any principal plane of the finite strain ellipsoid. In such a case, we can simply use Equations (4-13) to determine the shape of the strain ellipsoid, if there are two non-parallel sections available, on each of which an apparent strain ratio can be obtained.

CHAPTER V

DETERMINATION OF THE ORIGINAL ORIENTATION OF DEFORMED PEBBLES ON IDENTICAL AND PARALLEL PRINCIPAL PLANES

1. PEBBLE FABRICS IN SEDIMENTARY DEPOSITS

Because the final shape and orientation of deformed pebbles depend in part on the original orientation of the pebbles before deformation, it is necessary to know the general fabric of pebbles in sedimentary deposits. Commonly, the variation in original fabric reflects differences in the dynamics of the transport medium and the depositional environments. Johansson (1965) has reviewed this field of study with extensive bibliographies on the fabrics of different sedimentary deposits. He concludes that "the preferred orientation of most particle sizes, transported in contact with a frictional substratum, is usually transverse to the direction of transport. Particles immersed in the transporting medium, such as glacier ice, gravitating mass, etc., tend to align themselves parallel with the direction of movement, owing to the shearing stress of the moving medium ". Regarding pebble inclination, Johansson

shows in his Table 1 that an upstream inclination of less than 30° seems to be the common rule for pebbles deposited in a running-water environment or those in gravitational deposits.

Recently, in a series of studies on mass movement, Lindsay (1966, 1968, and Lindsay et al., 1970) found that the shortest-axis fabrics "developed by mudflows have vertical modes ". He noted that "settling of the clasts under gravity after the flow has come to rest probably leads to a strengthening of the C (the shortest) axis fabric, as clasts would tend to reorient themselves with their plane of maximum projection normal to the force of gravity ".

In the map area, the medium-grained arenite beds beneath the Shoal Lake conglomerate contain abundant cross-lamination and are considered to have been deposited in an environment of running water, in which occasional isolated small pebbles, such as those of locality 280 near the Seine River Bridge, are found to sit in sands (a frictional bottom) and so their longest axes (X_o) probably lay perpendicular to the paleocurrent direction.

On the other hand, the majority of the Shoal Lake conglomerate beds in the map area are regarded as the product of resedimentation (pp. 20-21) - a kind of gravitational deposit; the shortest axes (Z_o) of their pebbles are likely to have originally stood vertically in the nearly

horizontal beds, similar to the clast fabric in mudflow described by Lindsay (1968).

2. MATHEMATICAL RELATIONSHIP BETWEEN THE ORIGINAL AND THE FINAL ORIENTATIONS OF DEFORMED PEBBLES

Mathematical equations derived to determine the X_f -orientations of the final deformed pebbles with respect to the principal axes of the tectonic strain ellipsoid were first developed by Gay (1968, pp. 219-223). However, all the deformations considered belong strictly to those "of inhomogeneous materials by simple and pure shear" (op. cit., p. 211). In other words, the deformations are of two-dimensional type only. These equations must be applied with caution to natural situations which are not two-dimensional.

For a general deformation not necessarily caused by simple or pure shear, Dunnet (1969) has successfully derived equations to "relate the final elliptical ratio and orientation of particles to their initial form and the magnitude and orientation of the finite ... strain ". However, it should be noted that the concentration of shape plots within a pair of initial-ratio contours (op. cit., Figure 7-9) does not represent the real population (frequency) of the initial-axial-ratio range in the case

of originally random fabric, because the majority of initial axial ratios on any section are of the apparent ones (see pp. 92-96); only the maximum cross-section of the initial ellipsoid is correctly shown on the outermost curve (see pp. 77-79).

In this study, the present writer has derived mathematical equations and developed a graphical expression to determine the complex relationship of orientation and shape among the original undeformed ellipsoid, the tectonic strain ellipsoid, and the final deformed ellipsoid. In order to obtain the real populations of the orientation and shape concerned, one has to find a final planar fabric on an exposed section parallel to a principal plane of the strain ellipsoid, on which the real (not the apparent) orientation and shape of the deformed pebbles can be measured and a suspected originally planar fabric may be detected. Such a section is extremely rare in nature. But for geologic purposes, complete coincidence of an exposed section and a final planar fabric may not be necessary; a deviation of $\pm 5^{\circ}$ is tolerated in this study*. Thus, a favorable section for measurement can be found, even though it is not the best possible plane.

* A pebble with its longest axis making an angle of 0° - 30° to the movement direction, is called "strictly parallel" (parallèles stricts) by Cailleux and Tricart (1965, p. 7).

In an orientation analysis of deformed pebbles, it is most convenient to establish a reference xyz -coordinate system with axes parallel to the three principal axes ($X_t > Y_t > Z_t$), respectively, of the tectonic strain ellipsoid. The strain ellipsoid in this system is:

$$x^2/\lambda_{tx} + y^2/\lambda_{ty} + z^2/\lambda_{tz} = 1 \quad (5-1)$$

or

$$\lambda'_{tx} x^2 + \lambda'_{ty} y^2 + \lambda'_{tz} z^2 = 1 \quad (5-2)$$

where $\lambda_{tx} > \lambda_{ty} > \lambda_{tz}$ are the principal quadratic extensions (Ramsay, 1967, p. 52; Nadai, 1950, p. 118), equivalent to $(X_t/2)^2 > (Y_t/2)^2 > (Z_t/2)^2$ in this study; $\lambda'_{tx} < \lambda'_{ty} < \lambda'_{tz}$ are the reciprocal quadratic extensions (Ramsay, 1967, p. 126), i. e., $\lambda'_{tx} = 1/\lambda_{tx}$, $\lambda'_{ty} = 1/\lambda_{ty}$, and $\lambda'_{tz} = 1/\lambda_{tz}$.

In nature, the most common of all the possible coincidences of principal planes among the original undeformed pebble, the tectonic strain ellipsoid, and the final deformed pebble probably is $X_o Y_o \parallel X_t Y_t \parallel X_f Y_f$. In such a case, the $X_o Y_o$ plane of the original pebble in an $\bar{x}\bar{y}$ -coordinate system with axes parallel to the X_o and Y_o directions is given by

$$\bar{x}^2/(X_o/2)^2 + \bar{y}^2/(Y_o/2)^2 = 1$$

which is reduced to

$$\lambda'_{o1} \bar{x}^2 + \lambda'_{o2} \bar{y}^2 = 1 \quad (5-3)$$

if we set $\lambda'_{o1} = 1/\lambda_{o1} = (X_o/2)^{-2}$ and $\lambda'_{o2} = 1/\lambda_{o2} = (Y_o/2)^{-2}$.

Equation (5-3) can be revised into a matrix equation as

$$\begin{pmatrix} \bar{x} & \bar{y} \end{pmatrix} \begin{pmatrix} \lambda'_{o1} & 0 \\ 0 & \lambda'_{o2} \end{pmatrix} \begin{pmatrix} \bar{x} \\ \bar{y} \end{pmatrix} = 1 \quad (5-4)$$

With reference to an $x'y'$ -system with coordinate axes taken parallel to the principal strain directions, the above equation should be transformed

to

$$\begin{pmatrix} x' & y' \end{pmatrix} \begin{pmatrix} \cos\theta & \sin\theta \\ -\sin\theta & \cos\theta \end{pmatrix} \begin{pmatrix} \lambda'_{o1} & 0 \\ 0 & \lambda'_{o2} \end{pmatrix} \begin{pmatrix} \cos\theta & -\sin\theta \\ \sin\theta & \cos\theta \end{pmatrix} \begin{pmatrix} x' \\ y' \end{pmatrix} = 1$$

$$\text{or } \begin{pmatrix} x' & y' \end{pmatrix} \begin{pmatrix} \lambda'_{o1} \cos^2\theta + \lambda'_{o2} \sin^2\theta & (\lambda'_{o2} - \lambda'_{o1}) \sin\theta \cos\theta \\ (\lambda'_{o2} - \lambda'_{o1}) \sin\theta \cos\theta & \lambda'_{o1} \sin^2\theta + \lambda'_{o2} \cos^2\theta \end{pmatrix} \begin{pmatrix} x' \\ y' \end{pmatrix} = 1 \quad (5-5)$$

where θ is the angle between the X_o and X_t directions, or between the coordinate axes \bar{x} and x' (Figure 8(A)). Equation (5-5) can be expressed

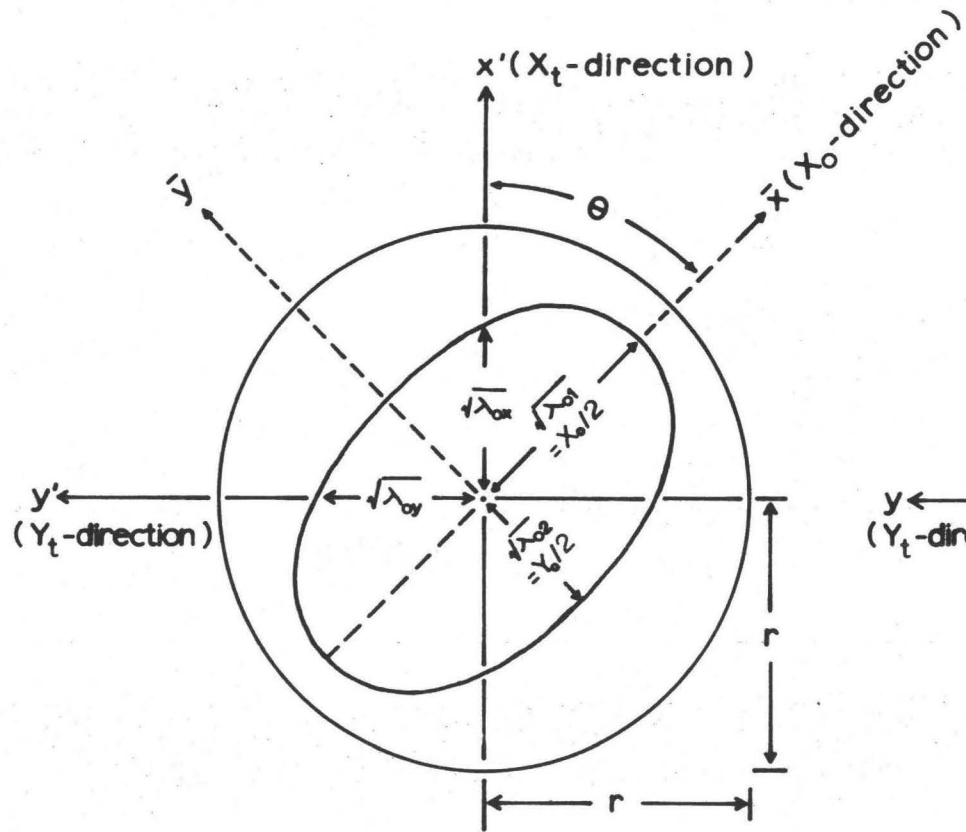
in a simple form as

$$\begin{pmatrix} x' & y' \end{pmatrix} \begin{pmatrix} \lambda'_{ox} & \gamma'_{o} \\ \gamma'_{o} & \lambda'_{oy} \end{pmatrix} \begin{pmatrix} x' \\ y' \end{pmatrix} = 1 \quad (5-6)$$

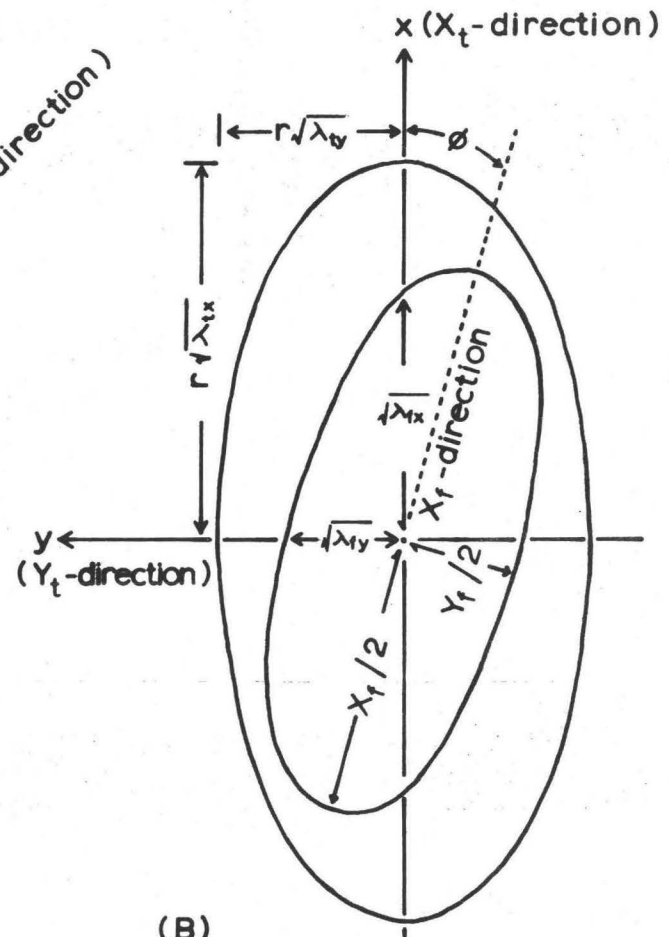
Figure 8. Homogeneous deformation of an $X_0 Y_0$ ellipse in a coordinate system with axes taken parallel to the principal strain directions.

(A), before deformation; a reference circle has a radius of r .

(B), after deformation; the reference circle becomes an ellipse with $r(\lambda_{tx})^{1/2}$ and $r(\lambda_{ty})^{1/2}$ as its semimajor and semiminor axes, respectively.



(A)



(B)

where

$$\lambda'_{ox} = \lambda'_{o1} \cos^2 \theta + \lambda'_{o2} \sin^2 \theta$$

$$\lambda'_{oy} = \lambda'_{o1} \sin^2 \theta + \lambda'_{o2} \cos^2 \theta$$

$$\gamma'_{o} = (\lambda'_{o2} - \lambda'_{o1}) \sin \theta \cos \theta$$

Now let us subject this $X_o Y_o$ ellipse to a homogeneous deformation, an irrotational strain with principal axes parallel to the x' and y' axes and with principal reciprocal quadratic extensions of λ'_{tx} and λ'_{ty} (Figure 8(B)). The transformation equations can be expressed in a simple vector notation as

$$\begin{pmatrix} x \\ y \end{pmatrix} = \begin{pmatrix} x' \sqrt{\lambda_{tx}} \\ y' \sqrt{\lambda_{ty}} \end{pmatrix}$$

or

$$\begin{pmatrix} x' \\ y' \end{pmatrix} = \begin{pmatrix} x \sqrt{\lambda'_{tx}} \\ y \sqrt{\lambda'_{ty}} \end{pmatrix}$$

which can be rewritten as

$$\begin{pmatrix} x' \\ y' \end{pmatrix} = \begin{pmatrix} \sqrt{\lambda'_{tx}} & 0 \\ 0 & \sqrt{\lambda'_{ty}} \end{pmatrix} \begin{pmatrix} x \\ y \end{pmatrix} \quad (5-7)$$

Substituting Equation (5-7) in Equation (5-6), we have

$$\begin{pmatrix} x & y \end{pmatrix} \begin{pmatrix} \sqrt{\lambda'_{tx}} & 0 \\ 0 & \sqrt{\lambda'_{ty}} \end{pmatrix} \begin{pmatrix} \sqrt{\lambda'_{ox}} & 0 \\ 0 & \sqrt{\lambda'_{oy}} \end{pmatrix} \begin{pmatrix} \sqrt{\lambda'_{tx}} & 0 \\ 0 & \sqrt{\lambda'_{ty}} \end{pmatrix} \begin{pmatrix} x \\ y \end{pmatrix} = 1$$

or

$$\begin{pmatrix} x & y \end{pmatrix} \begin{pmatrix} \lambda'_{tx} & \lambda'_{ox} & \sqrt{\lambda'_{tx} \lambda'_{ty}} \cdot \gamma'_o \\ \sqrt{\lambda'_{tx} \lambda'_{ty}} \cdot \gamma'_o & \lambda'_{ty} & \lambda'_{oy} \end{pmatrix} \begin{pmatrix} x \\ y \end{pmatrix} = 1$$

which can be expressed in a simple form as

$$\begin{pmatrix} x & y \end{pmatrix} \begin{pmatrix} \lambda'_{fx} & \gamma'_f \\ \gamma'_f & \lambda'_{fy} \end{pmatrix} \begin{pmatrix} x \\ y \end{pmatrix} = 1 \quad (5-8)$$

where

$$\lambda'_{fx} = \lambda'_{tx} \lambda'_{ox} = \lambda'_{tx} (\lambda'_{o1} \cos^2 \theta + \lambda'_{o2} \sin^2 \theta) \quad (5-9a)$$

$$\lambda'_{fy} = \lambda'_{ty} \lambda'_{oy} = \lambda'_{ty} (\lambda'_{o1} \sin^2 \theta + \lambda'_{o2} \cos^2 \theta) \quad (5-9b)$$

$$\gamma'_f = \sqrt{\lambda'_{tx} \lambda'_{ty}} \cdot \gamma'_o = \sqrt{\lambda'_{tx} \lambda'_{ty}} \cdot (\lambda'_{o2} - \lambda'_{o1}) \sin \theta \cos \theta \quad (5-9c)$$

Equation (5-8) with its elements shown in Equations (5-9), is a matrix equation of the final deformed pebble on the $X_f Y_f$ plane in terms of the principal tectonic strains and the shape and orientation of the original undeformed pebble, all with reference to the coordinate system with axes taken parallel to the principal strain directions.

Letting J_1 and J_2 be the first and the second strain invariants of the final strained $X_f Y_f$ ellipse, respectively (Ramsay, 1967, pp. 81-82), we have (see also Figure 8(B))

$$J_1 = \lambda'_{fx} + \lambda'_{fy} = 1/(X_f/2)^2 + 1/(Y_f/2)^2 \quad (5-10)$$

$$J_2 = \lambda'_{fx} \lambda'_{fy} - \gamma_f'^2 = 1/((X_f/2)^2 (Y_f/2)^2) \quad (5-11)$$

Because

$$1/(X_f/2)^2 + 1/(Y_f/2)^2 = \frac{1}{(X_f/2)^2} \left(1 + a_f^2 \right)$$

Equation (5-10) becomes

$$(X_f/2)^2 = (a_f^2 + 1)/(\lambda'_{fx} + \lambda'_{fy}) \quad (5-12)$$

Because

$$\frac{1}{(X_f/2)^2 (Y_f/2)^2} = \frac{a_f^2}{(X_f/2)^4} = \left(\frac{a_f}{(X_f/2)^2} \right)^2$$

Equation (5-11) becomes

$$(X_f/2)^2 = a_f / (\lambda'_{fx} \lambda'_{fy} - \gamma_f'^2)^{1/2} \quad (5-13)$$

Since Equation (5-8) is the equation of an ellipse, the discriminant

$$\begin{vmatrix} \lambda'_{fx} & \gamma'_f \\ \gamma'_f & \lambda'_{fy} \end{vmatrix} \text{ must be greater than zero, i.e. } (\lambda'_{fx} \lambda'_{fy} - \gamma'^2_f) > 0.$$

Moreover, because $(X_f/2)^2 > 0$ and $a_f > 0$, it follows that $(\lambda'_{fx} \lambda'_{fy} - \gamma'^2_f)^{1/2}$ can only be positive (see Equation (5-13)).

Equating Equations (5-12) and (5-13), we obtain

$$a_f(\lambda'_{fx} + \lambda'_{fy}) = (a_f^2 + 1)(\lambda'_{fx} \lambda'_{fy} - \gamma'^2_f)^{1/2} \quad (5-14)$$

Substituting Equations (5-9) in Equation (5-14) and dividing by

$$\lambda'_{tx} \lambda'_{oy} \text{ (note that } \lambda'_{ty} / \lambda'_{tx} = (X_t/2)^2 / (Y_t/2)^2 = a_t^2 \text{ and}$$

$$\lambda'_{oz} / \lambda'_{oy} = (X_o/2)^2 / (Y_o/2)^2 = a_o^2 \text{), we get}$$

$$\begin{aligned} & a_f \left[(\cos^2 \theta + a_o^2 \sin^2 \theta) + a_t^2 (\sin^2 \theta + a_o^2 \cos^2 \theta) \right] \\ &= (a_f^2 + 1) \left[a_t^2 (\cos^2 \theta + a_o^2 \sin^2 \theta) (\sin^2 \theta + a_o^2 \cos^2 \theta) \right. \\ & \quad \left. - a_t^2 (a_o^2 - 1)^2 \sin^2 \theta \cos^2 \theta \right]^{1/2} \end{aligned}$$

which, upon simplification, becomes

$$a_f \left[(a_t^2 + a_o^2) + (a_t^2 - 1)(a_o^2 - 1) \cos^2 \theta \right] = a_t a_o (a_f^2 + 1)$$

By transforming terms, we obtain

$$\cos^2 \theta = \frac{a_t a_o (a_f^2 + 1) - a_f (a_t^2 + a_o^2)}{a_f (a_t^2 - 1) (a_o^2 - 1)} \quad (5-15)$$

Multiplying by 2 and then subtracting 1 from both sides of Equation (5-15), we find

$$\cos 2\theta = \frac{2 a_t a_o (a_f^2 + 1) - a_f (a_t^2 + 1)(a_o^2 + 1)}{a_f (a_t^2 - 1)(a_o^2 - 1)} \quad (5-16)$$

If the angle between the X_f and X_t directions is designated as \emptyset in the case of coaxial deformation of $X_f Y_f \parallel X_t Y_t \parallel X_o Y_o$, we can follow similar approach to obtain

$$\cos^2 \emptyset = \frac{a_o (a_t^2 a_f^2 + 1) - a_t a_f (a_o^2 + 1)}{a_o (a_t^2 - 1)(a_f^2 - 1)}$$

which can be changed into

$$\cos 2\emptyset = \frac{a_o (a_t^2 + 1)(a_f^2 + 1) - 2a_t a_f (a_o^2 + 1)}{a_o (a_t^2 - 1)(a_f^2 - 1)} \quad (5-17)*$$

* This is the same equation as the one having been developed by Dunnet (1969, Equation 16), except that he has a needless wrong "+" sign between the two terms in the numerator.

It must be noted here that by definition (Ramsay, 1967, pp. 52-53), the true strain (ϵ) recording the change of length is:

$\epsilon = \ln \lambda^{1/2} = \frac{1}{2} \ln \lambda$, where λ is the quadratic elongation. Hence,
 $e^{2\epsilon} = \lambda$ or $e^{\epsilon} = \lambda^{1/2}$. In Equations (5-16) and (5-17), only a_t

can be expressed in terms of true strain because $a_t = X_t / Y_t$
 $= 2 \lambda_{tx}^{1/2} / 2 \lambda_{ty}^{1/2} = e^{\epsilon_x} / e^{\epsilon_y}$. All the others cannot. Unfortunately, confusions about the true strain frequently can be found in many papers, if the definition is not modified.

3. DEFORMATION OF ELLIPSES WITH VARIOUS ORIENTATIONS

Utilizing Equations (5-16) and (5-17), we can demonstrate how an original ellipse being homogeneously deformed, changes its orientation and shape during strain history.

First, suppose we have seven ellipses with an identical shape (say, $a_o = X_o / Y_o = 1.6$) but different orientations. The θ angles of these seven ellipses are 0° , 15° , 30° , 45° , 60° , 75° , and 90° .

Secondly, subject these ellipses to a tectonic strain with axial ratio (a_t) increasing progressively from 1.0 to 2.0, passing through, say, 1.2, 1.4, 1.6, and 1.8.

Thirdly, substitute the known data θ , a_o , and a_t in Equation (5-16) to obtain the a_f ratios.

Finally, substitute a_o , a_t , and a_f in Equation (5-17) to get the corresponding ϕ angles.

The above processes can be done easily by the computer all at once. The results are plotted in Figures 9-11 using the a_f ratio as ordinate and the ϕ angle as abscissa. This kind of plot is here called the orientation plot.

Some characteristics of the deformed ellipses during progressive deformation are outlined below:

(1) The ellipse with $\theta = 0^\circ$ keeps its orientation parallel to the X_t -axis of the tectonic strain ellipse throughout the deformation. In addition, the final axial ratio of this ellipse, a_f , is a product of a_o and a_t . This relationship can be derived by the following mathematical method:

Since $\theta = 0^\circ$, $\cos 2\theta = 1$;

so Equation (5-16) becomes, upon simplifying:

$$a_o a_t a_f^2 - (a_o^2 a_t^2 + 1) a_f + a_o a_t = 0$$

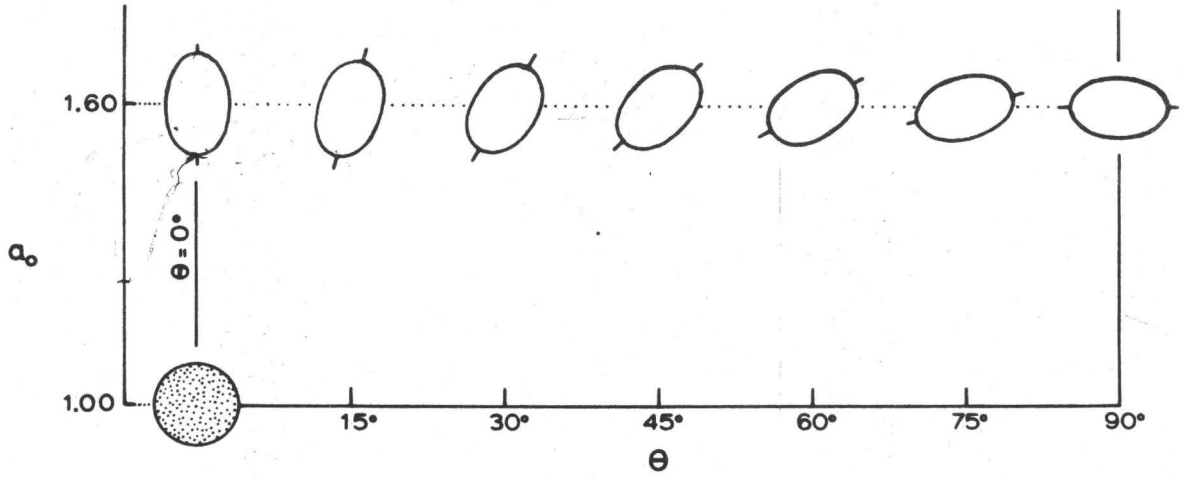
or

$$a_f^2 - \left(a_o a_t + \frac{1}{a_o a_t} \right) a_f + 1 = 0$$

Figure 9. Orientation plot of deformed ellipses during progressive deformation ($a_t = 1.40$).

(A), unstrained original ellipses with various orientations. (B), when $a_t = 1.40$, the reference circle (dotted) becomes an ellipse with axial ratio of 1.40. Solid curve, isostrain curve; broken lines, orientation curves; shaded ellipses, deformed ellipses.

(A)



(B)

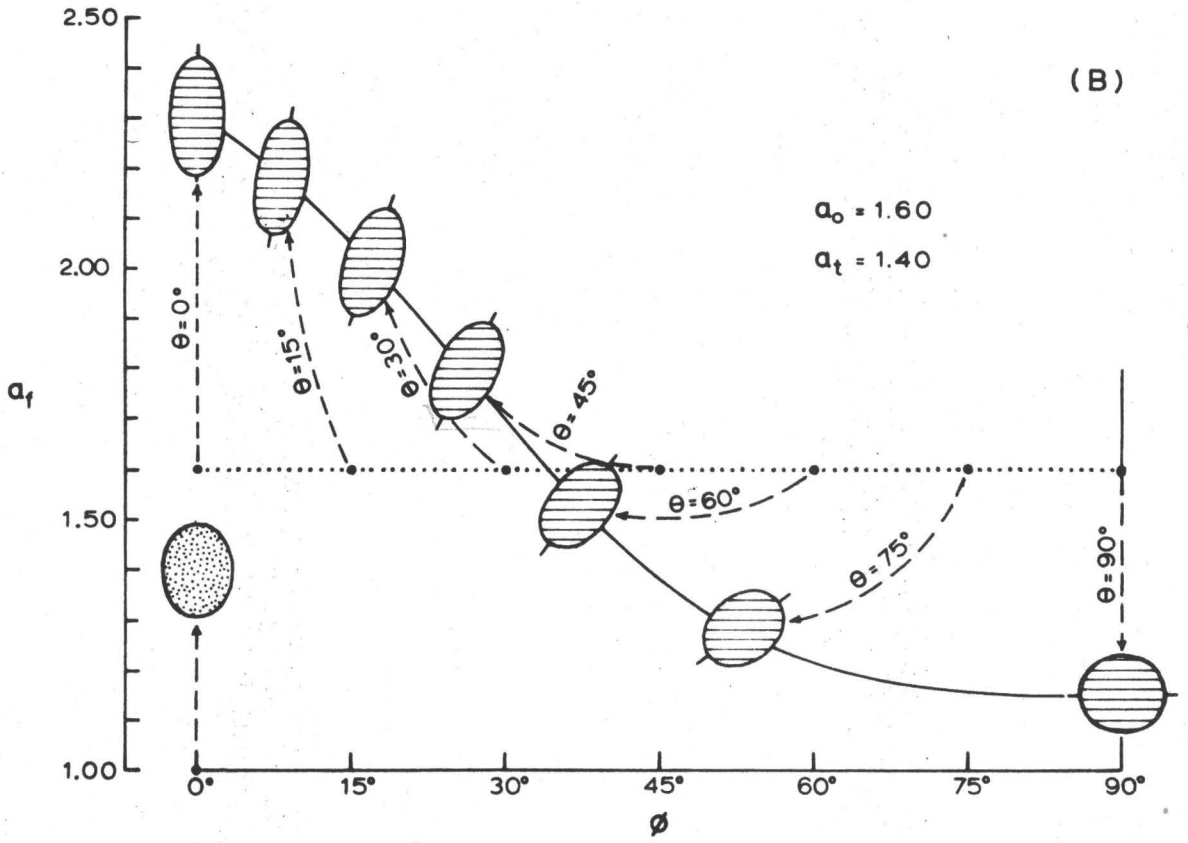


Figure 10. Orientation plot of deformed ellipses during progressive deformation ($a_t = 1.60$). See Figure 9 for explanation.

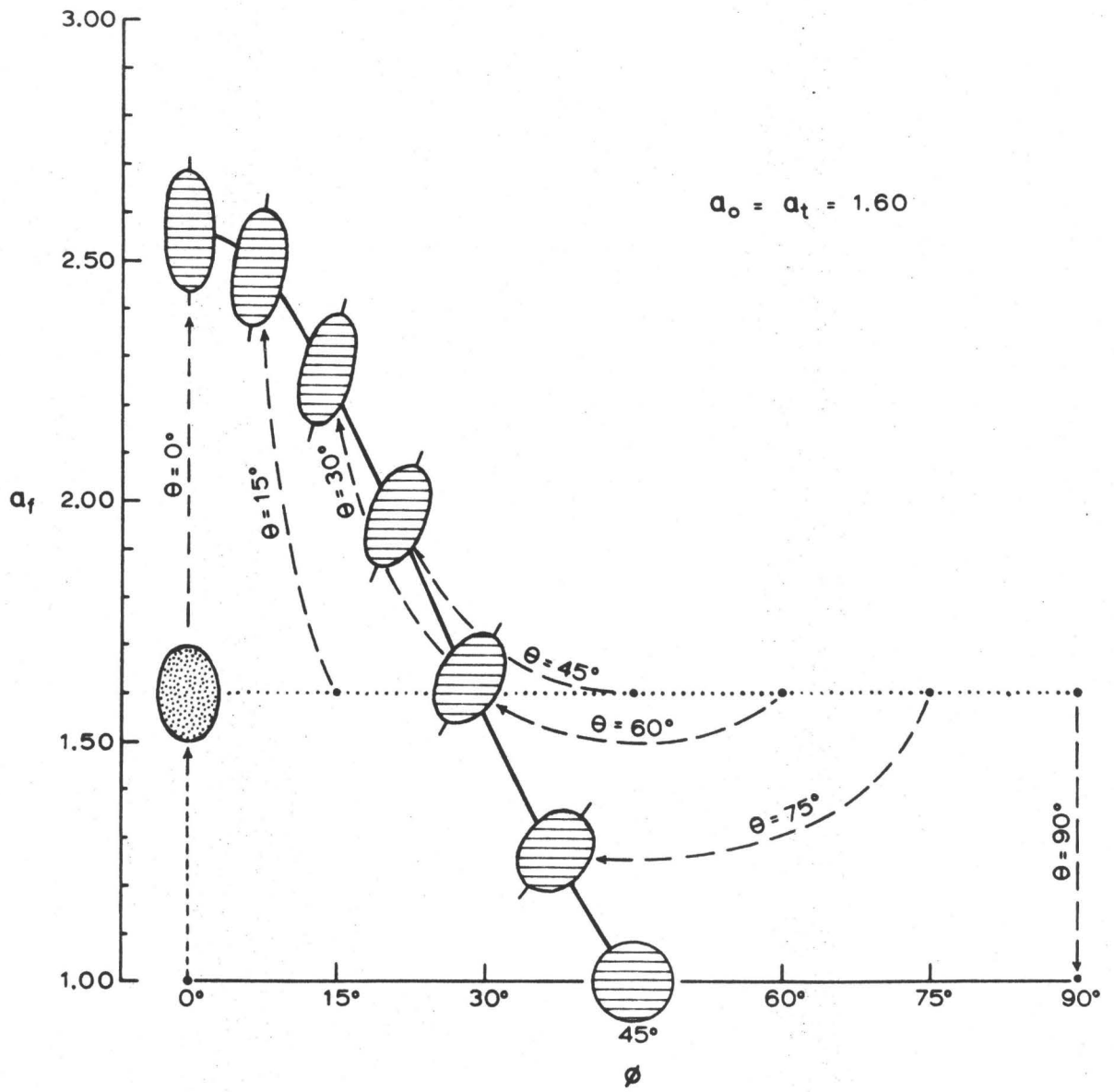
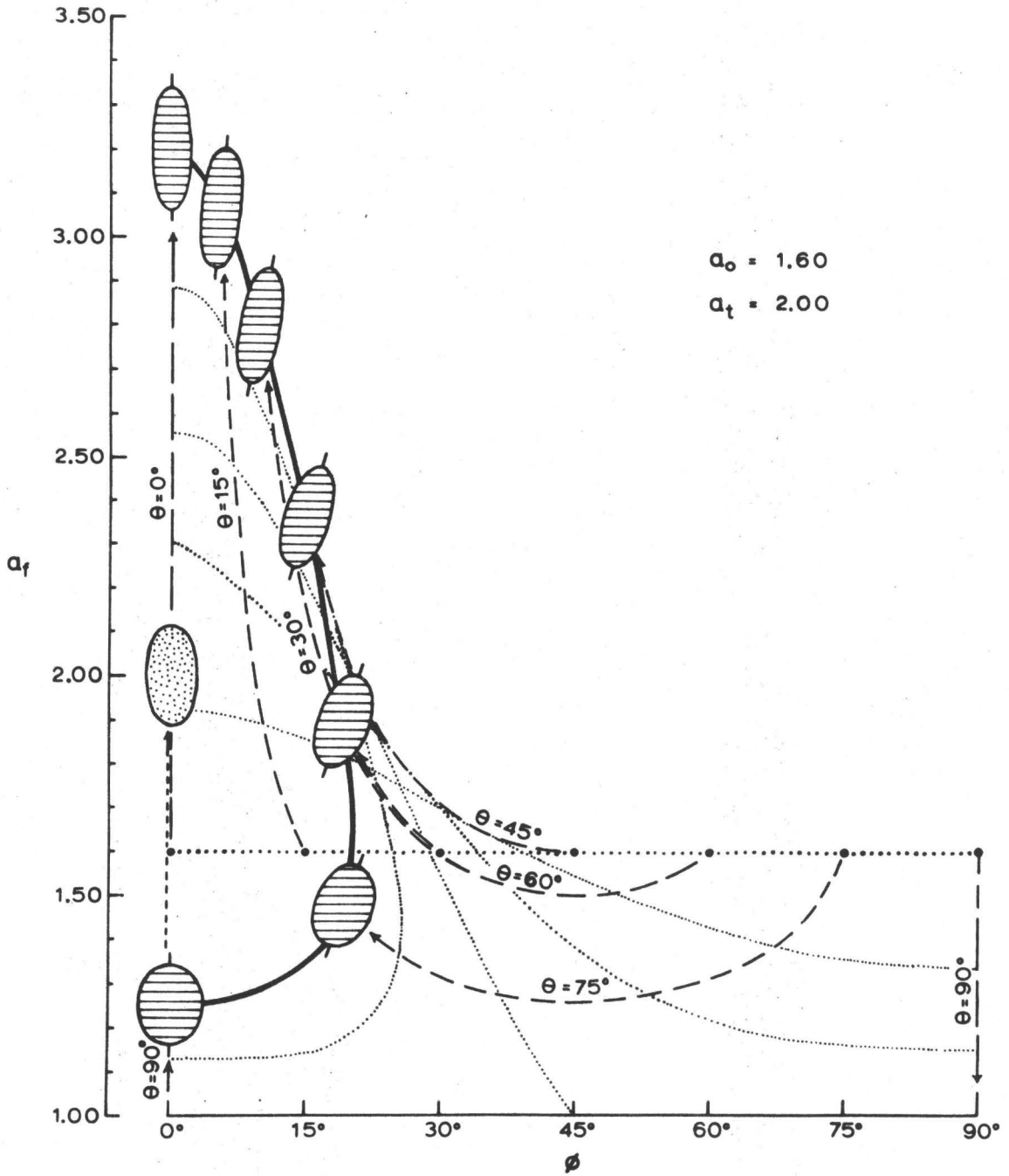


Figure 11. Orientation plot of deformed ellipses during progressive deformation ($a_t = 2.00$). Dotted lines, isostrain curves of a_t equal to 1.2, 1.4, 1.6, and 1.8; heavy line, isostrain curve of $a_t = 2.00$. For the rest, see Figure 9.



hence

$$(a_f - a_o a_t) \left(a_f - \frac{1}{a_o a_t} \right) = 0 \quad (5-18)$$

Because $a_o > 1$, $a_t \geq 1$, and $a_f \geq 1$, it follows that

$$\left(\frac{1}{(a_o a_t)} \right) < 1 \text{ and } a_f - \frac{1}{(a_o a_t)} \neq 0.$$

Therefore, from Equation (5-18), we know

$$a_f - a_o a_t = 0$$

$$\therefore a_f = a_o a_t \quad (5-19)$$

Substituting Equation (5-19) in Equation (5-17) yields

$$\begin{aligned} \cos 2\theta &= \frac{a_o^2 (a_t^2 + 1)(a_o^2 a_t^2 + 1) - 2 a_o a_t^2 (a_o^2 + 1)}{a_o^2 (a_t^2 - 1)(a_o^2 a_t^2 - 1)} \\ &= \frac{a_o^2 a_t^4 + a_o^2 a_t^2 + a_t^2 + 1 - 2 a_o^2 a_t^2 - 2 a_t^2}{a_o^2 a_t^4 - a_o^2 a_t^2 - a_t^2 + 1} \\ &= 1 \end{aligned}$$

$$\text{So } 2\theta = 0^\circ \text{ or } 360^\circ$$

$$\text{or } \theta = 0^\circ \text{ or } 180^\circ$$

In pebble orientation, $\theta = 180^\circ$ is the same as $\theta = 0^\circ$.

(2) The ellipse with $\theta = 90^\circ$ first maintains its orientation normal to the X_t -axis but gradually reduces its eccentricity until it becomes a circular shape when $a_t = a_o$, and then it progressively increases the eccentricity but always parallels the X_t -axis, i. e., $\phi = 0^\circ$.

Mathematical foundation of these relationships is shown below:

Since $\theta = 90^\circ$, $\cos 2\theta = -1$, so Equation (5-16) becomes

$$a_o a_t a_f^2 - (a_o^2 + a_t^2) a_f + a_o a_t = 0$$

Dividing by $a_o a_t$,

$$a_f^2 - (a_o/a_t + a_t/a_o) a_f + 1 = 0$$

so

$$(a_f - a_o/a_t)(a_f - a_t/a_o) = 0$$

If $a_f - a_o/a_t = 0$, then $a_f = a_o/a_t$ when $a_o > a_t$ (5-20)

If $a_f - a_t/a_o = 0$, then $a_f = a_t/a_o$ when $a_t > a_o$ (5-21)

If $a_t = a_o$, then $a_f = a_o/a_t = a_t/a_o = 1$

Substituting $a_o = a_f a_t$ from Equation (5-20) in Equation (5-17) yields

$$\cos 2\phi = -1$$

so $2\phi = 180^\circ$, or $\phi = 90^\circ$ when $a_t < a_o$.

Substituting $a_t = a_f a_o$ from Equation (5-21) in Equation (5-17) yields

$$\cos 2\phi = 1$$

so $2\phi = 0^\circ$ or 360°

or $\phi = 0^\circ$ or 180° , when $a_t > a_o$.

(3) All the ellipses having original orientations between $\theta = 45^\circ$ and $\theta = 90^\circ$ (e.g., the ellipses with θ -angles of 60° and 75° in Figure 11) become less eccentric at early stage of deformation and change their orientations with increasing rate towards the direction of the maximum tectonic elongation (X_t). When the long axes of the deformed ellipses pass through $\phi = 45^\circ$, the ellipses become more and more eccentric but change their orientations at a decreasing rate. The curves showing these paths are here called the orientation curves, which are symmetric about the vertical axis $\phi = 45^\circ$ in Figure 11.

(4) All the ellipses having initial orientations $\theta \leq 45^\circ$ (e.g., the ellipses with θ -angles of 15° and 30° in Figures 9-11) simply become more and more eccentric and change their orientations towards the X_t -axis during strain history. They follow the same orientation curves of those ellipses with original high angles equal to $(90^\circ - \theta)$ but advance further.

(5) Theoretically, all the ellipses having initial orientations $\theta \neq 0$ approach closer and closer to the direction of the principal tectonic elongation as strain increases; they become parallel to the X_t -axis only after having been deformed to an infinitely large strain.

(6) The curves showing equal tectonic strain ratio are here called the isostrain curves. The isostrain curve becomes steeper and steeper as strain increases until $a_t = a_o$ when the maximum \emptyset angle among all the deformed ellipses changes instantly from 90° to 45° . Wherever $a_t > a_o$, the isostrain curve has a pear-like closed form which increases its elongation as strain intensifies.

(7) The isostrain curves can be used to determine the fluctuation (Cloos, 1947, pp. 861-862) of deformed ellipsoids. The range of fluctuation in the orientation of deformed ellipses on a section parallel to the identical principal plane, can be determined readily from the maximum $2\emptyset$ of the isostrain curve. When $a_t > a_o$, the fluctuation range is always less than 90° , because $\max. \emptyset < 45^\circ$. If $a_t < a_o$, $\max. \emptyset = 90^\circ$, the fluctuation range is theoretically 180° , though the individual ellipses have considerably changed their orientations towards the X_t -axis. Thus, a simple rule can be set up here that wherever the fluctuation range (maximum $2\emptyset$) is greater than 90° , i. e., $\max. \emptyset > 45^\circ$, a_t must be smaller than a_o .

(8) Both orientation curve and isostrain curve in an orientation plot are symmetrical with respect to the X_t -axis, because $\cos 2\theta = \cos (-2\theta)$ and $\cos 2\phi = \cos (-2\phi)$.

4. CONCEPT OF MEAN ORIENTATION OF ELLISOIDAL PEBBLES

Figure 12 shows some orientation plots of the deformed pebbles in the map area in order to demonstrate the general fabric in three dimensional space. Figure 12(A) is an orientation plot made from the data measured on a section parallel to the common Z_f -direction (see Plate 6(A)) of the flattened pebbles but oblique to the mineral lineation. One sees in this diagram that the majority of the quartzose pebbles lie between the bedding trace and the foliation trace; whereas most of the granitic pebbles lie around the bedding trace with a wide range of fluctuation greater than 120° . In Figure 12(B) which is obtained from the data measured on a section normal to the mineral lineation --- a section equivalent to some authors' "YZ plane" -----, where the bedding is parallel to the foliation plane, both the volcanic and granitic pebbles have preferred orientation parallel to the bedding-foliation trace. Figure 12(C) shows an orientation plot of the deformed pebbles measured on a foliation plane which subparallels the local bedding at locality 144. In this diagram, the deformed volcanic pebbles have an

Figure 12. General feature of the final pebble-fabrics in the map area.

Dots, granitic pebbles; crosses, quartzose pebbles; triangles, volcanic pebbles. (A), a fabric of deformed pebbles on a section parallel to the common Z_f -direction. (B), a pebble-fabric on a section normal to the mineral lineation. (C), an orientation plot on a foliation/bedding plane.

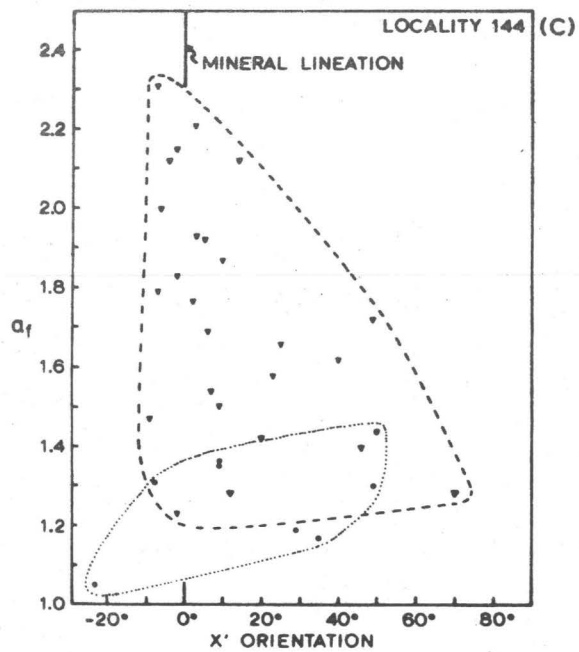
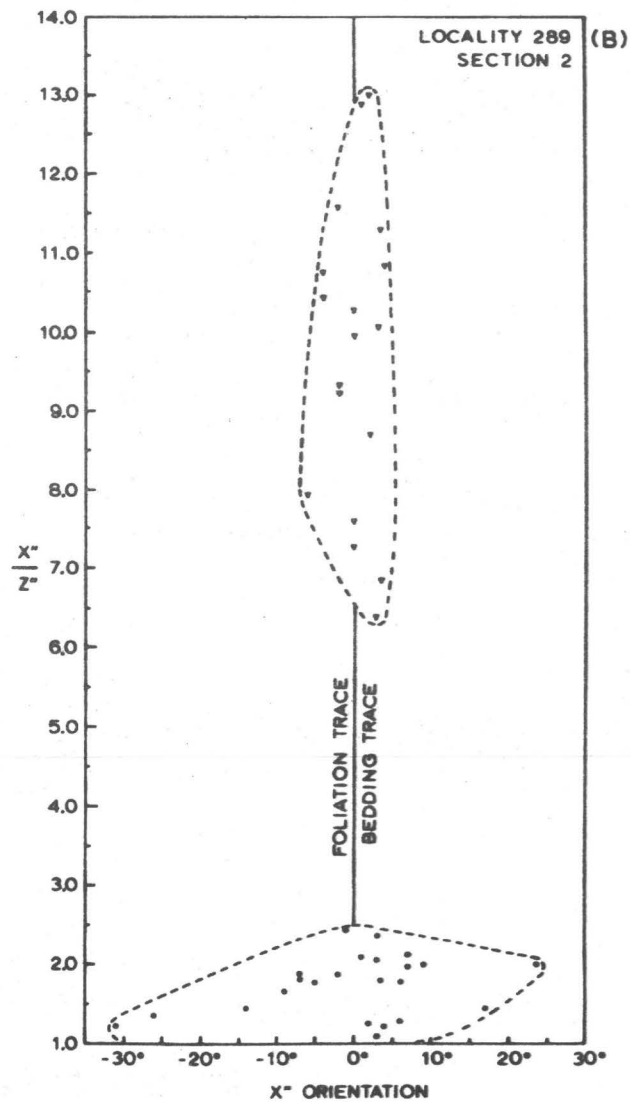
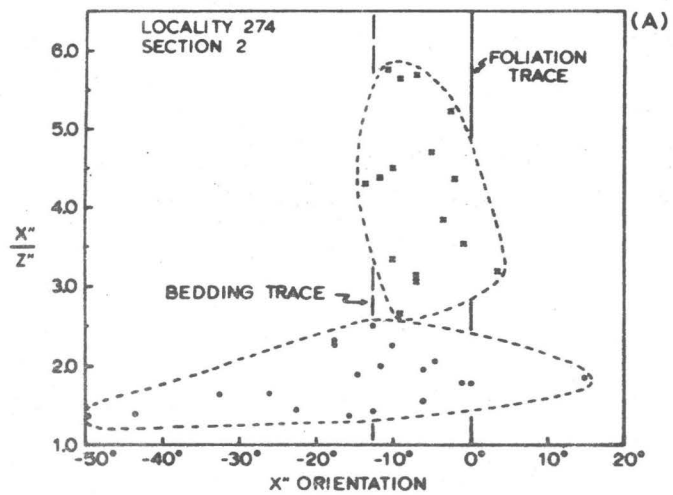


Plate 6

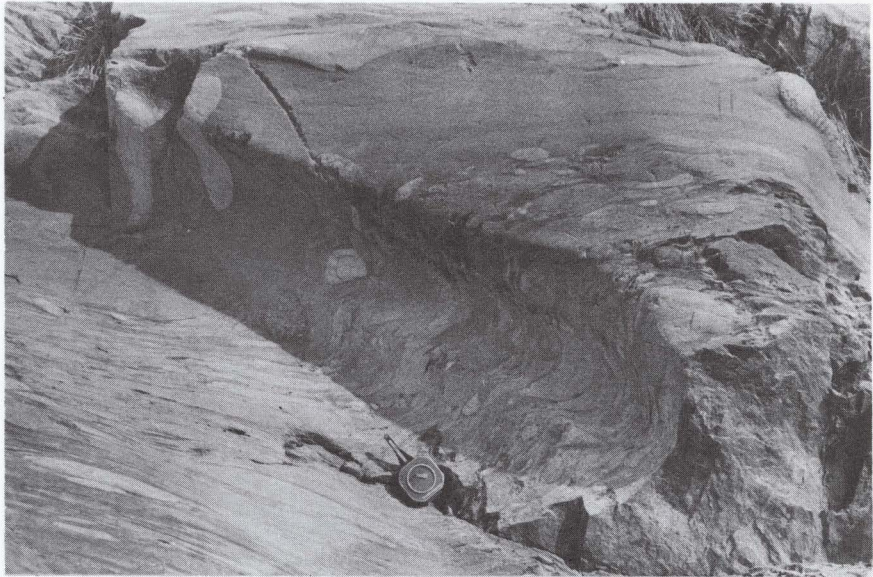
(A) Dextral kink band developed in rocks containing already deformed pebbles. Note that the minor axes of the exposed ellipses of most deformed pebbles are parallel to one another and are normal to the foliation trace.

(B) Three-dimensional view of the deformed pebbles.

The more deformed ones commonly parallel the foliation trace on any section. Pebbles are difficult to recognize on the foliation plane.



(A)



(B)

asymmetric distribution in the orientation plot, indicating that, before deformation, the pebbles must have had some preferred orientation pattern. On the other hand, the granitic pebbles do not show any appreciable preferred orientation, probably due to only eight counts.

Together with the evidence that pebbles are not so flattened in shape at the fold hinge as in fold limbs, the general final pebble-fabric represented by those shown in Figure 12 suggests that the majority of the original pebbles, regardless of the lithology, might have lain flat on the bedding plane although the range of fluctuation around the bedding might have been very large. The orientation plot on a foliation-bedding plane even indicates an original preferred orientation within the bedding plane (Figure 12(C)). Unfortunately, only one outcrop could be measured to give this kind of information in the map area.

In view of the asymmetric distribution of ellipse plots in the orientation plot of Figure 12(C), we come to the question: what is the mean orientation of these ellipses?

Imitating the pebble fabrics observed in the map area, suppose we have ten ellipsoids lying flat with their maximum cross-sections (the $X_f Y_f$ planes) parallel to one another on the foliation plane. Suppose these ellipsoids have equal intermediate axes (Y_f) of one unit length and equal shortest axes (Z_f) of 0.125 unit length, but their X_f -axes vary

from 2.00 to 1.10 unit length with an interval of 0.10 unit length and their orientations from $\emptyset = 0^\circ$ to $\emptyset = 90^\circ$ with 10° intervals as shown on the common $X_f Y_f$ plane in Figure 13. Hence, the axial ratios $b_f = Y_f/Z_f$ are all 8.00, but $a_f = X_f/Y_f$ range from 2.00 to 1.10 with an average of 1.55.

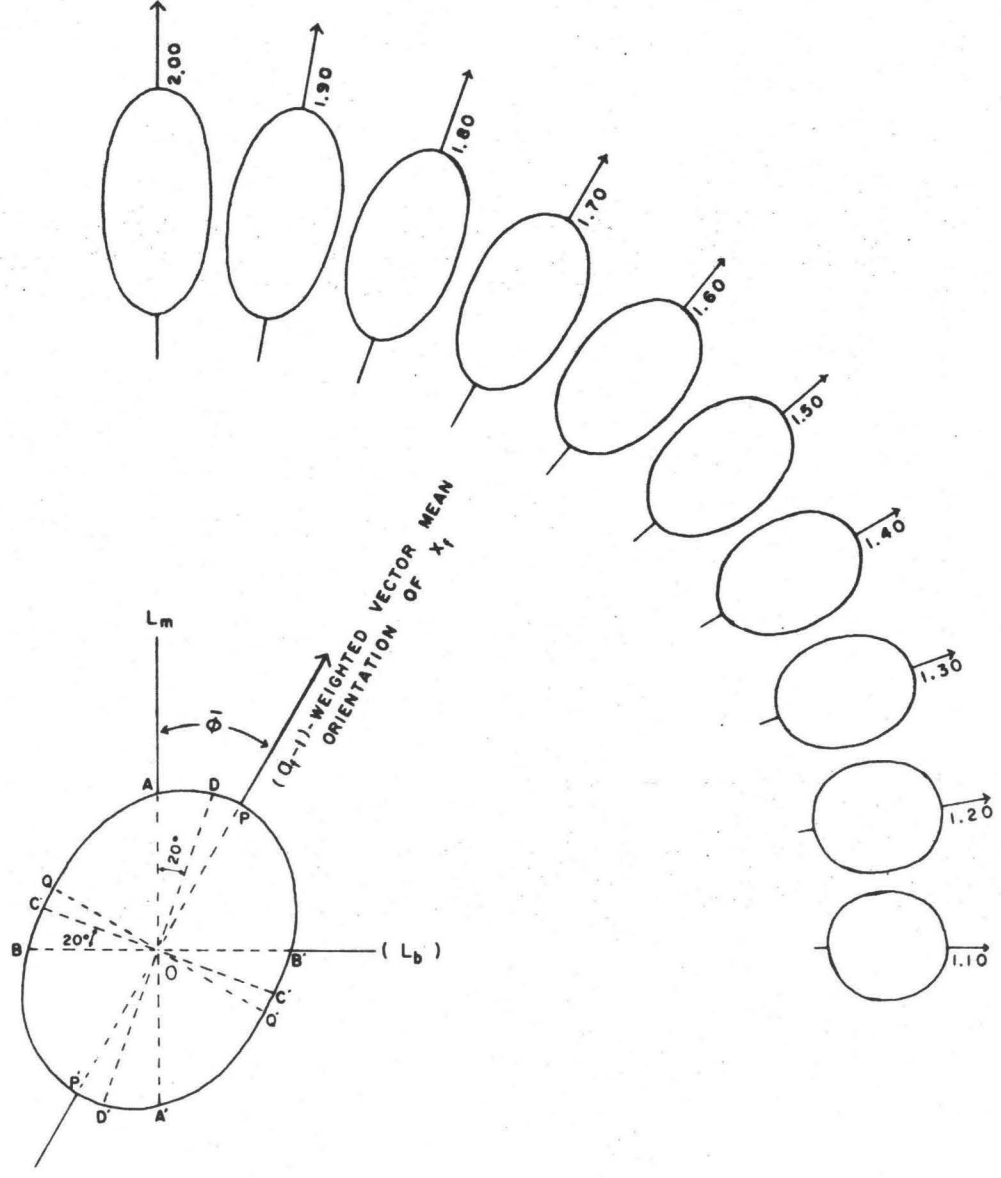
Now, if we cut each of these ellipsoids in an infinite number of orientations but always containing the Z_f -axis, we will have an infinite number of elliptical cross-sections of each ellipsoid, all have the same short axes but different long axes. In one orientation, let us measure all the long axes of the ten ellipses and average them. Each average of the long axes in one orientation is then drawn through a common center, point 0, with its two ends plotted as two points (see the lower left-hand-side diagram of Figure 13). The infinite points thus obtained form a nearly perfect ellipse on the $X_f Y_f$ plane, whose major axis has a \emptyset -angle of 30.5° .

Conventional statistical treatment of orientation data would lead one to use the vector mean orientation of the X_f -axes, which is $\emptyset = 45^\circ$ in this case. The large difference clearly is caused by the fact that in conventional treatment a nearly circular ellipse has an importance in expressing orientation equal to that of a strongly eccentric one on a common plane. In order to reduce this difference, the present writer employs a more realistic mean for analysis of the orientation

Figure 13. Determination of the mean X_f -orientation of deformed pebbles.

All the Z_f -axes are perpendicular to the plane of the diagram.

L_m , mineral lineation; L_b , boudinage axis. See the text for explanation.



data using (R - 1)-weighted vector expression, where R is the axial ratio of an individual ellipse involved. The weighting factor (R - 1) means that a sphere, with R = 1 in any orientation, does not have any value in expressing orientation, while a more eccentric ellipsoid has a higher value than a less eccentric one has.

The (R - 1)-weighted vector mean orientation of the above ten ellipsoids is $\bar{\phi} = 29.5^\circ$, which is very close to $\phi = 30.5^\circ$ obtained from infinite cuttings. Therefore, it is felt that the weight (R - 1) is well suited to the orientation analysis of this study.

On a cross-section through a rock which contains a number of ellipsoids, an ellipse which has its axial ratio equal to the arithmetic mean (see p. 81) of those of the individual exposed ellipses and which has its major axis parallel to the (R - 1)-weighted vector mean orientation of the individual major axes, is called the representative ellipse on that section.

5. SIMULTANEOUS DETERMINATION OF THE TECTONIC STRAIN RATIO AND THE ORIGINAL ORIENTATION AND SHAPE OF DEFORMED PEBBLES

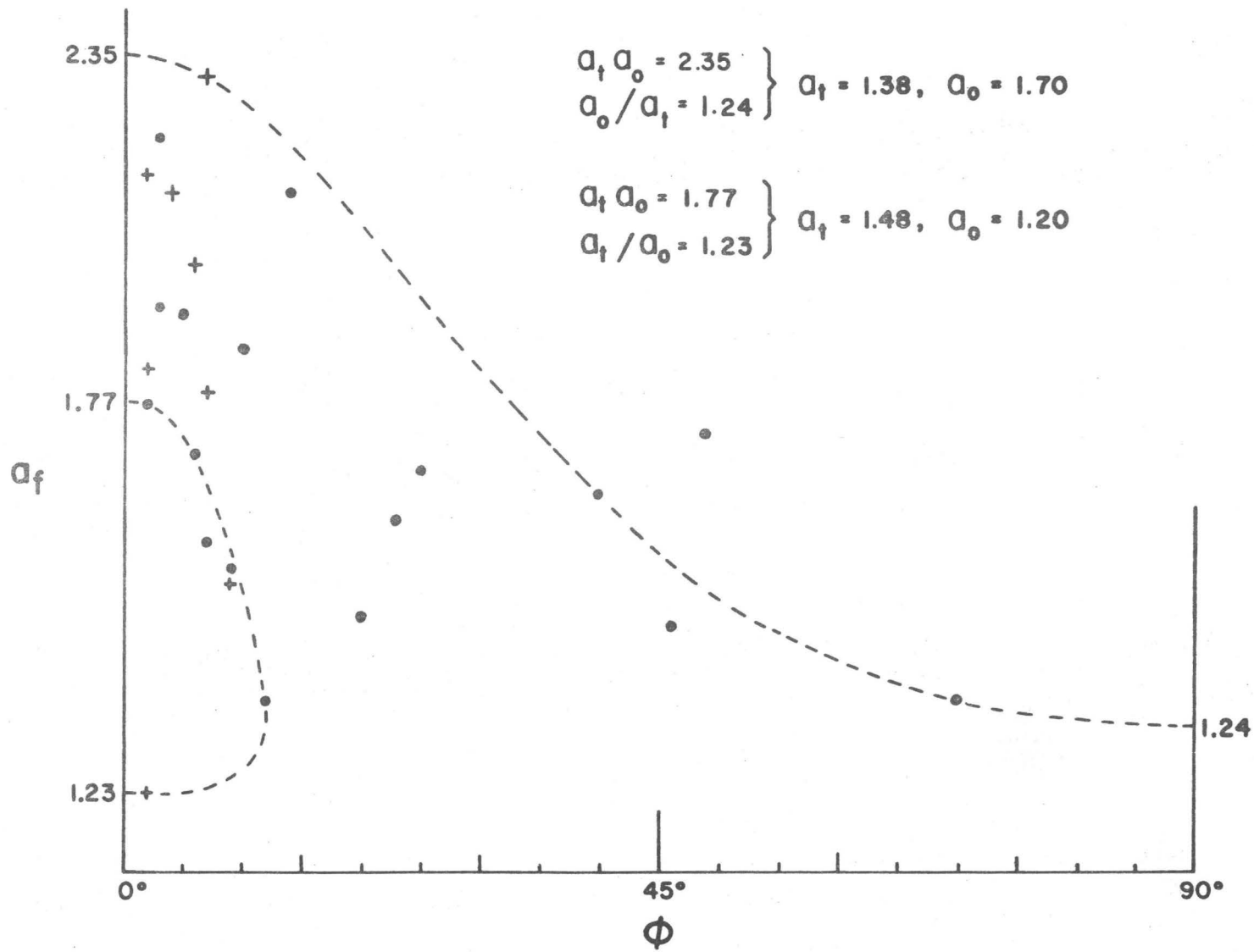
The final fabric of volcanic pebbles shown in Figure 12(C) is obtained from a plane parallel to all the individual $X_f Y_f$ planes and

the local foliation—bedding plane. In other words, $X_f Y_f \parallel X_t Y_t$
 \parallel bedding. Therefore, it is very likely that all the Z_o axes had
 been perpendicular to the bedding before the homogeneous deformation
 commenced. If we assume that the tectonic strain ratio (not magnitude)
 is all the same for pebbles of identical lithology at one single outcrop,
 then the spread of the ellipse plots in the orientation plot of Figure
 12(C) could result from different original shapes and orientations.

It has been remarked (p. 70) that the isostrain curve in an
 orientation plot is symmetrical with respect to the direction of the X_t -
 axis ($\theta = 0^\circ$). Therefore, when we construct an isostrain curve in an
 orientation plot, it is helpful to reflect those ellipse plots with negative
 θ -angles to the side of positive θ -angles. This improves the definition
 of the field of points. Figure 14 is redrawn from Figure 12(C) but with
 reflected ellipse-plots shown as crosses.

Connecting the outer-most dots and/or crosses on the upper
 right-hand side of the orientation plot in Figure 14 would form the
 possible highest- a_o isostrain curve, while connecting the innermost dots
 and/or crosses on the left-hand side would form the possible lowest- a_o
 isostrain curve. It is important to keep in mind that the constructed iso-
 strain curves must maintain the general trend of the scattered ellipse-
 plots. Occasionally, a remote ellipse-plot may appear in an orienta-
 tion plot, but by judging the general trend, we can probably ignore it

Figure 14. Construction of the bounding isostrain curves from the final pebble-fabric of Figure 12(C).



for the moment when we construct the curve, though this is quite subjective.

In our example, the outer curve intersects the axes $\emptyset = 0^\circ$ and $\emptyset = 90^\circ$ at points $a_f = 2.35$ and $a_f = 1.24$, respectively (Figure 14). Solving the following simultaneous equations (see Equations (5-19) and (5-20)):

$$\begin{cases} a_o a_t = 2.35 \\ a_o / a_t = 1.24 \end{cases}$$

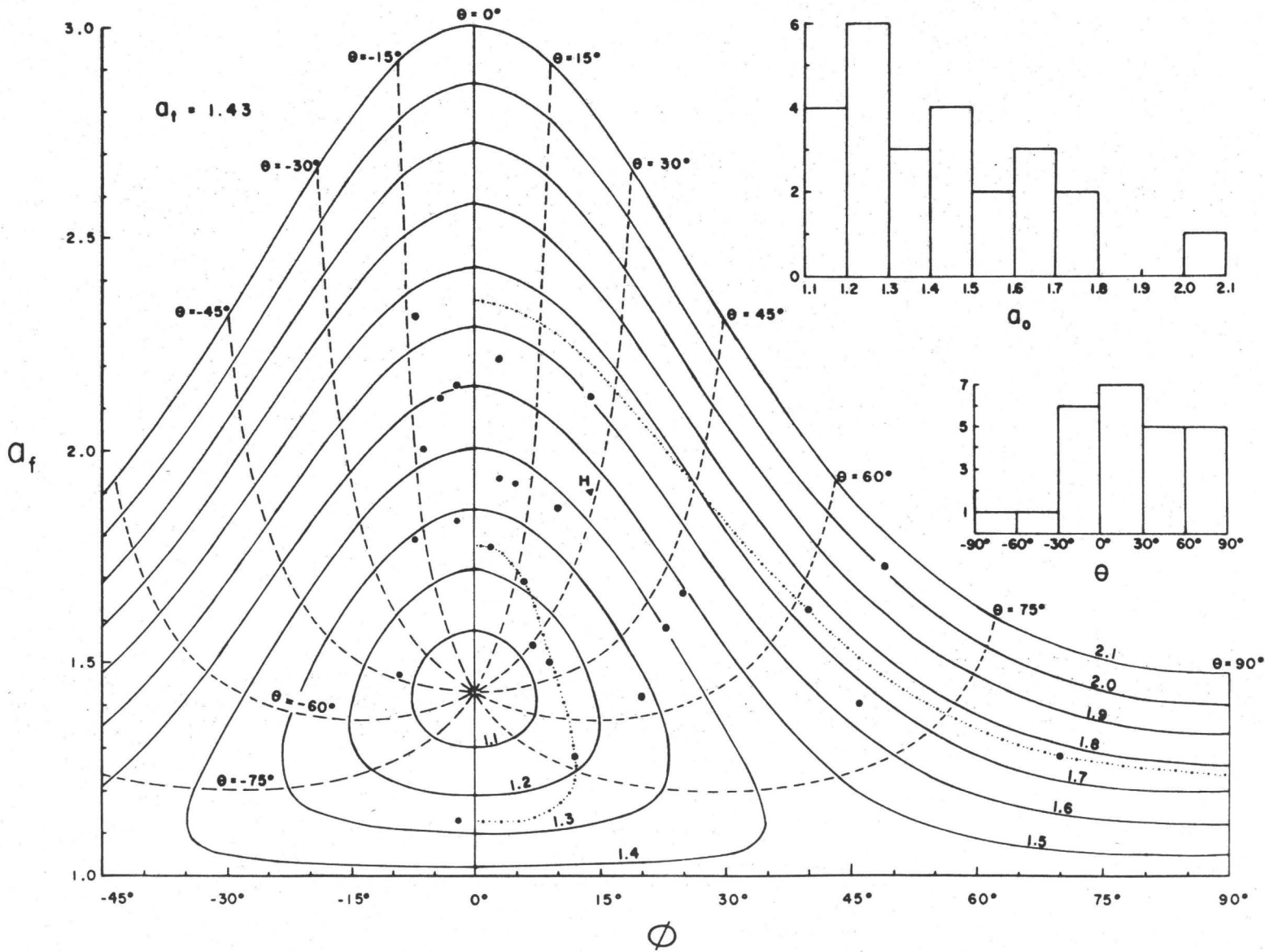
we obtain $a_t = 1.38$ and $a_o = 1.70$. On the other hand, the inner curve intersects the axis $\emptyset = 0^\circ$ at two points $a_{f(\emptyset = 0^\circ)} = 1.77$ and $a_{f(\emptyset = 90^\circ)} = 1.23$. Similarly, solving the simultaneous equations (see Equations (5-19) and (5-21)):

$$\begin{cases} a_o a_t = 1.77 \\ a_t / a_o = 1.23 \end{cases}$$

we get $a_t = 1.48$ and $a_o = 1.20$.

Although we have already assumed that a_t is all the same in this case, the calculated ones still have a range of $1.48 - 1.38 = 0.10$. Let us take their average $a_t = 1.43$ and compute Equations (5-16) and (5-17) by feeding the a_o -ratios from 1.10 to 2.10 with 0.10 intervals and the possible corresponding a_f -ratios. The resultant data are shown in Figure 15 which is based on the same orientation plot of Figure 12(C).

Figure 15. Expanded diagram showing the complex relationship among a_o , a_f , θ , and ϕ , from the final pebble-fabric of locality 144. The frequencies of the original axial ratios and orientations are shown in inset diagrams. Solid curves, isostrain curves (all are $a_t = 1.43$) with various a_o shown as numbers.



The upper inset diagram of Figure 15 shows the frequency of the original axial ratios collected from the main diagram; whereas the lower inset presents the frequency of the original X_o -orientations with reference to the mineral lineation ($\theta = 0^\circ$). The $(a_f - 1)$ -weighted vector mean X_f - orientation is $\bar{\phi} = 14^\circ$; while the $(a_o - 1)$ -weighted vector mean X_o - orientation calculated from the lower inset diagram is $\bar{\theta} = 29^\circ$.

It is obvious from Figures 11 and 15 that the axial ratios a_f and a_o , respectively, have by no means any simple normal or logarithmic distribution. These can also be seen from the complex relationship among a_f , a_t , a_o , ϕ , and θ in Equations (5-16) and (5-17). Further investigation on the statistical means of a_o and a_f is urgently needed. At this stage, we can use temporarily the arithmetic mean for lack of a better method. The average axial ratios in Figure 15 are $a_f = 1.74$ and $a_o = 1.42$. On the other hand, if we locate a point with $\phi = 14^\circ$ and $\theta = 29^\circ$ (point H) in Figure 15, we get $a_f = 1.90$ and $a_o = 1.45$. Surprisingly enough, the two a_o -ratios happen to be nearly equal.

CHAPTER VI

DETERMINATION OF THE STRAIN ELLIPSOID AND THE ORIGINAL SHAPE OF DEFORMED PEBBLES

If the original pebbles are spherical in shape, i. e. , $a_o = b_o = 1$, then the axial ratios of the pebbles after homogeneous deformation will be the same as those of the tectonic strain ellipsoid, i. e. , $a_f = a_t$ and $b_f = b_t$. If the principal planes of the final pebbles cannot be observed in the field or the sawed sections containing deformed ooids (or the like) are not the principal planes, we can use Equations (4-13) to compute the axial ratios a_f and b_f by measuring the orientations and the apparent axial ratios of the exposed ellipses on two cross-sections. The angles between the principal axes of the exposed ellipses and those of the tectonic strain ellipsoid can be obtained by means of stereographic projection.

If the original pebbles are not spherical in shape, i. e. , $a_o \neq 1$ and/or $b_o \neq 1$, as are most cases in nature, then the final deformed pebbles can have an infinite number of different shapes with

all possible fabrics depending upon the original fabric of the pebbles before deformation and the shape and orientation of the tectonic strain ellipsoid. The discussions which follow will describe the most practical ways of determining the strain ellipsoid and the originally ellipsoidal shape of deformed pebbles.

1. EXTRACTABLE INDIVIDUAL PEBBLES

The best way to study deformed pebbles is to extract them entirely from their matrix. Wherever extraction of deformed pebbles is possible, the strain ratios and the original pebble shape can be determined if the following conditions are met.

Original Pebbles with Random Fabric

If the originally ellipsoidal pebbles, having an identical shape with axial ratios of $a_o = X_o/Y_o$ and $b_o = Y_o/Z_o$, and being randomly oriented, are deformed homogeneously by a tectonic strain with axial ratios of $a_t = X_t/Y_t$ and $b_t = Y_t/Z_t$, we will obtain the final deformed pebbles with a large number of different axial ratios $a_f = X_f/Y_f$ and $b_f = Y_f/Z_f$, depending upon how the tectonic strain ellipsoid is superimposed on the original pebbles.

Suppose we reach a region where an almost infinite number of final deformed pebbles show that the orientation fluctuation of pebble

ellipses on any section parallel to a principal plane of the tectonic strain ellipsoid, is always less than 90° (this restriction means that any axial ratio of the strain ellipsoid, be it a_t or b_t , is always greater than any axial ratio of the original pebble, including $a_o b_o = X_o / Z_o$).

If the axial ratios a_f and b_f of these final pebbles are plotted in a deformation plot, there will be six limiting ellipsoids bounding a hexagon-like deformation field* (notice the curved lines in Figure 16(A)), within which all the possible shapes of the final pebbles fall. These six ellipsoids result from special coaxial superpositions of the tectonic strain ellipsoid upon the original pebbles, and are shown (clockwise in Figure 16) as follows:

$$(1) b_f = b_t b_o \text{ and } a_f = a_t a_o \quad (6-1)$$

$$\text{when } X_t X_o > Y_t Y_o > Z_t Z_o$$

$$(2) b_f = b_t a_o b_o \text{ (maximum } b_f) \text{ and } a_f = a_t / a_o \quad (6-2)$$

$$\text{when } X_t Y_o > Y_t X_o > Z_t Z_o$$

$$(3) b_f = b_t a_o \text{ and } a_f = a_t / a_o b_o \text{ (minimum } a_f) \quad (6-3)$$

$$\text{when } X_t Z_o > Y_t X_o > Z_t Y_o$$

* This deformation field becomes a double-isosceles-trapezoid with a common base when $\ln a_f$ and $\ln b_f$ are plotted in a logarithmic deformation plot (Figure 16(C)).

Figure 16. Deformation field of extractable deformed pebbles in the case of originally random orientation. (A), hexagon-like deformation field of the final pebbles resulting from deformation of original randomly-oriented pebbles. See the text for the restriction of this graph and the six bounding ellipsoids. (B), only three corners, Nos. 1, 2, and 3, of the hexagonal deformation field are shown up, indicating $b_t < a_o$ and $b_t < b_o$. (C), the deformation field of (A) becomes a double-isoseles-trapezoid with a common base (line 1-4) in a logarithmic deformation plot. The shape of the double-isoseles-trapezoid is dependent on the values of a_o and b_o .

$$(4) b_f = b_t/a_o \text{ and } a_f = a_t/b_o \quad (6-4)$$

$$\text{when } X_t Z_o > Y_t Y_o > Z_t X_o$$

$$(5) b_f = b_t/a_o b_o \text{ (minimum } b_f) \text{ and } a_f = a_t b_o \quad (6-5)$$

$$\text{when } X_t Y_o > Y_t Z_o > Z_t X_o$$

$$(6) b_f = b_t/b_o \text{ and } a_f = a_t a_o b_o \text{ (maximum } a_f) \quad (6-6)$$

$$\text{when } X_t X_o > Y_t Z_o > Z_t Y_o$$

Clearly, if we simply draw two vertical and two horizontal lines to touch such a hexagonal deformation field in the deformation plot, we can obtain the maxima and the minima of the axial ratios a_f and b_f (these can be also obtained directly from the measured data, though). The coordinates of the maxima and the minima, in turn, yield totally eight separate equations in terms of the four unknown variables a_o , b_o , a_t , and b_t . Any three of the maxima and the minima are sufficient to solve the problems.

If the orientation fluctuation on sections parallel to one or more principal planes of the strain ellipsoid exceeds 90° , then the hexagonal deformation field will be shifted towards and "swallowed" by the axes $a_f = 1$ or/and $b_f = 1$. For instance, if an infinite number of extracted, final, deformed pebbles which are known to have had an

originally random fabric, show only three corners, Nos. 1, 2, and 3, of the hexagonal deformation field (Figure 16(B)), then one can be sure that Equations (6-4) - (6-6) do not hold true. In other words, there must be $b_t < b_o$ and $b_t < a_o$, and the orientation fluctuation on sections parallel to the $Y_t Z_t$ plane must exceed 90° .

In some cases, only two angles of the hexagonal deformation field appear and their coordinates do not permit a solution of the unknown variables. We must find a third coaxially deformed pebble other than the two at the two angles, and measure its orientation as well as its axial ratios. Then we shall be able to solve the problem using additional two equations derived from the third coaxially deformed pebble.

Original Pebbles with a Planar Fabric

Commonly, pebbles in a conglomerate bed have an original planar fabric with their shortest axes (Z_o) subperpendicular to the bedding plane (pp. 50-51). In strongly deformed rocks, we frequently observe that foliation is parallel to or lies close to bedding (Ramsay, 1967, p. 218). In such a case, Z_t is parallel to Z_o and the special coaxial superpositions are given by

(1) $X_t X_o \rangle Y_t Y_o \rangle Z_t Z_o$ which result in a final, coaxially deformed pebble with axial ratios

$$b_f = b_t b_o \text{ and } a_f = a_t a_o \quad (6-7)$$

(2) $(X_t Y_o : Y_t X_o) > Z_t Z_o$ which has two possibilities:

a) If $X_t Y_o < Y_t X_o$, $a_t < a_o$, then

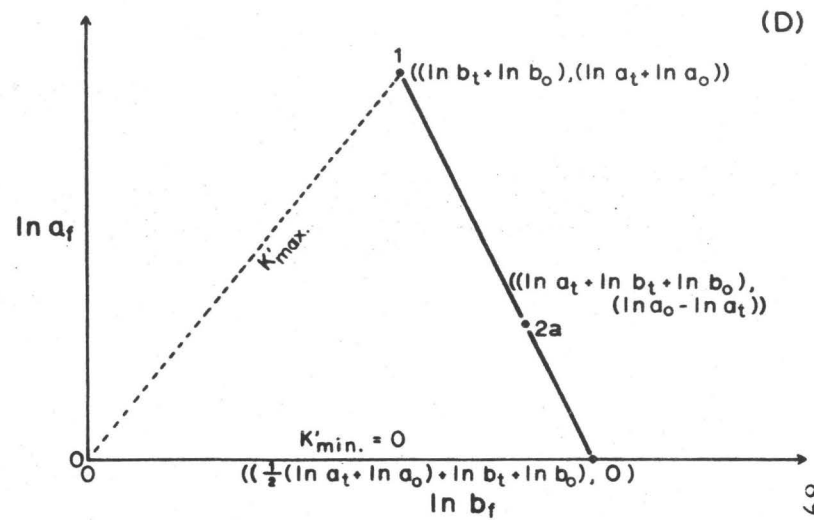
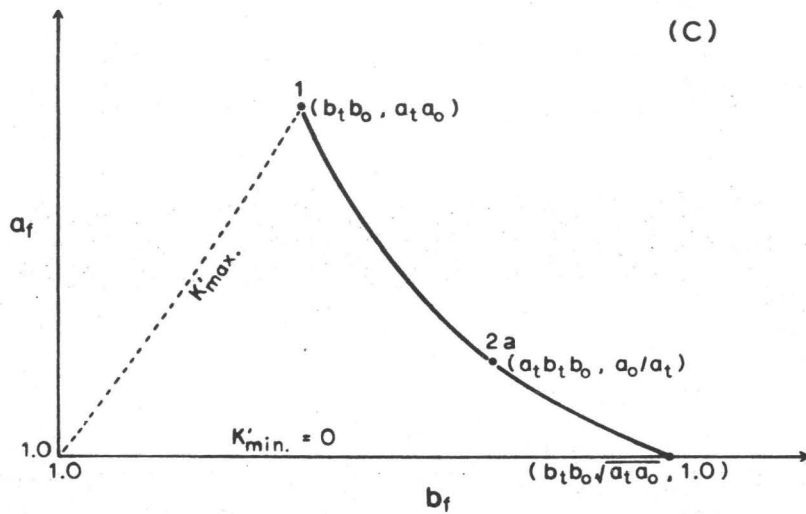
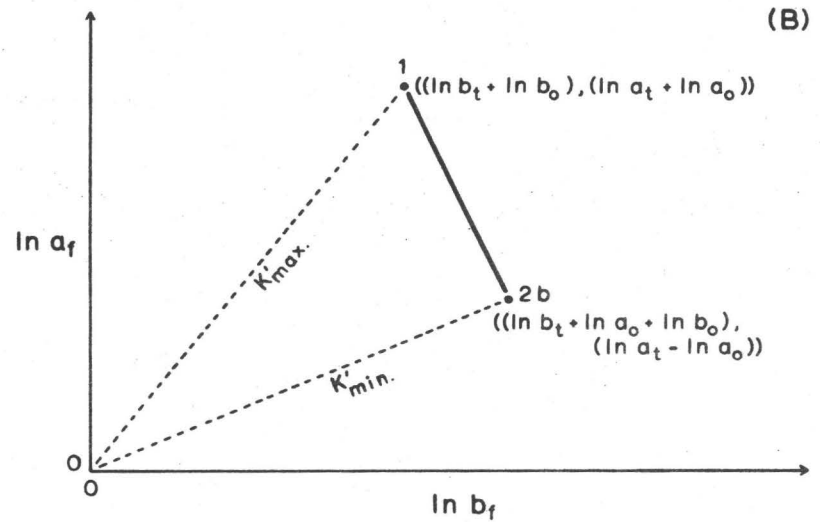
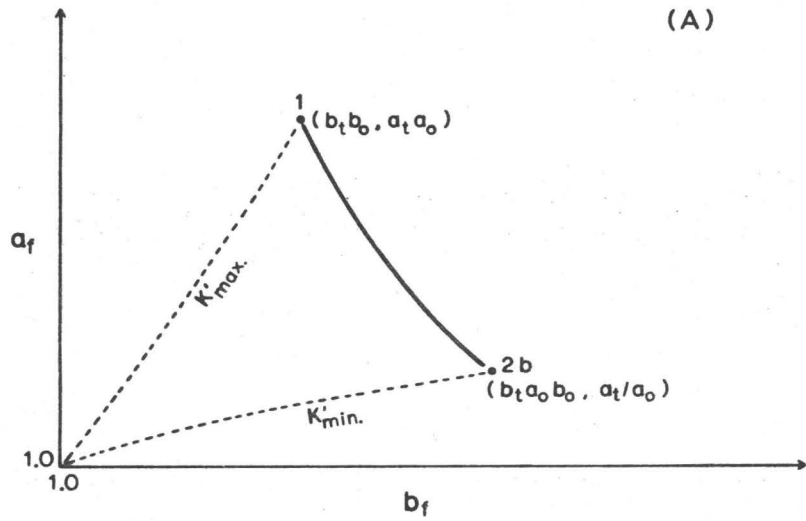
$$b_f = a_t b_o b_o \text{ and } a_f = a_o / a_t \quad (6-8a)$$

b) If $X_t Y_o > Y_t X_o$, $a_t > a_o$, then

$$b_f = b_t a_o b_o \text{ and } a_f = a_t / a_o \quad (6-8b)$$

If the line connecting the origin and the shape plot of a final deformed pebble in a logarithmic deformation plot is called the apparent deformation path (cf. Figure 4), then its slope, K' , can be expressed as $K' = (\ln a_f) / (\ln b_f)$. Assuming the original pebbles were of the same shape, the coaxially deformed pebble of the above Case 1 (Equations (6-7)) has a maximum K' value among all the possible final deformed pebbles; whereas that of Case 2b (Equations (6-8b)) has a minimum K' value. In the case of $a_t < a_o$, the minimum K' value is zero. All the other possible final pebbles will fall in the linear field between the above two K' extremities (Figure 17), which is parallel to the Z_f/d contour discussed in Chapter III, because the unit length reductions in the shortest axes of the deformed pebbles, $2 \xi_z$, are all equal to one another for the same lithology. Note that in the logarithmic deformation plots of Figure 17, both the apparent deformation paths and the deformation fields are straight lines.

Figure 17. Deformation field of extractable deformed pebbles in the case of coaxial superposition of $Z_f || Z_t || Z_o$. Heavy lines, deformation field. (A) and (B), $a_t > a_o$. (C) and (D), $a_t < a_o$.



If the pebbles have different ductilities, then the deformation field will become a broad band instead of a single line. In the case of $a_t > a_o$, the most ductile pebbles should fall in the line between points 1 and 2 of Figure 18; the coaxially deformed pebble of point 1 has a maximum K' value among the most ductile pebbles and an overall maximum a_f ratio, while that of point 2 has a minimum K' value among the most ductile pebbles and an overall maximum b_f ratio. Similarly, points 1' and 2' bound the deformation field of the least ductile pebbles (Figure 18); the former has an overall minimum b_f ratio, while the latter has an overall minimum K' value and an overall minimum a_f ratio.

In the case of the coaxial deformation of $X_t \parallel X_o$, we have a deformation field parallel to the X_f/d contours (Figure 19; cf. Figure 5). The two special coaxial superpositions are:

$$(1) \quad X_t X_o \rangle Y_t Y_o \rangle Z_t Z_o \text{ where}$$

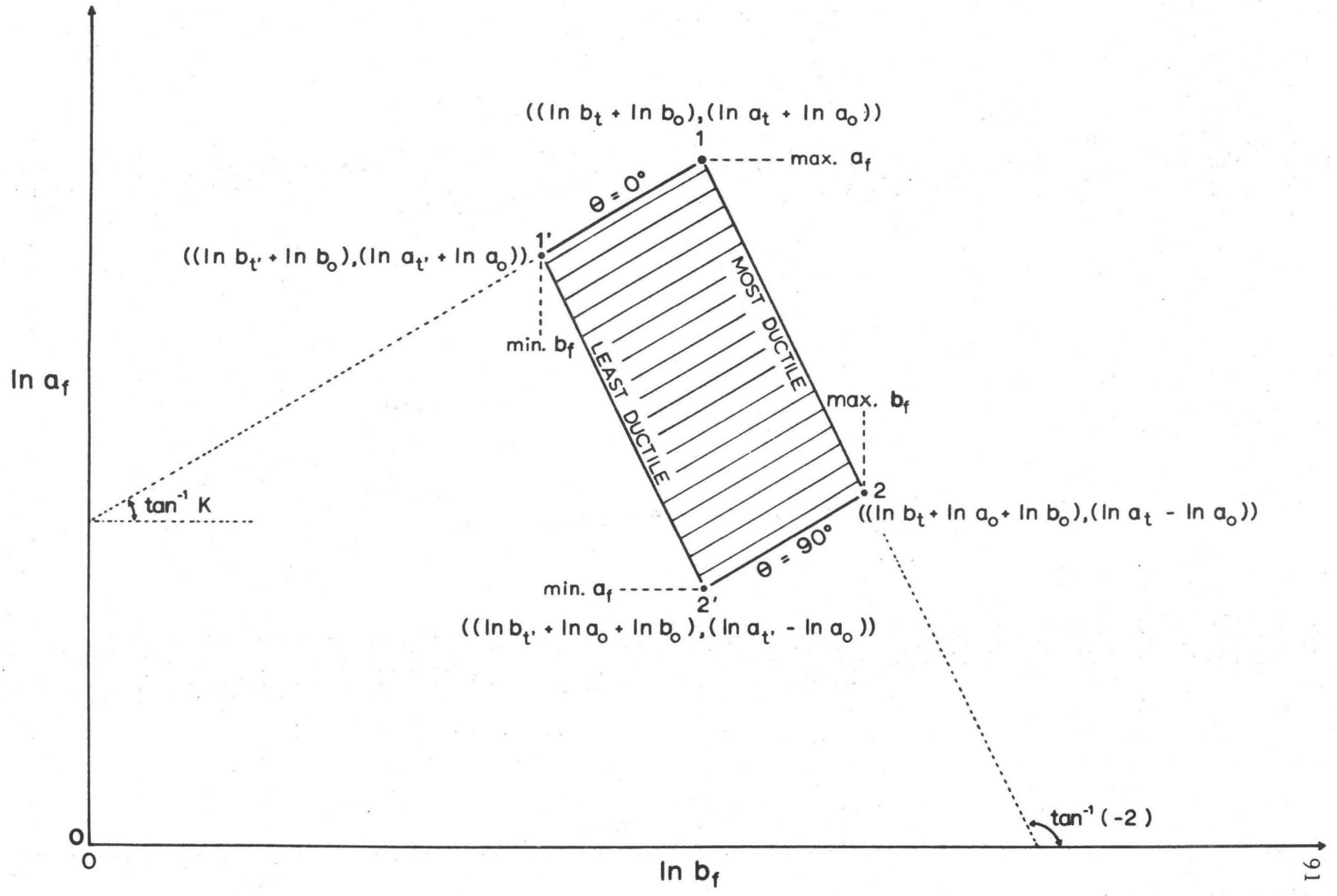
$$b_f = b_t b_o \text{ and } a_f = a_t a_o \quad (6-9)$$

$$(2) \quad X_t X_o \rangle (Y_t Z_o : Z_t Y_o) \text{ which has two possibilities:}$$

$$a) \text{ If } Y_t Z_o \langle Z_t Y_o, b_t \langle b_o, \text{ then}$$

$$b_f = b_o / b_t \text{ and } a_f = a_t b_t a_o \quad (6-10a)$$

Figure 18. Deformation field of extractable deformed pebbles with different ductilities in the case of $Z_f || Z_t || Z_o$. All the other conditions are the same as those of Figure 17(B).



b) If $Y_t Z_o > Z_t Y_o$, $b_t > b_o$, then

$$b_f = b_t / b_o \text{ and } a_f = a_t a_o b_o \quad (6-10b)$$

The coaxially deformed pebble of the above Case 1 (Equations (6-9)) has a minimum K' value among all the possible deformed shapes, while that of Case 2b (Equations (6-10b)) has a maximum K' value. In the case of $b_t < b_o$, the maximum K' value is infinite (Figure 19).

From the nature of Equations (6-7)-(6-10), we can only obtain a_o and a_t in the case of $Z_f || Z_t || Z_o$ and only obtain b_o and b_t in the case of $X_f || X_t || X_o$. It follows that we must have some knowledge of the original, ellipsoidal shape, otherwise the strain ellipsoid is not determinable (Ramsay, 1967, p. 219).

2. UNEXTRACTABLE PEBBLES

Concept of Average Axial Ratio

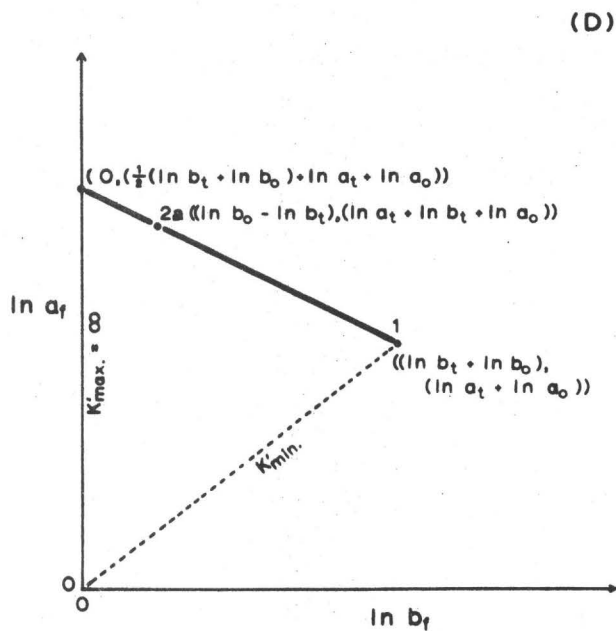
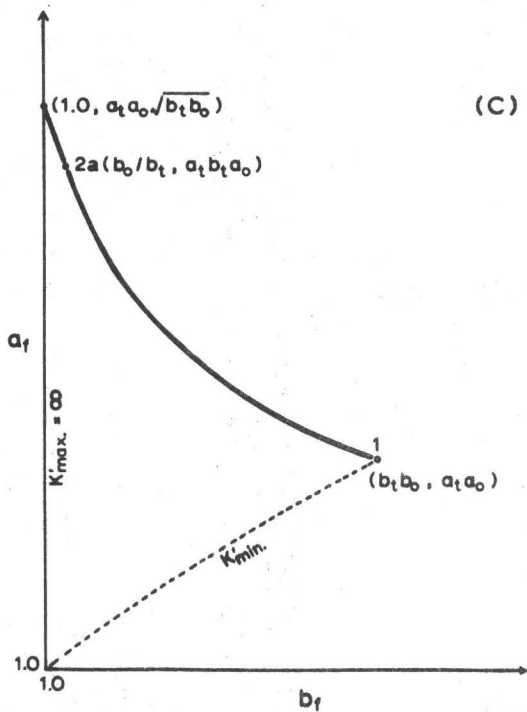
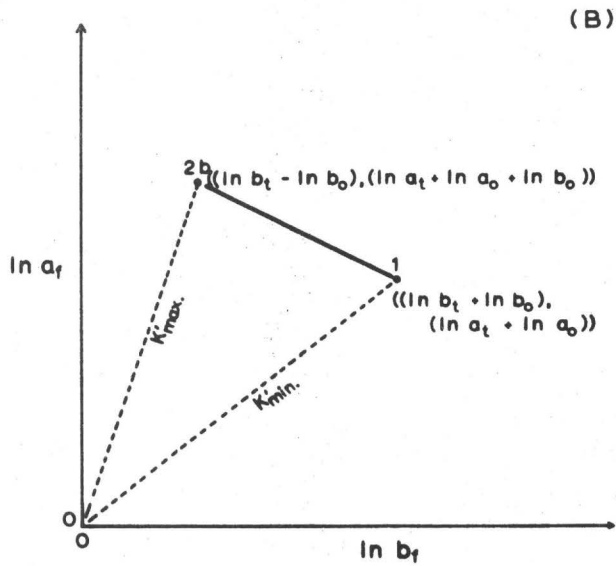
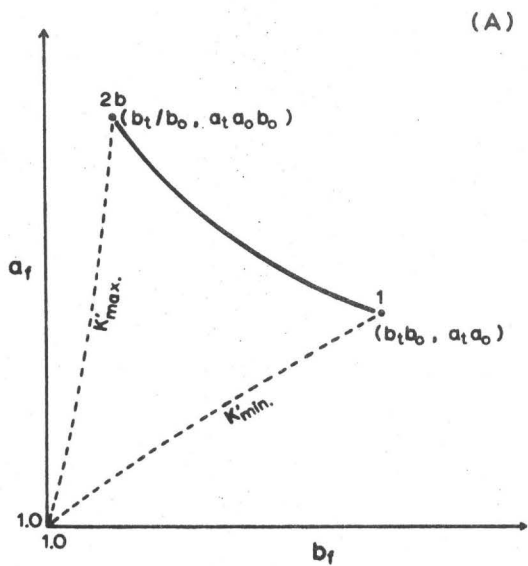
Average axial ratios obtained from extracted individual pebbles have unfortunately been mixed up with the average of the axial ratios of unextractable pebbles measured on certain cross-sections by many authors before. In fact, unextractable pebbles measured on a cross-section of an outcrop usually contain a large number of apparent

Figure 19. Deformation field of extractable deformed pebbles

in the case of coaxial deformation of $X_f || X_t || X_o$.

Heavy lines, deformation field. (A) and (B), $b_t > b_o$.

(C) and (D), $b_t < b_o$.



axial ratios. Hence, their average axial ratios, \bar{a}'_f and/or \bar{b}'_f , will not be the same as those of the extracted individual pebbles.

The example of ten ellipsoids given in Chapter V (pp. 73-76) is now used for showing the difference between average axial ratio obtained from extracted pebbles and that from measurements on some specific cross-sections (Table 1). Sections AA' and BB' in Figure 13 are parallel to the X_tZ_t and Y_tZ_t planes, respectively. They are easily mistaken as the X_fZ_f and Y_fZ_f planes. The large error derived from the measurements on sections AA' and BB' can readily be seen in Table 1.

The average axial ratio of unextractable pebbles obtained on a section of an outcrop can be equal to that of extracted individual pebbles only when the section is perpendicular to the same principal axis of all the final deformed pebbles. Such measurements, however, are commonly impossible because it is rare for there to be no axial fluctuation in a deformed pebble-fabric. In the map area, only two outcrops of deformed pebbles belong to this category. One is that shown in Figure 12(C), where the individual axial ratios, a_f , are the real ones, because all the measurements are made on a plane normal to their shortest axes Z_f ; the other is locality 280 near the Seine River Bridge, where one of the two sections measured is a foliation plane which is perpendicular to the Z_f axis of all the flattened pebbles right at the hinge of the Seine River anticline.

Table 1. Comparison of average axial ratios

Sections measured in Figure 13	Average axial ratios	
	a	b
Individual principal planes of the extracted pebbles	1.55	8.00
Principal planes PP' and QQ' of the representative ellipsoid	1.35	8.78
Cross-sections AA' and BB' parallel to the $X_t Z_t$ and $Y_t Z_t$ planes, respectively	1.17	9.53

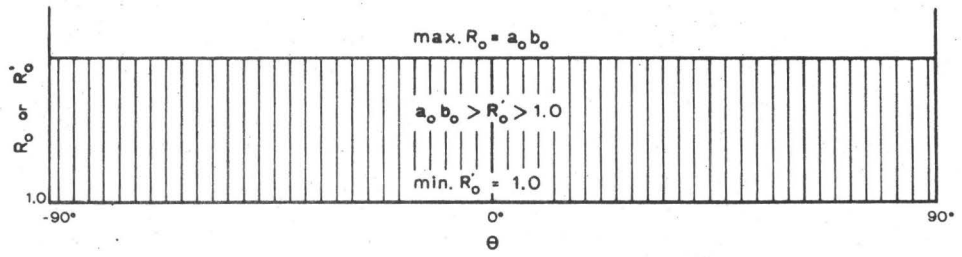
Original Pebbles with Random Orientations

Ramsay (1967, pp. 209-211) introduces a technique to isolate the tectonic strains and the original pebble shape from the final shape and orientation of deformed pebbles. However, this technique must be applied with caution, or mistakes can easily arise. Though the present writer agrees that "by using this method on three mutually perpendicular sections through a rock which contains deformed particles that were initially ellipsoidal and variably oriented, it is possible to isolate the tectonic strains in each section" (op. cit.), yet the original pebble shape remains unsolved. Discussion of this problem follows.

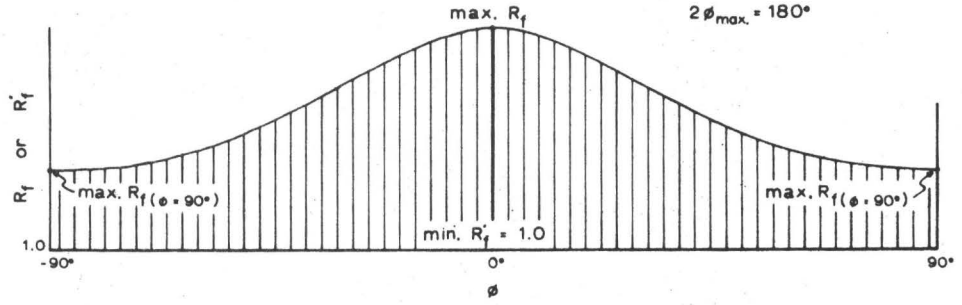
Let us first assume that all the original pebbles had an identical ellipsoidal shape with three principal axes $X_o > Y_o > Z_o$ and their axial ratios $X_o/Y_o = a_o$, $Y_o/Z_o = b_o$, and $X_o/Z_o = a_o b_o$. Because of the originally random orientation, any section through the undeformed rock will show elliptical cross-sections with axial ratios ranging from 1.0 (the circular section through an ellipsoid) passing through all possible apparent axial ratios, R'_o (including the real axial ratios a_o and b_o), to $a_o b_o$ (Figure 20(A)). Now, subject these original pebbles to a homogeneous deformation having a strain ellipsoid with three principal axes $X_t > Y_t > Z_t$ and their axial ratios $X_t/Y_t = a_t$, $Y_t/Z_t = b_t$, and $X_t/Z_t = a_t b_t$. Any unspecified true axial ratio is designated as R which may be

Figure 20. Orientation plots on sections parallel to a principal plane of the tectonic strain ellipsoid in the case of original randomly-oriented pebbles. (A), original fabric before deformation. (B), final deformed pebble-fabric in the case of $2\phi_{\max} = 180^\circ$. (C), final deformed pebble-fabric in the case of $2\phi_{\max} < 90^\circ$. (D), final deformed pebble-fabric in the special case of $2\phi_{\max} = 90^\circ$.

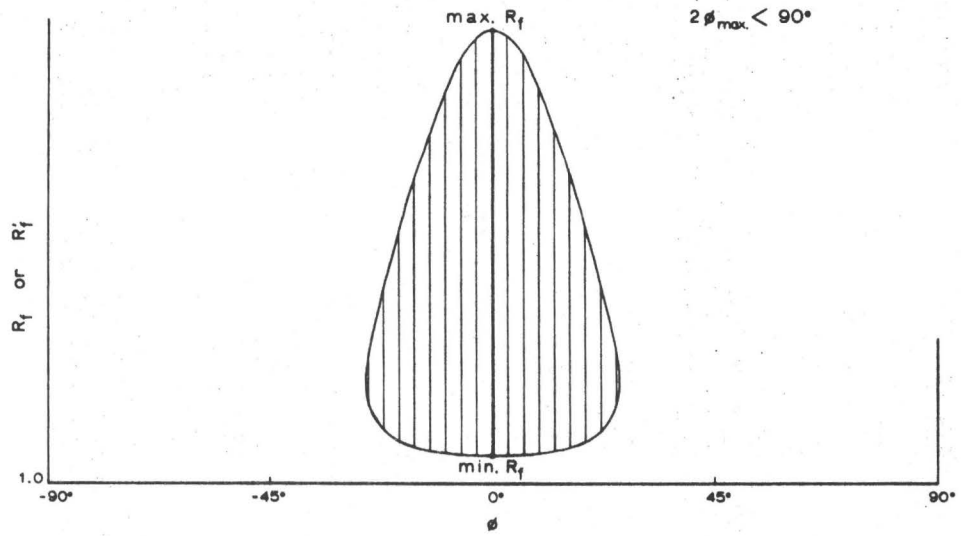
(A)



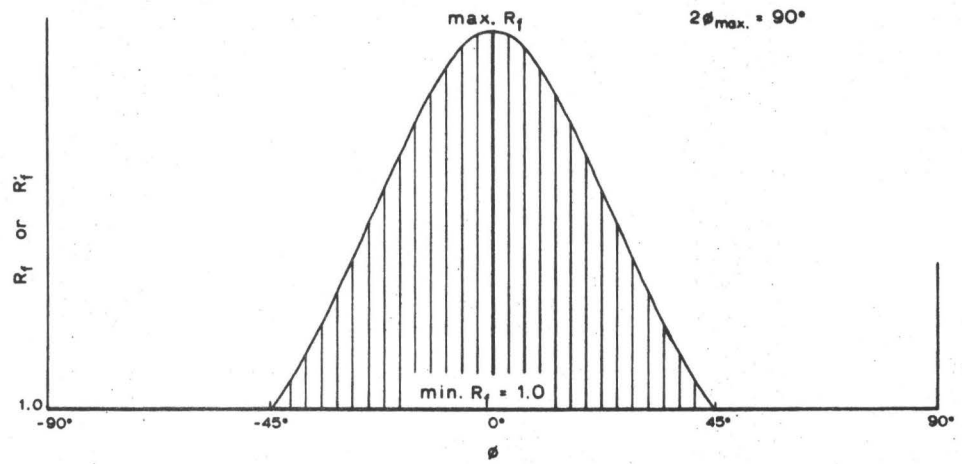
(B)



(C)



(D)



either \underline{a} or \underline{b} or \underline{ab} , whereas any apparent axial ratio is represented by R' ; the subscripts \underline{o} , \underline{t} , \underline{f} refer to that of the original pebble, the strain ellipsoid, and the final deformed pebble, respectively. θ and \emptyset are the angles between the major axis of the strain ellipse and the major axis of the exposed ellipse of an original pebble and a final deformed pebble, respectively, on a plane. Hence, on a section through the rock parallel to the $X_t Y_t$ plane, the axial ratios of the elliptical cross-sections of the deformed pebbles will range from the maximum R_f , which can be either

$$\max. a_f = a_t a_o b_o \quad (6-11)$$

for $X_t X_o > Y_t Z_o$ ($> Z_t Y_o$), if $b_t > b_o$,

$$\text{or } \max. a_f b_f = a_t a_o b_o \quad (6-12)$$

for $X_t X_o > (Z_t Y_o >) Y_t Z_o$, if $b_t < b_o$,

to the minimum R_f , which may be either

$$\min. R_f' = 1.0^* \text{ if } a_t < a_o b_o \text{ or } 2\emptyset_{\max.} > 90^\circ \text{ (Figure 20(B))}$$

where $2\emptyset_{\max.}$ is the orientation fluctuation range of the deformed pebble ellipses on that section (p. 69), or

$$\min. a_f = a_t / a_o b_o \quad (6-13)$$

* Min. $R_f = 1.0$ is a special case when R_t is equal to R_o which may be a_o , b_o , or $a_o b_o$. In the case of $R_t = a_o b_o$, $2\emptyset_{\max.} = 90^\circ$ (Figure 20(D)).

for $X_t Z_o \rangle Y_t X_o$ ($\rangle Z_t Y_o$), if $2\phi_{\max.} < 90^\circ$ or $a_t \rangle a_o b_o$ (Figure 20(C)).

Note that in the case of $2\phi_{\max.} = 180^\circ$ ($a_o b_o \rangle a_t$ (see p. 69)), among all the final pebble ellipses with $\phi = 90^\circ$ (Figure 20(B)), the maximum $R_{f(\phi = 90^\circ)}$ in that orientation may be either

$$\max. a_{f(\phi = 90^\circ)} = a_o b_o / a_t \quad (6-14)$$

for $Y_t X_o \rangle X_t Z_o$ ($\rangle Z_t Y_o$), if $a_t b_t \rangle b_o$, or

$$\max. a_{f(\phi = 90^\circ)}^b = a_o b_o / a_t \quad (6-15)$$

for $Y_t X_o \rangle (Z_t Y_o \rangle) X_t Z_o$, if $b_o \rangle a_t b_t$.

Similarly, on a section parallel to the $Y_t Z_t$ plane, we shall have axial ratios of the final deformed pebble ellipses ranging from the maximum R_f , which may be either

$$\max. b_f = b_t a_o b_o \quad (6-16)$$

for $(X_t Y_o \rangle) Y_t X_o \rangle Z_t Z_o$, if $a_t \rangle a_o$,

$$\text{or } \max. a_{f_f} = b_t a_o b_o \quad (6-17)$$

for $Y_t X_o$ ($\rangle X_t Y_o$) $\rangle Z_t Z_o$, if $a_t < a_o$,

to the minimum R_f , which may be either

$$\min. R_f = 1.0^* \text{ if } b_t < a_o b_o \text{ or } 2\phi_{\max.} > 90^\circ \text{ (Figure 20(B))}$$

* See footnote on previous page.

$$\text{or } \min. b_f = b_t / a_o b_o \quad (6-18)$$

for $(X_t Y_o) > Y_t Z_o > Z_t X_o$ if $b_t > a_o b_o$ or $2\theta_{\max.} < 90^\circ$ (Figure 20(C)).

In the case of $2\theta_{\max.} = 180^\circ$ (Figure 20(B)), the maximum $R_{f(\theta = 90^\circ)}$ in the orientation $\theta = 90^\circ$ may be either

$$\max. b_{f(\theta = 90^\circ)} = a_o b_o / b_t \quad (6-19)$$

for $(X_t Y_o) > Z_t X_o > Y_t Z_o$, if $a_t b_t > a_o$,

$$\text{or } \max. a_{f(\theta = 90^\circ)} = a_o b_o / b_t \quad (6-20)$$

for $Z_t X_o > (X_t Y_o) > Y_t Z_o$, if $a_t b_t < a_o$.

Finally, on a section parallel to the $X_t Z_t$ plane, we shall

have the maximum R_f which is

$$\max. a_f b_f = a_t b_t a_o b_o \quad (6-21)$$

for $X_t X_o > (Y_t Y_o) > Z_t Z_o$

and the minimum R_f , which may be either

$$\min. R'_f = 1.0^* \text{ if } a_t b_t < a_o b_o \text{ or } 2\theta_{\max.} > 90^\circ \text{ (Figure 20(B)),}$$

$$\text{or } \min. R_f = a_t b_t / a_o b_o \text{ if } a_t b_t > a_o b_o \text{ or } 2\theta_{\max.} < 90^\circ \text{ (Figure 20(C)).}$$

The latter has three possibilities as follows:

* See footnote on previous page.

$$a) \min. a_f b_f = a_t b_t / a_o b_o \quad (6-22)$$

for $X_t Z_o (> Y_t Y_o) > Z_t X_o$, if $a_t > b_o$ and $b_t > a_o$;

$$b) \min. a_f = a_t b_t / a_o b_o \quad (6-23)$$

for $X_t Z_o > Z_t X_o (> Y_t Y_o)$, if $a_o > b_t$;

$$c) \min. b_f = a_t b_t / a_o b_o \quad (6-24)$$

for $(Y_t Y_o >) X_t Z_o > Z_t X_o$, if $b_o > a_t$.

In the case of $2\phi_{\max.} = 180^\circ$ (Figure 20(B)), the maximum $R_{f(\phi=90^\circ)}$

in the orientation $\phi = 90^\circ$ may be either

$$\max. a_f b_{f(\phi=90^\circ)} = a_o b_o / a_t b_t \quad (6-25)$$

for $Z_t X_o > (Y_t Y_o >) X_t Z_o$, if $a_o > b_t$ and $b_o > a_t$,

$$\text{or } \max. a_{f(\phi=90^\circ)} = a_o b_o / a_t b_t \quad (6-26)$$

for $Z_t X_o > X_t Z_o (> Y_t Y_o)$, if $a_t > b_o$

$$\text{or } \max. b_{f(\phi=90^\circ)} = a_o b_o / a_t b_t \quad (6-27)$$

for $(Y_t Y_o >) Z_t X_o > X_t Z_o$, if $b_t > a_o$.

Of all the above possibilities which may be encountered on the sections parallel to the three principal planes of the tectonic strain ellipsoid, we can be certain of Equation (6-21) only and possibly Equations (6-13) and (6-16), or Equations (6-11) and (6-18),

provided that the fluctuation range ($2\phi_{\max.}$) on the section parallel to the $X_t Y_t$ or $Y_t Z_t$ plane, respectively, is smaller than 90° (Equation (6-22) also holds, if $2\phi_{\max.} < 90^\circ$ occurs on both sections). Moreover, even if all these equations are known, we can only obtain a_t , b_t , and $a_o b_o$. In fact, by looking over Equations (6-11)-(6-27), it is impossible to separate a_o and b_o . So the original pebble shape cannot be determined.

If the original pebbles were variably oriented and had different shapes with various axial ratios a_o and b_o , then their maximum axial ratio ($R_{o(\max.)}$) before deformation can be shown as

$$a_{o(\max.)} \cdot b_{o(\max.)} \geq R_{o(\max.)} = (a_o b_o)_{\max.}$$

All the possible maxima and minima of R_f or R'_f in Equations (6-11)-(6-27) remain true except that every factor $a_o b_o$ in these equations should be substituted by $R_{o(\max.)}$. It follows, similarly, that we can at most solve the variables a_t , b_t , and $R_{o(\max.)}$ only.

Original Pebbles with a Planar Fabric

If the deformed pebbles are not extractable in the case of an originally planar fabric, it is best, though usually difficult, to find in the field the special superposition of a principal plane of the tectonic strain ellipsoid upon that of the original pebbles showing planar fabric.

For instance, if we can measure the deformed pebble ellipses on a section parallel to the plane $X_f Y_f \parallel X_t Y_t \parallel X_o Y_o$ which is perpendicular to the shortest axes $Z_f \parallel Z_t \parallel Z_o$, we shall be able to determine simultaneously the tectonic strain ratio and the original shape and orientation of the deformed pebbles on that plane, as has been discussed in detail in Chapter V. However, this solution yields only a_o and a_t , similar to the result given on page 92 in the case of extractable pebbles.

Deformed Pebbles with Unknown Final Fabric on the Foliation Plane

The mathematical method developed in Chapter IV can be used to determine the final shape of deformed pebbles only if the final fabric is known. Unfortunately, in the map area, not only are the pebbles unextractable, but also the pebbles are rarely exposed on the foliation plane - a clear-cut section parallel to the $X_f Y_f$ plane of most deformed pebbles (Plate 6(B)); or the pebble lithology and margin are scarcely distinguishable on that plane, because there is always some matrix glued firmly on the surface of pebbles. In other words, the final pebble orientation of any lithology on section parallel to the general $X_f Y_f$ plane at any outcrop, except that shown in Figure 12(C) and that of locality 280, is indeterminate.

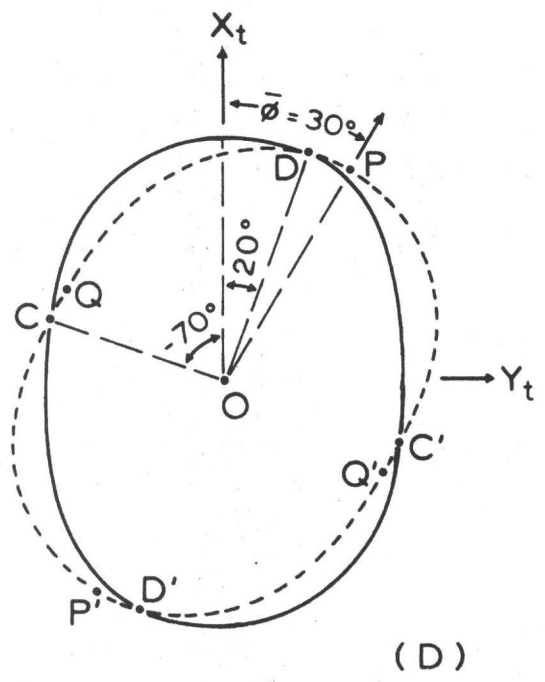
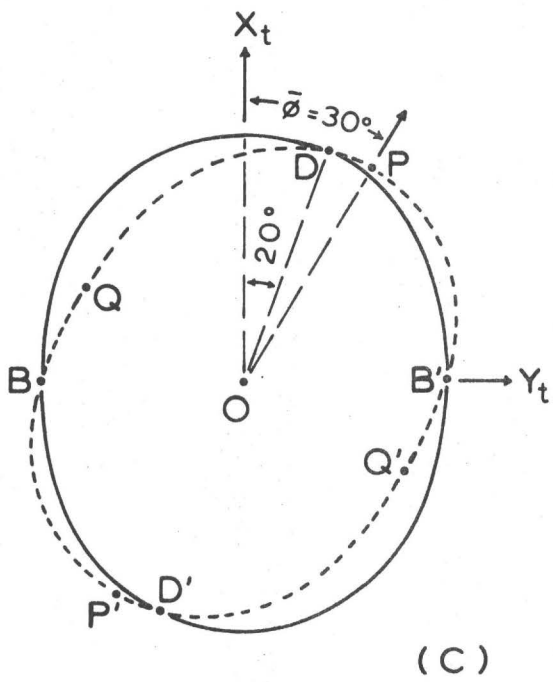
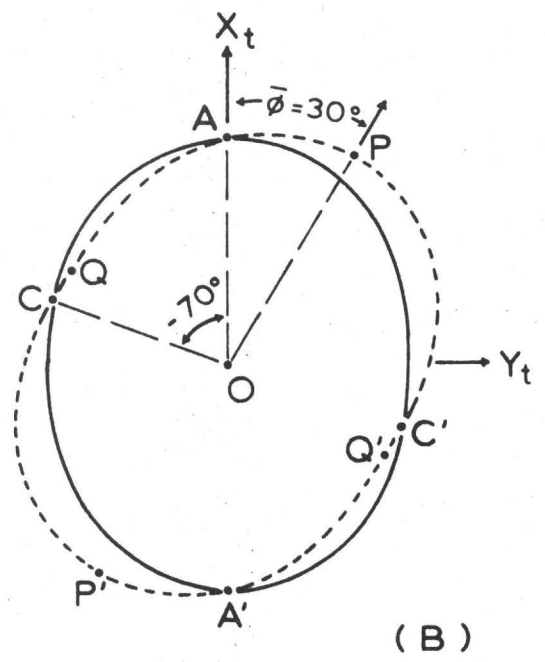
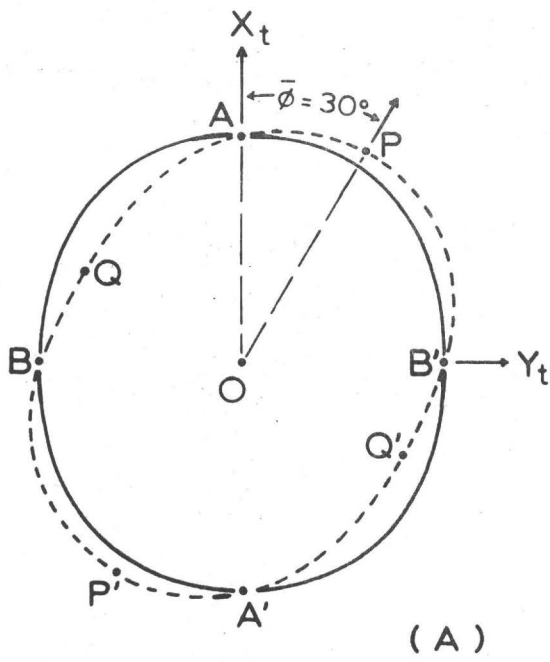
(A) Construction of the Imaginary Ellipsoid:

Under such adverse circumstances as stated above, we construct an imaginary ellipsoid to represent the deformed pebbles at each outcrop, from two representative ellipses obtained on two cross-sections of an outcrop, using Equations (4-13). The principal axes of a constructed ellipsoid are designated as X_{fc} , Y_{fc} , and Z_{fc} which are taken parallel to X_t , Y_t , and Z_t , respectively. For easier explanation, we use the same example of Figure 13 to demonstrate how the constructed ellipsoids are formed and how large the errors involved may be (Figure 21).

The representative ellipse on the common $X_f Y_f$ plane of the ten ellipsoids in Figure 13 is shown as dashed lines in Figure 21. Its X_f -axis (the $(a_f - 1)$ -weighted vector mean X_f -orientation of the ten ellipses) makes an angle of $\bar{\theta} = 30^\circ$ with the direction of the X_t -axis (principal tectonic elongation). This representative orientation of pebbles of the same lithology is an unknown parameter in practical cases, because the final pebble fabric of a particular lithology on a section parallel to most of the $X_f Y_f$ planes is generally unknown. However, an approximate position of the representative orientation of all pebbles of unknown lithology can be estimated from the vague outlines of the matrix-glued pebbles lying on the foliation plane. For instance,

Figure 21. Construction of imaginary ellipsoids from one of sections AA', DD' and one of sections CC', BB', when $\bar{\varphi} = 30^\circ$. Solid curves, constructed ellipsoids; dashed curves, the representative ellipsoid.

$Z_f \parallel Z_t$, perpendicular to the plane of the diagram.

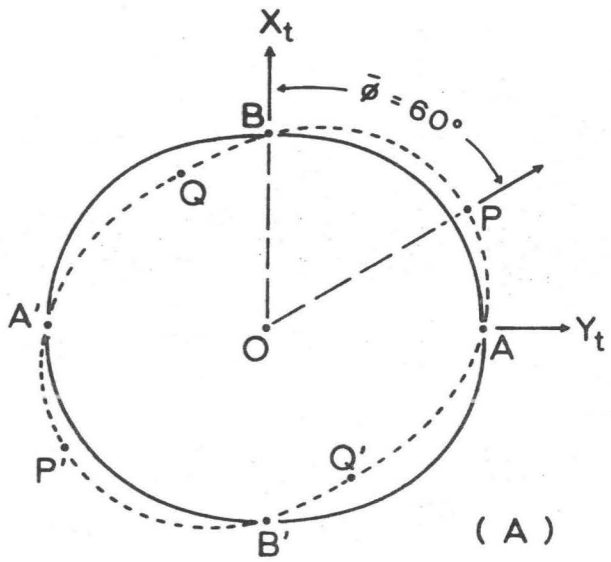


there should be no difficulty finding that the representative orientation of the ten ellipses in Figure 13 lies between 0° and 45° with the X_t -direction. In this case, the next step is to find a section between sections DD' and AA' in Figure 13, which intersects the mineral lineation—the assumed X_t -direction—at an angle between 0° and 20° . Roughly normal to this section, we try to find another section between sections CC' and BB' in Figure 13, which makes an angle with the X_t -direction between -70° and -90° (angle measured clockwise with respect to the X_t -direction is positive). At least one of the two sections should parallel the Z_f -axes which are all subparallel to one another, because the average length of the Z_f -axes may be used to calculate the average size of the deformed pebbles at each outcrop after their final axial ratios are obtained (see Chapter VII).

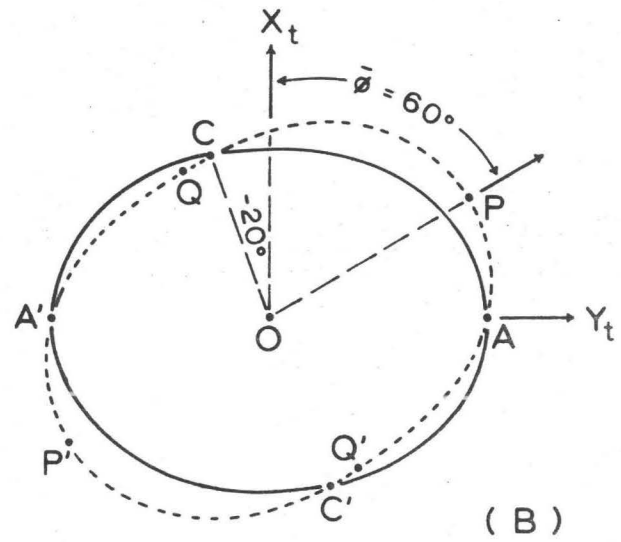
If the estimated, representative orientation is greater than 45° to the X_t -direction, then the first section to be chosen should make an angle between 70° and 90° with the mineral lineation (Figure 22), while the second one intersects the X_t -direction at an angle between 0° and -20° .

The above selection of cross-sections is taken in an attempt to minimize the error derived from the construction of the imaginary ellipsoid.

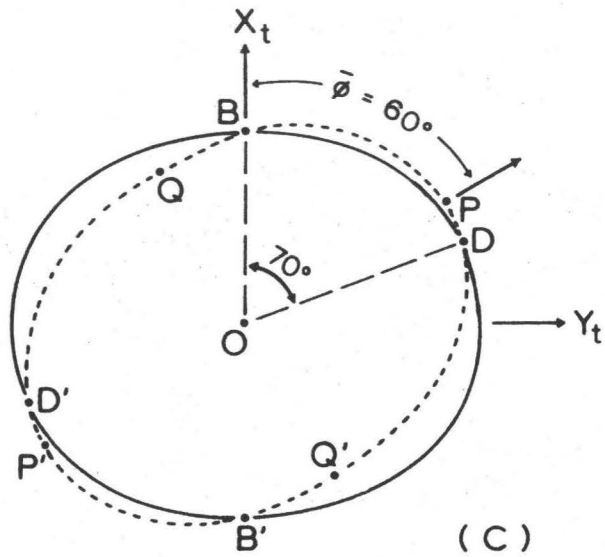
Figure 22. Construction of imaginary ellipsoids from one of sections
AA', DD' and one of sections CC', BB', when $\bar{\theta} = 60^\circ$. See
Figure 21 for explanation.



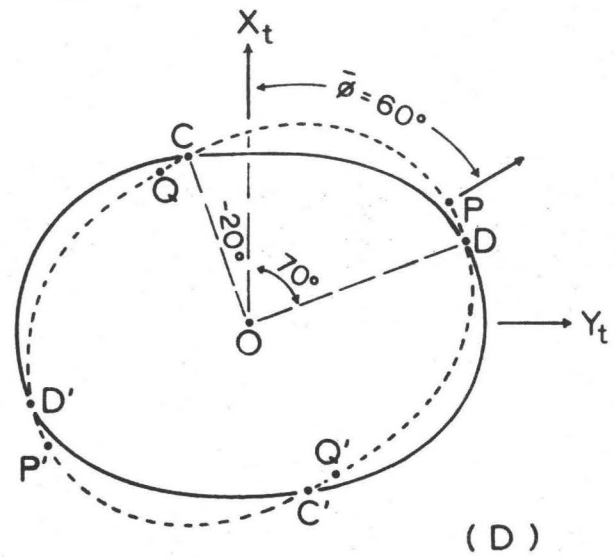
(A)



(B)



(C)



(D)

Now suppose at one outcrop where the final pebble fabric is the same as the one shown in Figure 13, we find two sections DD' and CC' which parallel the common Z_f -direction and intersect the mineral lineation on the foliation plane at angles of 20° and -70° , respectively (Figure 21(D)). On section DD', the average apparent axial ratio is $\bar{R}' = (X'/Z')_{av.} = 11.72$; whereas $\bar{R}'' = (X''/Z'')_{av.} = 8.85$ on section CC'. The twelve angles concerned are shown below:

Section DD'

$$\begin{aligned}\phi'_{11} &= 20^\circ \\ \phi'_{12} &= 70^\circ \\ \phi'_{13} &= 90^\circ \\ \phi'_{31} &= 90^\circ \\ \phi'_{32} &= 90^\circ \\ \phi'_{33} &= 0^\circ\end{aligned}$$

Section CC'

$$\begin{aligned}\phi''_{11} &= -70^\circ \\ \phi''_{12} &= 160^\circ \\ \phi''_{13} &= 90^\circ \\ \phi''_{31} &= 90^\circ \\ \phi''_{32} &= 90^\circ \\ \phi''_{33} &= 0^\circ\end{aligned}$$

where ϕ'_{13} is the angle between the $(R' - 1)$ -weighted vector mean X' -orientation on section DD' and the Z_t -direction, while ϕ''_{13} is the angle between the $(R'' - 1)$ -weighted vector mean X'' -orientation on section CC' and the Z_t -direction (note the order of the subscript numbers; see p. 41), etc. Applying all the above known data in Equations (4-13), we obtain

$$a_{fc} = X_{fc} / Y_{fc} = 1.45$$

and
$$b_{fc} = Y_{fc} / Z_{fc} = 8.85$$

Similarly, we can use the same method to construct another imaginary ellipsoid if another set of sections is available. Table 2 shows the possible range of a_{fc} and b_{fc} which may be obtained from the same final pebble fabric by different sets of cross-sections.

In the case of $\bar{\phi} > 45^\circ$, i. e., the representative X_f -direction makes a high angle with the X_t -direction, the constructed ellipsoid will be perpendicular to the strain ellipsoid on the $X_f Y_f$ plane (Figure 22). Because of the definition that $X_{fc} \parallel X_t$ and $Y_{fc} \parallel Y_t$, $a_{fc}(\bar{\phi} > 45^\circ)$ will be less than 1.0 and equal to $1/a_{fc}(90^\circ - \bar{\phi})$, while $b_{fc}(\bar{\phi} > 45^\circ)$ will be equal to $a_{fc}(90^\circ - \bar{\phi}) \cdot b_{fc}(90^\circ - \bar{\phi})$, where $a_{fc}(90^\circ - \bar{\phi})$ and $b_{fc}(90^\circ - \bar{\phi})$ are the a_{fc} and b_{fc} , respectively, of an ellipsoid which has the same shape as the one with $\bar{\phi} > 45^\circ$ but has its X' -orientation at a low angle of $(90^\circ - \bar{\phi})$ with the X_t -direction.

Except for $\bar{\phi} = 0^\circ$ or $\bar{\phi} = 90^\circ$, all the axial ratios of the constructed ellipsoids will be in error to a certain extent. Maximum error occurs when $\bar{\phi} = 45^\circ$. A representative ellipsoid, which has the same shape as that of Figure 13 but with $\bar{\phi} = 45^\circ$, is shown in Figure 23. Table 3 lists the possible maximum deviations of a_{fc} and b_{fc} which may be derived from the construction of the imaginary ellipsoid when the final deformed pebbles have a representative ellipsoid with unknown X -orientation on the XY plane but of the same shape as that in Figure 13.

Table 2. Axial ratios of the imaginary ellipsoids
constructed from different sections on Figure 21

Sections measured	a_{fc}	b_{fc}	$\ln a_{fc}$	$\ln b_{fc}$	$(Z/d)_{fc}$
AA' and BB'	1.17	9.53	0.157	2.254	0.211
AA' and CC'	1.28	8.64	0.247	2.156	0.219
BB' and DD'	1.27	9.53	0.239	2.254	0.205
CC' and DD'	1.45	8.57	0.372	2.148	0.211

The representative ellipsoid has $a_f = 1.35$, $b_f = 8.78$, and

$$Z_f/d = 0.213.$$

Figure 23. Construction of imaginary ellipsoids from one of sections AA', DD' and one of sections CC', BB', when $\bar{\varphi} = 45^\circ$. See Figure 21 for explanation.

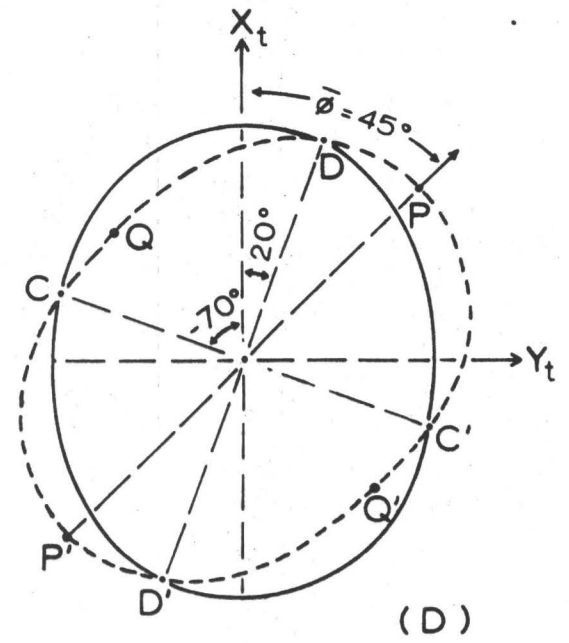
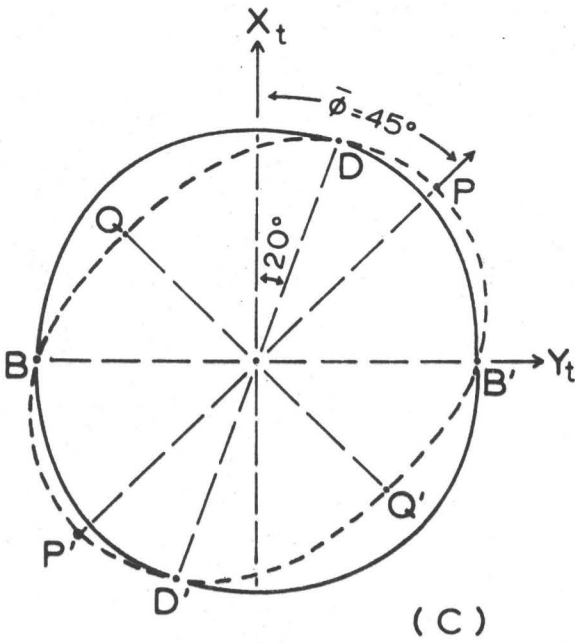
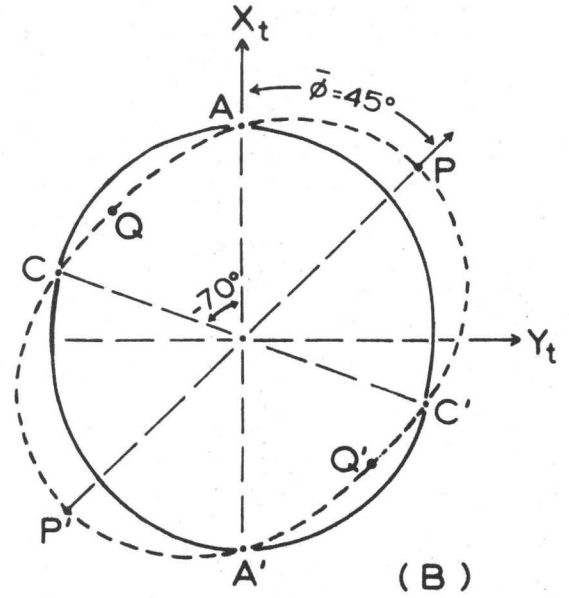
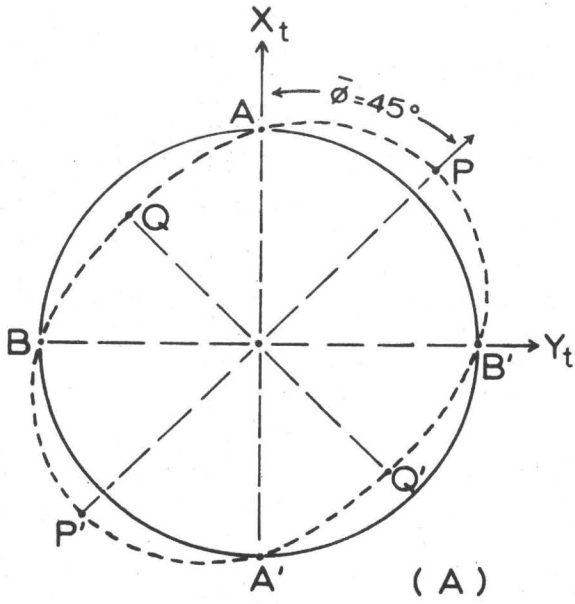


Table 3. Axial ratios of the imaginary
ellipsoids constructed from different
sections on Figure 23

Sections measured	a_{fc}	b_{fc}	$\ln a_{fc}$	$\ln b_{fc}$	$(Z/d)_{fc}$
AA' and BB'	1.00	10.37	0.000	2.339	0.210
AA' and CC'	1.13	9.19	0.122	2.218	0.219
BB' and DD'	1.10	10.37	0.095	2.339	0.204
CC' and DD'	1.29	9.09	0.255	2.207	0.211

The representative ellipsoid has $a_f = 1.35$, $b_f = 8.78$, and $Z_f/d = 0.213$.

Using Equations (4-13), the constructed axial ratios a_{fc} and b_{fc} of the deformed pebbles in the map area have been calculated. The resultant data are presented in Table 4-6. The constructed imaginary ellipsoid of the same pebble lithology at each locality is plotted as a point in the logarithmic deformation plot shown in Figure 24. The $(Z/d)_{fc}$ ratio of each shape plot is computed from the corresponding $\ln a_{fc}$ and $\ln b_{fc}$ (Tables 4-6) using Equation (3-5). It can be seen in Figure 24 that the variation in average shape of the final pebbles of the same lithology at different localities is unrelated to geographical position (cf. Figure 1).

The range of $(Z/d)_{fc}$ ratio for the volcanic pebbles is from 0.314 to 0.211; for the quartzose pebbles is from 0.425 to 0.324; and for the granitic pebbles is from 0.720 to 0.553. The circumscribing polygons representing the possible deformation fields of the three major pebble lithologies in the fold limbs, are all roughly parallel to the Z_f/d contour (cf. Figure 5), suggesting that most pebbles probably were originally lying flat on the bedding plane and were deformed under a condition such that Z_t paralleled Z_o . This can be also inferred from the final fabrics shown in Figure 12.

Table 4. Axial ratios and Z/d ratios of the constructed ellipsoids of the deformed granitic pebbles

Locality number	Number of measurements		a_{fc}	b_{fc}	$\ln a_{fc}$	$\ln b_{fc}$	$(Z/d)_{fc}$
	Section 1	Section 2					
264	12	25	1.21	2,21	0.191	0.793	0.553
265	20	12	1.21	1,87	0.191	0.626	0.618
266	38	29	1.47	1.82	0.385	0.599	0.590
267	21	24	1.14	1.89	0.131	0.637	0.626
268	13	24	0.87	2.03	-0.139	0.708	0.653
272	23	27	0.89	1.84	-0.117	0.610	0.692
273	15	14	0.85	2.12	-0.163	0.751	0.640
274	23	19	0.72	2.30	-0.329	0.833	0.640
277	10	10	1.07	1.81	0.068	0.593	9.658
278	20	14	0.91	1.84	-0.094	0.610	0.687
279	26	17	0.85	1.98	-0.163	0.683	0.669
509	16	16	1.12	1.56	0.113	0.445	0.716
286	14	11	1.17	1.92	0.157	0.652	0.614
287	5	13	1.11	1.83	0.104	0.604	0.646
289	9	23	0.91	1.75	-0.094	0.560	0.711
292	9	7	1.05	1.92	0.049	0.652	0.637
293	10	4	1.14	1.88	0.131	0.631	0.628
294	11	4	1.52	1.84	0.419	0.610	0.579
296	15	10	1.39	1.57	0.329	0.451	0.663
297	11	18	1.00	2.00	0.000	0.693	0.630
299	23	8	1.07	1.68	0.068	0.519	0.692
300	18	15	1.06	1.85	0.058	0.615	0.651
303	30	5	1.24	1.47	0.215	0.385	0.720
304	10	18	0.94	1.69	-0.062	0.525	0.720
321	19	14	1.16	1.84	0.148	0.610	0.634
413	19	8	1.50	1.67	0.405	0.513	0.621
305*	8	9	1.01	1.62	0.010	0.482	

* Not in fold limb.

Average $(Z/d)_{fc} = 0.652$

Table 5. Axial ratios and Z/d ratios
of the constructed ellipsoids of the
deformed quartzose pebbles

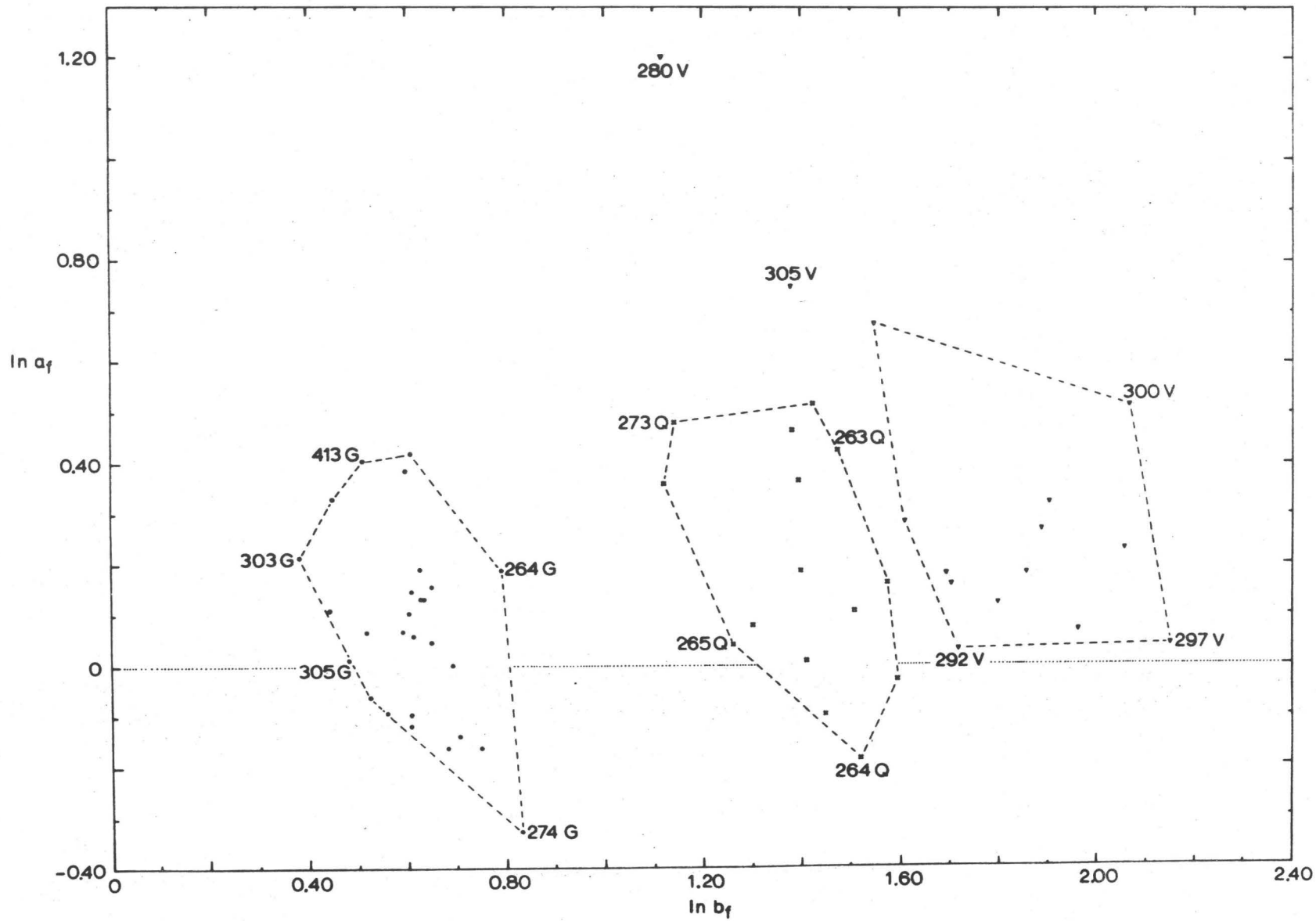
Locality number	Number of measurements		a_{fc}	b_{fc}	$\ln a_{fc}$	$\ln b_{fc}$	$(Z/d)_{fc}$
	Section 1	Section 2					
261	12	8	1.68	4.16	0.519	1.426	0.325
263	17	6	1.53	4.38	0.425	1.477	0.324
264	10	18	0.83	4.57	-0.186	1.520	0.386
265	25	12	1.04	3.54	0.039	1.264	0.425
266	34	13	1.20	4.85	0.182	1.579	0.328
268	8	18	1.11	4.52	0.104	1.509	0.353
272	19	27	1.43	3.07	0.358	1.122	0.420
273	7	12	1.62	3.13	0.482	1.141	0.398
274	21	16	0.97	4.94	-0.030	1.597	0.348
277	7	10	1.21	4.07	0.191	1.404	0.368
278	8	6	1.01	4.11	0.010	1.413	0.388
279	12	15	1.44	4.05	0.365	1.399	0.349
284	10	10	1.59	4.00	0.464	1.386	0.340
287	5	8	1.08	3.67	0.077	1.300	0.410
289	10	10	0.91	4.27	-0.094	1.452	0.392

Table 6. Axial ratios and Z/d ratios
of the constructed ellipsoids of the
deformed volcanic pebbles

Locality Number	Number of measurements		a_{fc}	b_{fc}	$\ln a_{fc}$	$\ln b_{fc}$	$(Z/d)_{fc}$
	Section 1	Section 2					
266	17	14	1.31	6.64	0.270	1.893	0.259
509	14	17	1.38	6.76	0.322	1.911	0.251
290	15	14	1.20	6.42	0.182	1.859	0.272
292	10	10	1.03	5.59	0.030	1.721	0.314
293	15	5	1.20	5.46	0.182	1.697	0.303
294	30	8	1.18	5.51	0.166	1.707	0.303
296	12	15	1.33	5.01	0.285	1.611	0.311
297	11	18	1.04	8.61	0.039	2.153	0.235
299	17	13	1.26	7.85	0.231	2.061	0.234
300	19	14	1.67	7.96	0.513	2.074	0.211
304	12	20	1.13	6.06	0.122	1.802	0.289
321	15	9	1.97	4.71	0.678	1.550	0.284
362	16	19	1.07	7.16	0.068	1.969	0.263
305*	17	19	2.12	3.99	0.751	1.384	
280*	11	8	3.33	3.06	1.203	1.118	

* Not in fold limb.

Figure 24. Logarithmic deformation plot of the imaginary ellipsoids constructed from the deformed pebbles in the Seine River area, Ontario. Localities 280 and 305 are situated in the fold hinge zones. G, Q, and V refer to the granitic (dots), quartzose (crosses), and volcanic pebbles (triangles), respectively.



(B) Computation for a_o , b_o , and a_t , b_t :

Locality 280 (Figure 1) is situated at the hinge of the Seine River anticline near the Seine River Bridge where the bedding is parallel to the mineral lineation but is normal to the foliation plane. Abundant cross-lamination in the arenites overlying and underlying the scattered volcanic pebbles of locality 280 indicates that the paleocurrent flowed towards the present south-southeast and is roughly normal to the fold axis as well as the mineral lineation (X_t -direction). It has been noted that under conditions of running water, the preferred X_o -orientation of most pebbles, as transported in contact with a frictional substratum such as the medium-grained sands of locality 280, is transverse to the current direction (p. 50). Therefore, it seems reasonable to assume that the X_o -axes of the original pebbles were statistically normal to the paleocurrent direction and that the original pebbles, which are scattered without contacting one another, lay flat on the bedding. It follows that $X_t \parallel X_o$, $Y_t \parallel Z_o$, and $Z_t \parallel Y_o$, approximately.

Because one of the measured sections at locality 280 was made on the foliation plane, and also because of the special coaxial superposition of strain ellipsoid upon the original pebbles, theoretically there should not be any error induced from construction of the representative ellipsoid. Since $X_t \parallel X_o$, $Y_t \parallel Z_o$, and $Z_t \parallel Y_o$ at locality 280, the shape plot of the representative ellipsoid, point

280V(1.118, 1.203) in Figure 25, should be one of the two extremities of the deformation field parallel to the X_f/d contour (see Figure 19).

In Figure 24 (see also Tables 4-6), point 297V(2.153, 0.039) has an overall maximum b_f ratio. Its K' value is

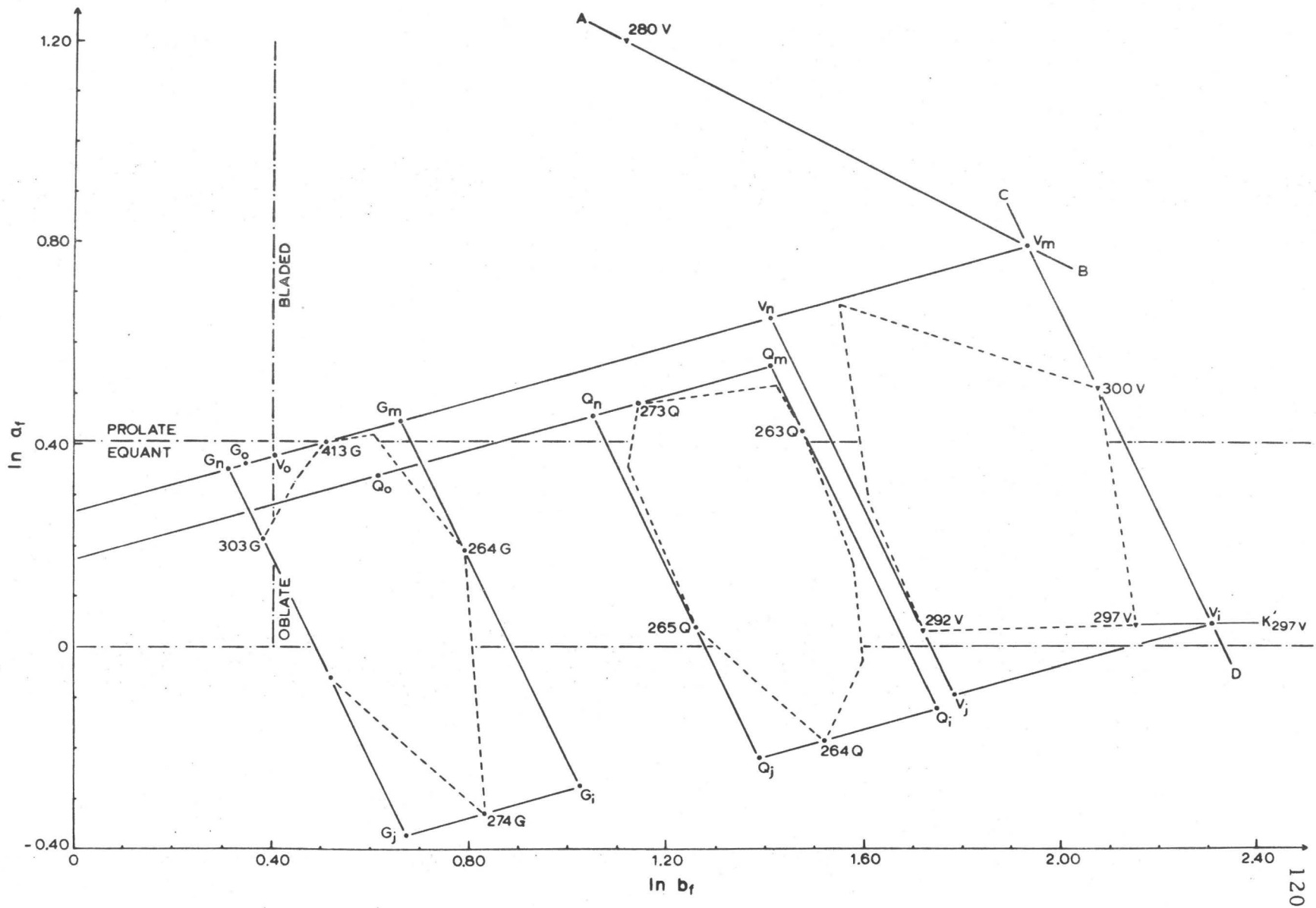
$$K'_{297V} = (\ln a_{297V}) / (\ln b_{297V}) = 0.039 / 2.153 = 0.018$$

The apparent deformation path (p. 88) passing through point 297V is then represented by

$$\ln a_f = 0.018 \ln b_f \quad (6-28)$$

On the other hand, point 300V has the lowest $(Z/d)_{fc}$ ratio and so is considered to have been subjected to a maximum compressional strain in the Z_t -direction among the volcanic pebbles of all the localities in the fold limbs. When a flow fold with a minor buckling component is developed, maximum shortening strain normal to the axial plane usually occurs at the fold hinge; because the fold limbs rotate more or less during folding, the incremental shortening strains in the fold limbs are not coaxially added as at the fold hinge. The maximum compressional strain in the fold limbs, as represented by the lowest $(Z/d)_{fc}$ ratio at locality 300, is therefore taken to compare with that of locality 280 at the fold hinge.

Figure 25. Determination of the tectonic strain ellipsoid and the original pebble shape on the logarithmic deformation plot of the final deformed pebbles in the map area. See the text for explanation.



Passing through point 280V in Figure 25, draw a line AB parallel to the X_f/d contour (see Figures 5 and 19). Line AB can be shown as

$$\ln a_f - 1.203 = -\frac{1}{2} (\ln b_f = 1.118)$$

$$\text{or } \ln a_f = -\frac{1}{2} \ln b_f + 1.762 \quad (6-29)$$

Passing through point 300V(2.074, 0.513), draw a line CD parallel to the Z_f/d contour (see Figures 5 and 17; see also the line between points 1 and 2 of Figure 18). Line CD is given by

$$\ln a_f - 0.513 = -2 (\ln b_f - 2.074)$$

$$\text{or } \ln a_f = -2 \ln b_f + 4.661 \quad (6-30)$$

Solving simultaneous equations (6-29) and (6-30), we get

$\ln a_f = 0.795$ and $\ln b_f = 1.933$. Coordinates (1.933, 0.795) shown by the intersection point V_m in Figure 25, represent the final ellipsoid of volcanic pebble with the same tectonic strain as those of localities 280 and 300, but resulting from coaxial superpositions of X_t, Y_t, Z_t on X_o, Y_o, Z_o respectively. Similarly, from Equations (6-28) and (6-30), we obtain $\ln a_f = 0.041$ and $\ln b_f = 2.310$. Point V_i with coordinates (2.310, 0.041) in Figure 25 is assumed to represent the final ellipsoid of volcanic pebble having the same tectonic strain ratios as those of localities 280 and 300, but resulting from coaxial deformation of

$Z_t \parallel Z_o$, $Y_t \parallel X_o$, and $X_t \parallel Y_o$. This assumption is only approximately true; the error involved depends on how far the shape plot with an overall maximum b_f ratio (point 297V in this case) is discrete from point 2 of Figure 18, and also on the deformation path (the true K value (see p. 30)).

Let us say that the volcanic pebbles of localities 280 and 300 have a strain ellipsoid with axial ratios a_{tvm} and b_{tvm} , and that the axial ratios of their original pebble shape are a_{ov} and b_{ov} . Then, from the coordinates of points 280V, V_m , and V_i , we have six separate equations (see Equations (6-10b), (6-7) or (6-9), and (6-8b), respectively) as follows:

$$\ln a_{ov} + \ln b_{ov} + \ln a_{tvm} = 1.203 \quad (6-31)$$

$$\ln b_{tvm} - \ln b_{ov} = 1.118 \quad (6-32)$$

$$\ln a_{ov} + \ln a_{tvm} = 0.795 \quad (6-33)$$

$$\ln b_{ov} + \ln b_{tvm} = 1.933 \quad (6-34)$$

$$\ln a_{tvm} - \ln a_{ov} = 0.041 \quad (6-35)$$

$$\ln a_{ov} + \ln b_{ov} + \ln b_{tvm} = 2.310 \quad (6-36)$$

Solving these equations, we obtain

$$\begin{cases} \ln a_{tvm} = 0.418 \\ \ln b_{tvm} = 1.525 \end{cases} \quad \text{or} \quad \begin{cases} a_{tvm} = 1.52 \\ b_{tvm} = 4.60 \end{cases}$$

$$\text{and} \quad \begin{cases} \ln a_{ov} = 0.377 \\ \ln b_{ov} = 0.408 \end{cases} \quad \text{or} \quad \begin{cases} a_{ov} = 1.46 \\ b_{ov} = 1.50 \end{cases}$$

Plot the coordinates $(0.408, 0.377)$ as point $V_o(\ln b_{ov}, \ln a_{ov})$ in

Figure 25, which represents the original shape of the volcanic pebbles at localities 280 and 300. The slope (K) of the simplest deformation path between points V_o and V_m in the case of irrotational strain (see Equation (3-1)) is

$$K = (\ln a_{tvm}) / (\ln b_{tvm}) = 0.274$$

Hence, the simplest deformation path of these volcanic pebbles can be represented by the following equation:

$$\ln a_f - 0.377 = 0.274 (\ln b_f - 0.408)$$

$$\text{or} \quad \ln a_f = 0.274 \ln b_f + 0.265 \quad (6-37)$$

Now let us assume that the average original pebble shape of the same lithology at one outcrop is identical with that of another outcrop, but that the tectonic strain may differ at different places and is solely responsible for the variation in the final $(Z/d)_{fc}$ ratios. Among volcanic

pebbles of all the localities in Figures 24 and 25, point 292V(1.721, 0.030) has a highest $(Z/d)_{fc}$ ratio (see also Table 6) and thus has a least strain in the Z_f -direction. The Z_f/d contour (see p. 34) passing through point 292V is given by

$$\ln a_f - 0.030 = -2 (\ln b_f - 1.721)$$

$$\text{or } \ln a_f = -2 \ln b_f + 3.472 \quad (6-38)$$

Substituting Equation (6-38) in Equation (6-37), we get $\ln b_f = 1.410$ and $\ln a_f = 0.652$. Coordinates (1.410, 0.652) are shown by intersection point $V_n (\ln b_{vn}, \ln a_{vn})$ in Figure 25. The finite strain ratios between points V_o and V_n are then

$$\begin{cases} \ln a_{tvn} = \ln a_{vn} - \ln a_{ov} = 0.275 \\ \ln b_{tvn} = \ln b_{vn} - \ln b_{ov} = 1.002 \end{cases}$$

$$\text{or } \begin{cases} a_{tvn} = 1.32 \\ b_{tvn} = 2.72 \end{cases}$$

Here we find that the average axial ratio $a_{ov} = 1.46$ of the original volcanic pebbles as calculated from the logarithmic deformation plot is surprisingly close to the average axial ratio $\bar{a}_o = 1.42$ as computed from the orientation plot on the special plane of $X_f Y_f \parallel X_t Y_t \parallel X_o Y_o$ (see p. 81). Furthermore, the tectonic strain ratio $a_t = 1.43 \pm 0.05$ (p. 79)

obtained from the special plane mentioned above at locality 144 (Figure 1), is correctly within the range between $a_{tvn} = 1.32$ and $a_{tvm} = 1.52$ as computed from the logarithmic deformation plot. These coincident results through different approaches suggest that either all the assumptions involved are quite valid or some of the errors happen to oppose one another.

For the granitic and quartzose pebbles, the calculations of a_o , b_o , a_t , and b_t are shown in Appendix C to avoid the tedious repetition of mathematical presentation. The calculated axial ratios of their original shape are $a_{og} = 1.43$ and $b_{og} = 1.42$ for the granitic pebbles; $a_{oq} = 1.40$ and $b_{oq} = 1.86$ for the quartzose pebbles. These original shapes are plotted as $G_o(0.351, 0.361)$ and $Q_o(0.621, 0.339)$ in the logarithmic deformation plot (Figure 25) for the granitic and quartzose pebbles, respectively.

According to Zingg's (1935) shape classification, the original pebble shape was equant for the granitic pebbles; oblate for the quartzose pebbles; and the original volcanic pebbles lay between equant and oblate shape (Figure 25).

CHAPTER VII

PEBBLE SIZE

There are several methods which we can employ to calculate the "size" of final deformed pebbles. If a number of pebbles, \underline{n} , can be extracted at one outcrop, their average nominal diameter, \bar{d} , will be given by

$$\bar{d} = \frac{1}{n} \sum_{i=1}^{i=n} d_i = \frac{1}{n} \sum_{i=1}^{i=n} (X_{f(i)} Y_{f(i)} Z_{f(i)})^{1/3} \quad (7-1)$$

If the deformed pebbles are not extractable by means of ordinary method, we must know the final fabric and compute the axial ratios a_f and b_f using Equations (4-13), if condition favors, before proceeding the calculation of pebble size.

By definition in a single pebble,

$$b_f = Y_f/Z_f, \quad a_f = X_f/Y_f, \quad \text{and } d = (X_f Y_f Z_f)^{1/3}$$

so $Y_f = b_f Z_f$, $X_f = a_f Y_f = a_f b_f Z_f$, and

$$d = ((a_f b_f Z_f)(b_f Z_f) Z_f)^{1/3} = Z_f (a_f b_f^2)^{1/3} \quad (7-2)$$

Infinite cross-sections through a flattened pebble parallel to its Z_f axis, will have a maximum length of Z_f and a minimum one of zero with an average slightly greater than $Z_f/2$ in the Z_f direction.

Similarly, on a section parallel to the common Z_f -direction through a rock containing an infinite number of flattened pebbles in the case of coaxial deformation of $Z_f \parallel Z_t \parallel Z_o$, the average length of the apparent Z_f -axes, \bar{Z}'_f , will be slightly greater than one half of the average Z_f -axis, \bar{Z}_f , of all the individual pebbles. In the map area, pebbles which have Z'_f axes less than 5.0 mm were not measured. By approximation, we may say:

$$\bar{Z}'_f \approx \frac{1}{2} (\bar{Z}_f + 5.0 \text{ mm})$$

$$\text{or } \bar{Z}_f \approx 2(\bar{Z}'_f - 2.5 \text{ mm}) \quad (7-3)$$

Substituting Equation (7-3) in Equation (7-2), we have an equation to determine the approximate average pebble size of the same lithology at each locality in the map area as:

$$\bar{d} \approx 2(a_f b_f)^{2/3} \left[\bar{Z}'_f - 2.5 \text{ mm} \right] \quad (7-4)$$

Because the imaginary ellipsoid constructed from the exposed pebble ellipses at each locality does not have the same shape and volume as those of the representative ellipsoid except for those co-

axially deformed ones, it follows that there must be a certain unknown error in computing pebble size under such circumstances. To see how great the error may be, we use the axial ratios a_{fc} and b_{fc} of the imaginary ellipsoid constructed from sections BB' and DD' in Figure 23(C), which shows the greatest deviation in our example (Table 3). Substituting $a_{fc} = 1.10$ and $b_{fc} = 10.37$ in the factor $(a_{fc} b_{fc}^2)^{1/3}$ of Equation (7-4), we get

$$(a_{fc} b_{fc}^2)^{1/3} = (118.29)^{1/3} = 4.91$$

Substituting in the same factor with the axial ratios $a_f = 1.35$ and $b_f = 8.78$ of the representative ellipsoid whose principal planes XZ and YZ are the sections PP' and QQ', respectively (Figure 23(C)), we obtain

$$(a_f b_f^2)^{1/3} = (104.07)^{1/3} = 4.70$$

Hence, the error involved in calculation of pebble size from the constructed ellipsoid through sections BB' and DD' of Figure 23, is

$$\frac{4.91 - 4.70}{4.70} \times 100\% = 4.46\%$$

It is considered from the above example that the error of pebble size induced by the construction of imaginary ellipsoid is unlikely to be too large. The pebble size of different lithologies at different localities in the map area is calculated using Equation (7-4) and is listed in Tables 7-9. Figure 26 shows the pebble sizes of all the localities within the Seine River anticline - the main structure of the area - plotted against their spatial distribution which is projected in a direction parallel to the bedding trace upon a reference line MF obliquely across the fold. Some conclusions of the pebble size can be drawn from this diagram together with field observations:

- 1) The pebble size of the granitic pebbles increases stratigraphically upwards in the north limb.
- 2) Within a single conglomerate bed, pebble size increases towards where the thickness of the bed is greatest.
- 3) The granitic pebbles are generally larger than the volcanic pebbles, both lie in the size range of cobbles with some of the former reaching the boulder size; whereas the quartzose pebbles are the smallest among the three major pebble lithologies and are mostly within the range of 40-100 mm.
- 4) Pebbles in the north limb are commonly bigger than their counterparts in the south limb.

Table 7. Calculated size of
the granitic pebbles

Locality number	a_f	b_f	b_f^2	$a_f b_f^2$	$(a_f b_f^2)^{1/3}$	$\bar{Z}'_f(\text{mm})$	$\bar{d}(\text{mm})$
264	1.21	2.21	4.88	5.90	1.81	31.8	106.1
265	1.21	1.87	3.50	4.24	1.62	29.6	87.8
266	1.47	1.82	3.31	4.87	1.70	51.3	165.9
267	1.14	1.89	3.57	4.07	1.60	45.9	138.9
268	0.87	2.03	4.12	3.58	1.53	41.8	120.3
272	0.89	1.84	3.39	3.02	1.44	43.8	118.9
273	0.85	2.12	4.49	3.82	1.56	26.0	104.5
274	0.72	2.30	5.29	3.81	1.56	52.9	157.2
277	1.07	1.81	3.28	3.51	1.52	49.5	142.9
278	0.91	1.84	3.39	3.08	1.45	29.6	78.6
279	0.85	1.98	3.92	3.33	1.49	48.3	136.5
509	1.12	1.56	2.43	2.72	1.40	35.2	91.6
286	1.17	1.92	3.69	4.32	1.63	24.6	72.0
287	1.11	1.83	3.35	3.72	1.55	25.9	72.5
289	0.91	1.75	3.06	2.78	1.41	46.4	123.8
292	1.05	1.92	3.69	3.87	1.57	42.9	126.9
293	1.14	1.88	3.53	4.02	1.59	34.0	100.2
294	1.52	1.84	3.39	5.15	1.73	49.3	161.9
296	1.39	1.57	2.46	3.42	1.51	68.9	200.5
297	1.00	2.00	4.00	4.00	1.59	80.9	249.3
299	1.07	1.68	2.82	3.02	1.44	92.2	258.3
300	1.06	1.85	3.42	3.62	1.54	83.7	250.1
303	1.24	1.47	2.16	2.68	1.39	81.9	220.7
304	0.94	1.69	2.86	2.69	1.39	94.6	256.0
321	1.16	1.84	3.39	3.93	1.58	28.8	83.1
413	1.50	1.67	2.79	4.19	1.61	61.4	189.7

Table 8. Calculated size of
the quartzose pebbles

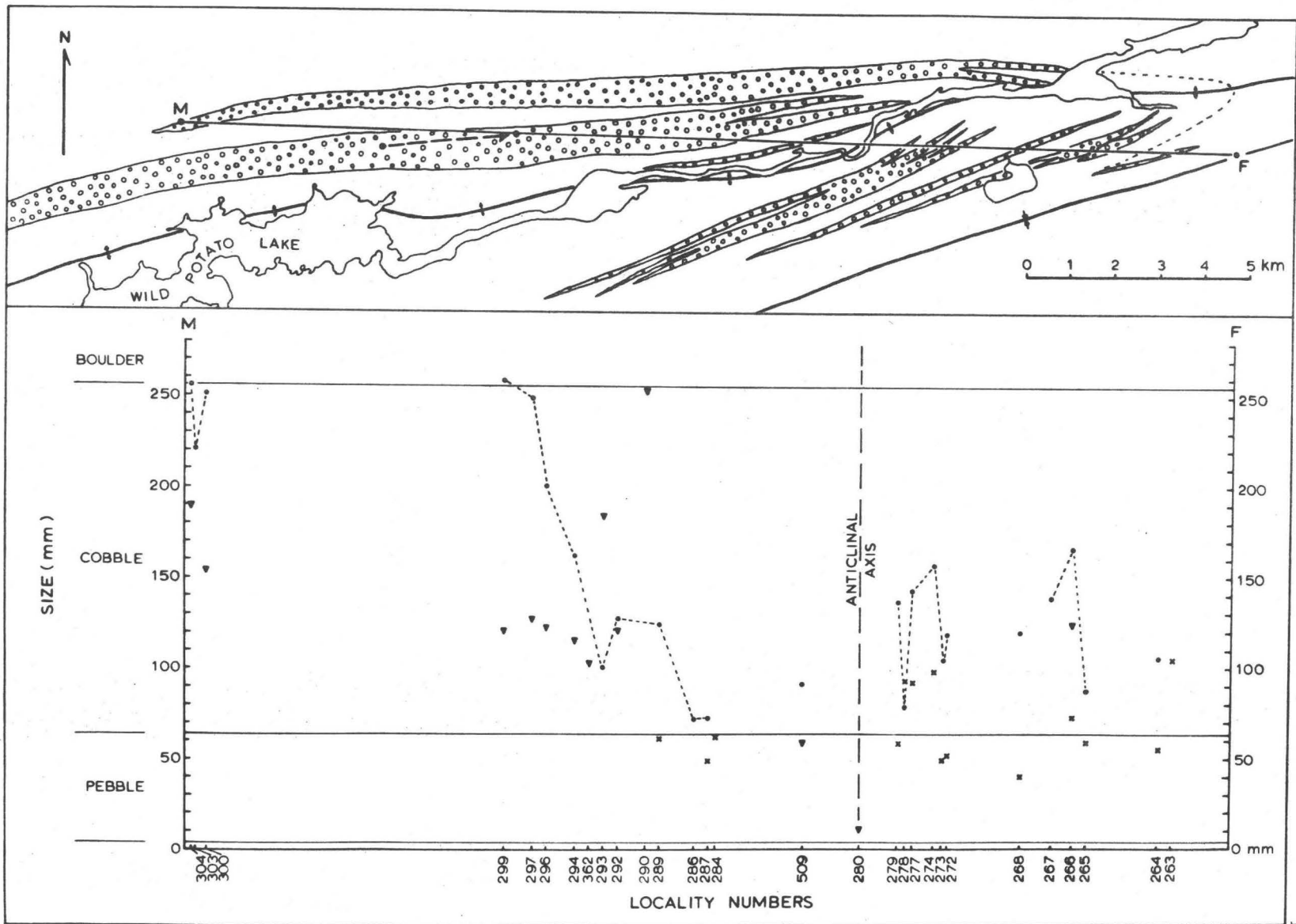
Locality number	a_f	b_f	b_f^2	$a_f b_f^2$	$(a_f b_f^2)^{1/3}$	$\bar{Z}'_f(\text{mm})$	$\bar{d}(\text{mm})$
261	1.68	4.16	17.31	29.08	3.08	6.9	27.2
263	1.53	4.38	19.19	29.35	3.08	19.6	105.3
264	0.83	4.57	20.88	17.33	2.59	13.3	55.9
265	1.04	3.54	12.53	13.03	2.35	15.0	58.8
266	1.20	4.85	23.52	28.22	3.04	14.5	73.0
268	1.11	4.52	20.43	22.68	2.83	9.6	40.2
272	1.43	3.07	9.42	13.47	2.38	13.4	51.9
273	1.62	3.13	9.80	15.88	2.51	12.4	49.7
274	0.97	4.94	24.40	23.67	2.87	19.6	98.2
277	1.21	4.07	16.56	20.04	2.72	19.5	92.5
278	1.01	4.11	16.89	17.06	2.57	20.6	93.0
279	1.44	4.05	16.40	23.62	2.87	12.8	59.1
284	1.59	4.00	16.00	25.44	2.94	13.1	62.3
287	1.08	3.67	13.47	14.55	2.44	12.6	49.3
289	0.91	4.27	18.23	16.59	2.55	14.4	60.7

Table 9. Calculated size of
the volcanic pebbles

Locality number	a_f	b_f	b_f^2	$a_f b_f^2$	$(a_f b_f^2)^{1/3}$	$\bar{Z}'_f(\text{mm})$	$\bar{d}(\text{mm})$
266	1.31	6.64	44.09	57.76	3.87	18.5	123.8
280	3.33	3.06					10.7*
509	1.38	6.76	45.70	63.07	3.98	9.9	58.9
290	1.20	6.42	41.22	49.46	3.67	37.0	253.2
292	1.03	5.59	31.25	32.19	3.18	21.5	120.8
293	1.20	5.46	29.81	35.77	3.29	30.4	183.6
362	1.07	7.16	51.27	54.86	3.80	16.0	102.6
294	1.18	5.51	30.36	35.82	3.30	19.9	114.8
296	1.33	5.01	25.10	33.38	3.22	21.6	123.0
297	1.04	8.61	74.13	77.10	4.26	17.4	126.9
299	1.26	7.85	61.62	77.64	4.27	16.7	121.3
300	1.67	7.96	63.36	105.81	4.73	18.8	154.2
304	1.13	6.06	36.72	41.49	3.46	29.9	189.6
321	1.97	4.71	22.18	43.69	3.52	11.8	65.5

* Calculated from $d = Y_f \sqrt[3]{a_f/b_f}$

Figure 26. Pebble size versus spatial distribution. All the localities are projected in a direction parallel to the bedding trace (see the broken arrow in the upper diagram), upon a reference line MF obliquely across the fold. Dots, granitic pebbles; crosses, quartzose pebbles; triangles, volcanic pebbles.



5) Within the domain of the anticline, buckling is seen to have developed at places where the pebbles are the smallest. In fact, no rocks in the hinge zone except those at locality 280 can be called conglomerate. This might imply an early local uplift which occurred at the deposition site during the resedimentation of the Shoal Lake conglomerate.

CHAPTER VIII

PEBBLE DUCTILITY

Based on a previous assumption that the average original shape of the deformed pebbles of the same lithology at one outcrop is identical with that of another outcrop (pp. 123-124), the variation in the Z_f/d ratio of the same lithology must be attributed to some other factors than the original shape, such as ductility difference of the same rock type, local stress variation, or the construction of imaginary ellipsoid, etc.

Local stress variation is always an unknown parameter. Its effect is assumed to be very small and is being ignored for simplicity. The effect of the construction of imaginary ellipsoid probably is not very great, because the maximum error in the Z_f/d ratio as calculated from the most deviated datum tabulated on Table 3 is

$$\frac{0.213 - 0.204}{0.213} \times 100\% = 4\%$$

Therefore, it may be assumed that only ductility difference was responsible for the variation in the Z_f/d ratio. By comparing the tectonic strain in the common Z_f -direction of the deformed pebbles, we can obtain the ductility ratio of different pebbles, provided that the shortening strain developed homogeneously throughout the pebbles during deformation (p. 28).

In the case of the coaxial deformation of $Z_f || Z_t || Z_o$, the shortening strain is calculated using the following equation:

$$\frac{(Z_o/d) - (Z_f/d)}{(Z_o/d)} \times 100\% = \text{strain (\%)} \text{ in the } Z_o \text{-direction} \quad (8-1)$$

where the Z_o/d ratio can be computed from the following equation which is similar to Equation (3-5):

$$\ln (Z_o/d) = - (\ln a_o + 2 \ln b_o) / 3$$

$$\text{or } Z_o/d = \exp (-(\ln a_o + 2 \ln b_o) / 3) \quad (8-2)$$

Substituting the original axial ratios of the deformed pebbles (pp. 123-125) in Equation (8-2), we obtain the Z_o/d ratio for the volcanic pebbles 0.672, for the quartzose pebbles 0.591, and for the granitic pebbles 0.702. It is interesting to note that the original, undeformed Z_o/d ratio of the granitic pebbles is smaller than the final, deformed

$(Z/d)_{fc}$ ratio at localities 303, 304, 509, and 289 (see Table 4), indicating that the granitic pebbles of these localities probably were subjected to little or even no deformation. For this reason, the shortening strain of the granitic pebbles at these localities is set as zero (Table 10).

The computed shortening strains in the common Z_f -direction of the deformed pebbles in the map area are listed on Table 10, with the locality numbers given in sequence from east to west. Except for the eastern part of the area (Nos. 261-268) where the strains are generally higher than those to the west, the variation in shortening strain does not reveal any systematic gradient with respect to geographical position. The average shortening strain of the granitic pebbles is calculated directly from the average $(Z/d)_{fc}$ ratio on Table 4 and the Z_o/d ratio of 0.702, using Equation (8-1). This is because the strains of the granitic pebbles are set to zero on Table 10 for certain localities mentioned above, and so the average of individual strains has been altered.

Comparing the average shortening strains of the three major pebble lithologies, we get their ductility ratio as follows:

$$\begin{aligned} &\text{Volcanic pebble : quartzose pebble : granitic pebble} \\ &= 8.4 : 5.3 : 1.0 \end{aligned}$$

Table 10. Shortening strain of the deformed pebbles
in the Seine River area

Locality Number	Shortening strain, %		
	Granitic Pebbles	Quartzose Pebbles	Volcanic Pebbles
261	-	45.0	
263	-	45.2	
264	21.2	34.7	
265	12.0	28.1	
266	16.0	44.5	61.5
267	10.8	-	
268	7.0	40.3	
272	1.4	28.9	
273	8.8	32.7	
274	8.8	41.1	
277	6.3	37.7	
278	2.1	34.3	
279	4.7	40.9	
509	0.0	-	62.6
284	-	42.5	
286	12.5	-	
287	8.0	30.6	
289	0.0	33.7	
290	-		59.5
292	9.3		53.3
293	10.5		54.9
294	17.5		54.9
296	5.6		53.7
362	-		60.9
297	10.3		65.0
299	1.4		65.2
300	7.3		68.6
303	0.0		-
304	0.0		57.0
321	9.7		57.7
413	11.5		
Average	(7.4)*	37.3	59.6

* Calculated directly from the average $(Z/d)_{fc}$ ratio of the granitic pebbles (Table 4).

It should be noted that this ductility ratio should not be taken as a standard value for use in other areas, because it is dependent upon the particular P-T conditions and strain rate which prevailed in the map area; these can hardly be the same elsewhere.

It is worth mentioning here that on any section approximately parallel to the common Z_f -direction, the foliation density of matrix is highest when the exposed major axis (X') of an enclosed granitic pebble is normal to the foliation trace, but it is less intense for situations where the X' axis of the same pebble lithology is nearly parallel to the foliation trace. On the other hand, rarely have volcanic pebbles with their X' axis at a high angle to the foliation trace been observed. In general, volcanic pebbles lie parallel to the foliation plane unless they are folded around a bigger but less deformed pebble. Moreover, there is little change in foliation density between a volcanic pebble and its surrounding matrix. The strain gradient along a line through a volcanic pebble and its surrounding matrix probably is approximately zero. This implies that the volcanic pebble and matrix must be of similar ductility.

CHAPTER IX

SELECTIVE VEINING IN PEBBLES

One of the most interesting features connected with the deformed pebbles in the map area is the occurrence of cross-veins in certain pebbles. In general, veins are rarely developed in the pebbles on the south limb of the Seine River anticline, but on the north limb about three or four out of every ten granitic pebbles contain one or more veins. Veins also are observed in some quartzite pebbles, but such occurrences are not common. It is clear in the field that less deformed pebbles have a better development of veins than more deformed ones. For instance, the slate and volcanic pebbles which show the strongest deformation among all kinds of pebbles, commonly are devoid of any veinlet. Furthermore, the matrix, which has suffered at least the same deformation as volcanic pebbles, contains no veins similar to those in pebbles, although one vein (among more than 200 counts) in a granitic pebble was observed to extend into the matrix (Plate 7(A)).

Plate 7

(A) One vein in a granitic pebble extends into the matrix.

(B) Offset along the shear-fracture trace, which usually is
straight and smooth.



(A)



(B)

The walls of veins are distinguished into two types of fracture, viz. extensional fracture and shear fracture. Extensional fractures are those with irregular and rough contact between vein and host pebble, whereas the walls of a shear fracture are straight and smooth. Moreover, a shear fracture commonly shows offset along the fracture trace (Plate 7(B)), while the trace of an extensional fracture usually lies close to the direction of maximum tectonic shortening (Plate 8(A)). By comparison, veins of the shear-fracture type are rare. Plate 8(B) shows that a transverse vein of the extensional-fracture type is cut off by an oblique vein of the shear-fracture type. They might have developed in response to the same stress system but with the shear fracture growing subsequently to the extensional fracture.

Veins have never been observed in any transverse granitic pebble which has an exposed major axis (X') at a high angle to the foliation trace and has an apparent axial ratio, X'/Z' , equal to 1.5 or more. This might indicate that rupture of granitic pebble is conditional upon the original X_0 -orientation relative to the tectonic strain axes.

1. VEIN ORIENTATION

Wherever a section of any orientation is cut through a rock containing a number of pebbles with veins of the extensional-fracture type, most of the veins appear to align subperpendicular to or make a high angle with the foliation trace.

Plate 8

(A) Veins of the extensional-fracture type commonly lie perpendicular to the foliation trace.

(B) A transverse vein of the extensional-fracture type is cut off by an oblique vein of the shear-fracture type.



(A)



(B)

A nicely exposed section at locality 297 containing eight granitic pebbles with veins of the extensional-fracture type, is demonstrated in Figure 27. The less deformed pebbles (Nos. 4-8) maintain their elongation roughly parallel to the bedding trace, whereas the more deformed ones (Nos. 1-3) are nearly parallel to the foliation trace (Figure 27, (A) and (B)).

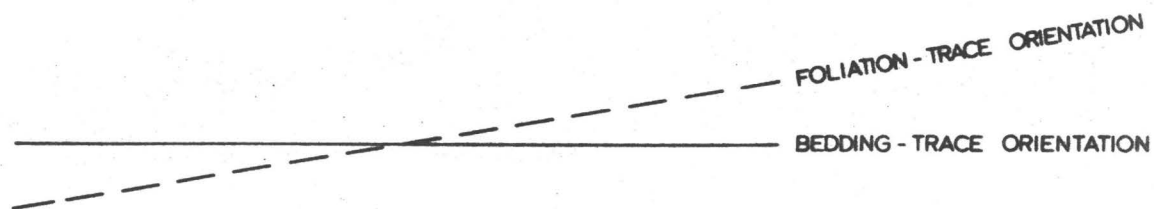
In Figure 27(B), the apparent axial ratio (X'/Z') of the deformed pebbles is plotted against both the orientation of the vein trace and the X' -direction of the corresponding pebbles. If we assume that the least principal stress axis is parallel to the mineral lineation and that the greatest principal stress axis is normal to the penetrative foliation plane, then we would expect that extensional fractures, if any, occur normal to the mineral lineation, considered statistically. In Figure 27(B), however, all the vein traces lie on the right-hand side of the trace of a plane normal to the mineral lineation. This might imply a reorientation of the forces which produced the finite foliation and mineral lineation in the rocks after the development of extensional fractures had completed.

In Figure 27(C), the X'/Z' ratio of the same pebbles is plotted against the angle α between the X' -direction and the vein trace. The distribution has a negative slope; i. e., the more deformed pebbles

Figure 27. Orientation of eight pebbles with veins of the extensional-
fracture type at locality 297. See the text for explanation.

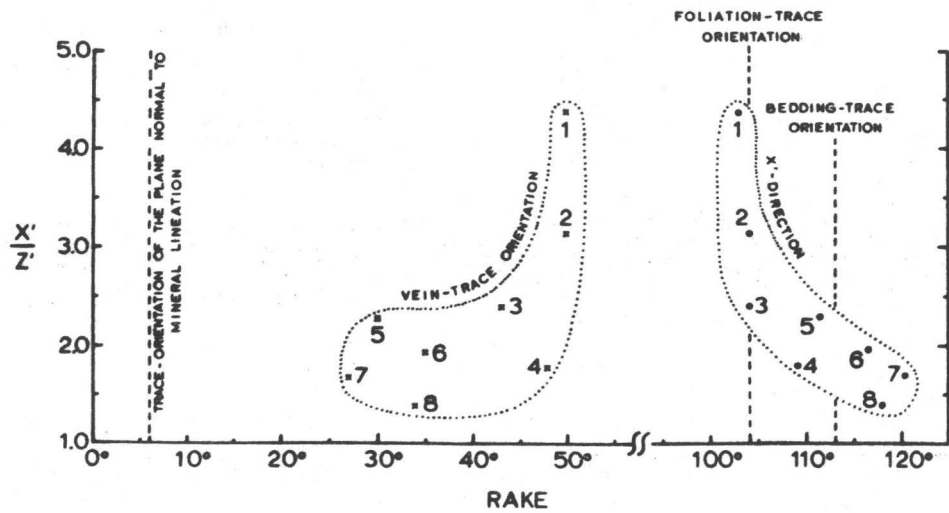


0 10 20 30 cm

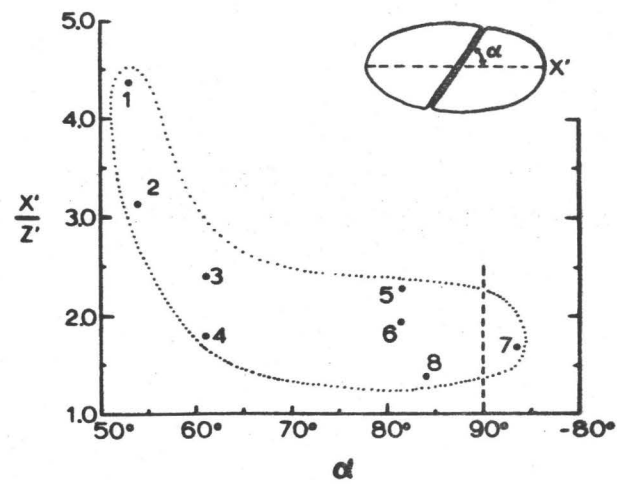


(A)

(B)



(C)



show a smaller α -angle (cf. the two dashed lines in Ramsay's (1967, p. 92) Figure 3-30), with an exception that any one pebble (not in this diagram), which had its three principal axes parallel to those of the tectonic strain ellipsoid and which had its vein perpendicular to the X_t -axis, would have maintained $\alpha = 90^\circ$ regardless of the deformation intensity.

2. CRYSTALLOGRAPHIC FABRICS OF QUARTZ

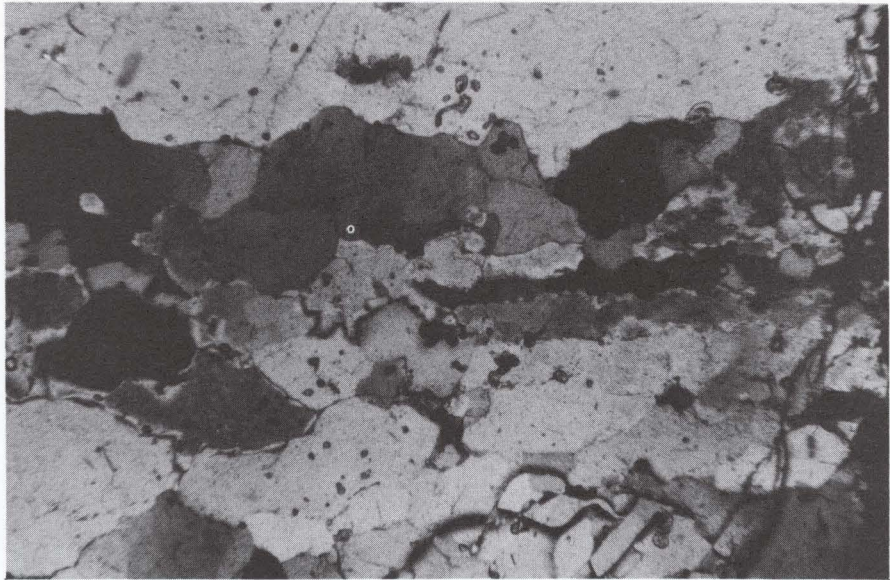
In order to get rid of the effect of original orientation on the final pebble fabric, only those pebbles which show special coaxial superpositions of $X_f \parallel X_t$, $Y_f \parallel Y_t$, and $Z_f \parallel Z_t$, are subjected to petrofabric analysis of quartz in both vein and host pebble.

Under the microscope, the constituent minerals of vein in deformed pebble of any lithology are mainly quartz with a small amount of calcite. These minerals form rod-like, columnar grains (Plate 9(A)), which are roughly parallel to the external mineral lineation surrounding the pebble. The cross-sections of these columnar grains generally show elliptical to irregular form (Plate 9(B)). The columnar grains and/or their aggregates commonly reach from side to side of the vein. Some of the quartz grains are found to have grown in crystallographical continuity across the vein from either a pure

Plate 9

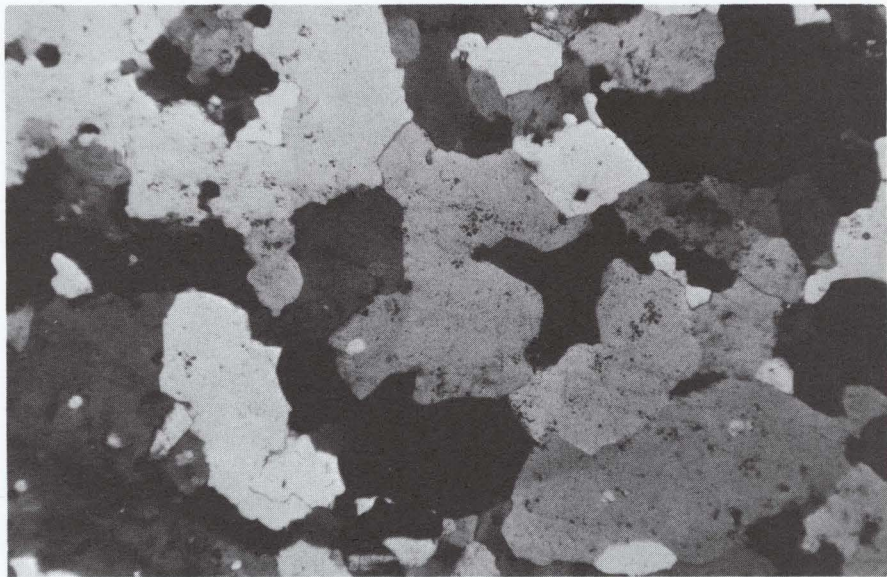
(A) Vein quartz shows rod-like columnar form on sections parallel to the direction of principal tectonic elongation. Crossed polarizers.

(B) Vein quartz shows irregular to crude elliptical form on sections perpendicular to the direction of principal tectonic elongation. Crossed polarizers.



(A)

1 mm



(B)

1 mm

quartz or a quartz pseudomorph of plagioclase in the host pebble (Plate 10(A)).

The optical orientations of quartz in both vein and pebble itself were determined with a universal stage in an attempt to investigate the geometric relationship between mesoscopic structures and quartz crystallographic fabrics. Lower hemisphere equal-area plots of quartz c-axis orientations are shown on Figure 28.

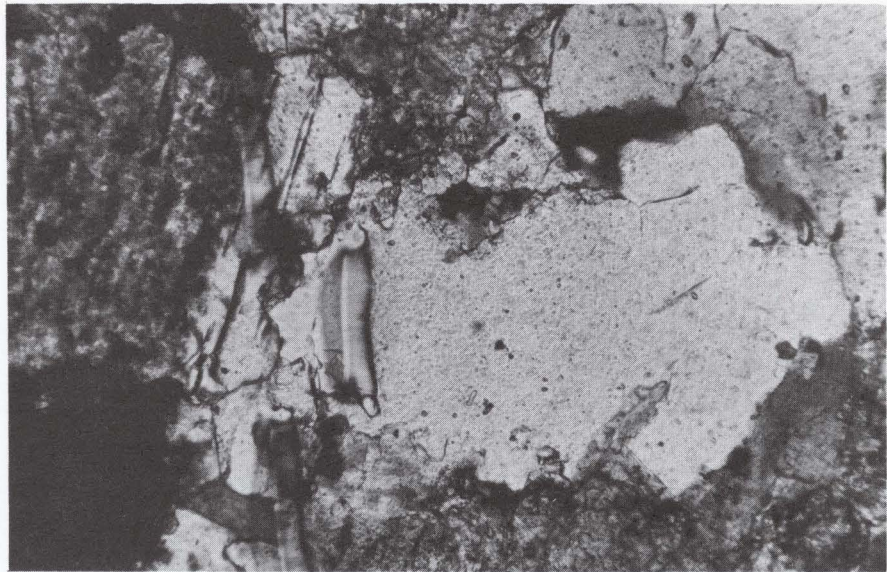
The c-axes of the constituent quartz in vein No. V8B show a very weak preferred orientation which seems to show a partial small-circle girdle at an angle of approximately 45° to the X_t -axis — the direction of maximum tectonic elongation. In another vein, No. V8A, of the same pebble, the quartz c-axes may be envisaged as showing composite small-circle girdles at angles of 45° and 65° to the X_t -axis and the Z_t -axis, respectively, although only 52 crystals can be measured in the thin section of that vein. In a third thin section made from sample No. V17B which does not show visible columnar form of the constituent minerals in the vein, the quartz optical fabric is a very broad small-circle girdle (20° - 70°) around the Z_t -axis. But the relic of the partial girdle around the X_t -axis at an angle of about 52° can be detected only with uncertainty.

In the pebble itself, quartz axial fabrics show interesting features which have never been reported before. Plate 10(B) shows

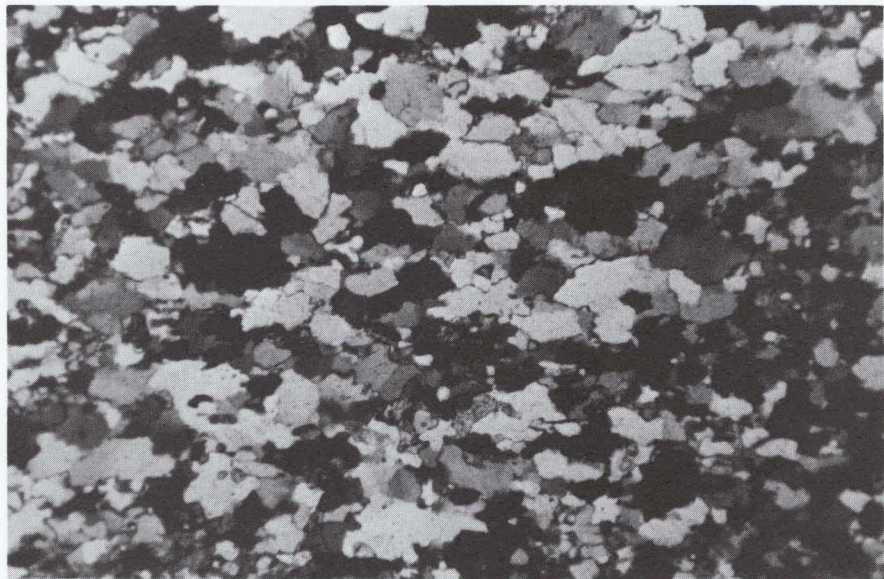
Plate 10

(A) Plagioclase of host pebble (on the left-hand side) is partly replaced by vein quartz which shows crystallographical continuity from the quartz pseudomorph of plagioclase to non-cleavage quartz. Crossed polarizers.

(B) Petrofabric of a quartzite pebble on section subparallel to the $X_t Z_t$ plane. Most individual quartz grains are elongated and parallel to the X_t -direction (E-W line of the photograph). Crossed polarizers.



(A) 0.25 mm



(B) 1 mm

Figure 28. Quartz c-axis fabrics.

V8B, 176 grains in vein; contours, 3.4%, 2.3%,

1.1% per 1% area.

V8A, 52 grains in vein.

V17B, 250 grains in vein; contours, 2% and 0.8%

per 1% area.

P13A and P13B, 200 grains per section in pebble;

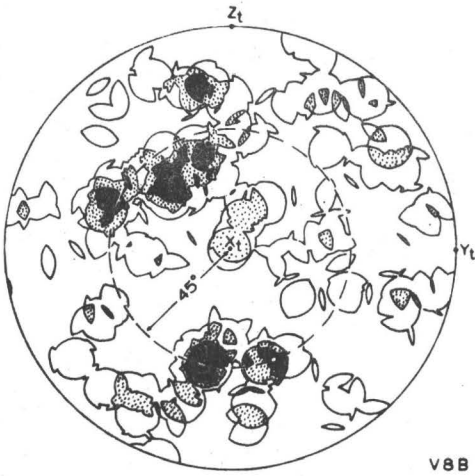
contours, 3% and 1% per 1% area.

P14, 200 grains in pebble; contours, 3%, 2%, 1%

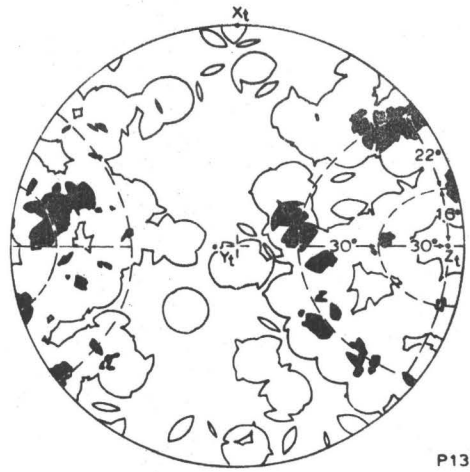
per 1% area.

VEIN

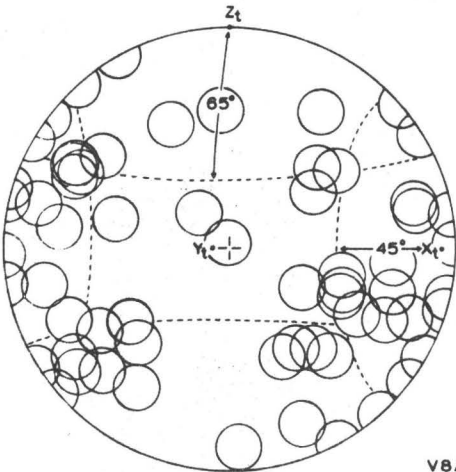
PEBBLE



V8B



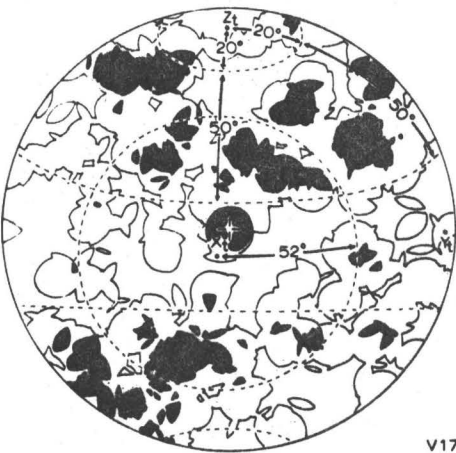
P13A



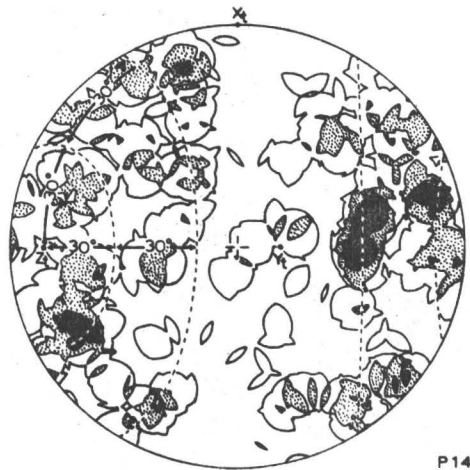
V8A



P13B



V17B



P14

the petrofabric of a quartzite pebble from locality 304. Here the quartz c-axes form double elliptical girdles (though incomplete) around the Z_t -axis (Figure 28, P13A). On the $Y_t Z_t$ plane the c-axis girdles make angles of 30° and 60° to the X_t -axis, whereas on the $X_t Z_t$ plane the angles are 16° and 38° . On another section, P13B, which is cut at right angle to section P13A in the same specimen, quartz c-axes roughly show double partial girdles of elliptical shape around the Z_t -axis, but they are less clear than those of P13A. On the $X_t Z_t$ plane of section P13B, the double girdles make angles of 25° and 55° to the Z_t -axis; while on the $Y_t Z_t$ plane the angles are 30° and 60° , same as those of P13A. Section P14 is made from a quartzite pebble at locality 279 where the mineral lineations were hardly recognized on strongly foliated rock, and so the tectonic strain ellipsoid there is considered as close to the pancake-type of $X_t = Y_t \gg Z_t$. The microfabric of the quartz c-axes seems to show double girdles with a symmetry similar to that of the postulated strain ellipsoid. The double girdles make angles of 30° and 60° around the Z_t -axis.

3. INTERPRETATION

It is considered that the development of veins in the less deformed pebbles (mainly granitic) was synchronous with a simultaneous deformation and metamorphism, proceeding by fracturing, followed by

simultaneous pull-apart of the pebble portions and emplacement of vein by a process of diffusion of soluble quartz from the immediate neighbourhood into the embryonic fractures.

The content of granitic pebbles in the Shoal Lake conglomerate commonly does not exceed 15%. Rarely are the granitic pebbles observed in contact with each other. The brittle failure which has occurred in this small volume fraction of dispersed granitic pebbles can best be explained on the basis of Drucker's (1966, pp. 891-893) analysis (see also Rector, 1970, pp. 135-137).

At a certain early stage of the deformation which probably was caused by a regional compressive stress system, all the conglomerates became ductile except for the dispersed granitic pebbles. Perhaps rigid-body rotation, if any, of the granitic pebbles occurred at this stage. With a continued application of compressive stress, the granitic pebbles remained elastic and deformed much less than the already ductile matrix and other constituents of the conglomerate. So the granitic pebbles did not expand laterally as much as the surrounding materials. The movement of these ductile materials probably was under conditions such that a moderate to high intergranular cohesion was maintained between the moving materials and the granitic pebbles (Stauffer, 1970, p. 504). This generated a tensile stress on the granitic

pebbles, which was balanced by a compressional stress in the ductile materials. The tensile stress might exceed the tensile strength of the granitic pebbles at some advanced stage of the deformation, resulting in extensional fracturing of the pebbles. Due to the continued movement of ductile materials, the less-deformed granitic pebbles must have carried more than their share of the compressional load. At a certain further advanced stage when some of the granitic pebbles became a bit ductile, the greatest shearing stress of the same stress system might exceed the cohesive shearing strength of the granitic pebbles, resulting in shear fracturing. The extensional fractures probably were originally normal to the least principal stress axis in a statistical sense. But a later, slightly reoriented, stress system caused the homogeneous deformation of all the pebbles and produced the finite penetrative foliation and mineral lineation in the rocks.

During the deformation, the already ruptured pebbles were pulled apart by the continued tensile stress. However, it seems unlikely that the fractures had ever been devoid of material, because commonly the columnar quartz grains extend in crystallographic continuity from wall to wall of the fracture, which might suggest that the crystallizing quartz grew in step with the dilation of the fracture. This is also an interpretation which has long been held by many other authors (Ramberg, 1961; Carstens, 1966; Roberts, 1969).

The optical orientation of vein quartz probably was determined by the chance orientation of the first nuclei which formed on the wall of fracture, but the direction of fast growth kept pace with the dilation, might have slightly favored the direction at 45° to the c-axis, as that revealed in section V8B of Figure 28. The resultant fabric of quartz c-axes would belong to the cigar-type of $X \gg Y = Z$, similar to the columnar form of the individual quartz grain. The orientation of quartz c-axes discussed above is assumed to have grown freely under a "pressure shelter" within the fracture of a then plastically undeformed, but already ruptured, pebble.

If the host pebble was deformed to a certain extent, the pressure shelter within the fracture walls of the host pebble would not have been strong enough to protect completely the vein quartz from suffering strain, and the final fabric of quartz c-axes would have been a mixture of fast-growth orientation and strain geometry. In the map area, the deformation path has a slope of $K = 0.274$ (p. 123), so the strain ellipsoid is of the flattening type ($X_t > Y_t \gg Z_t$). Locally strain ellipsoid of the pancake type ($X_t = Y_t \gg Z_t$, or $K = 0.0$) may be expected. Vein quartz affected by a pancake-type deformation would probably form composite fabric as that shown in section V8A of

Figure 28; i.e., a small-circle girdle around the X_t -axis and another around the Z_t -axis.

If the host pebble was severely deformed, the pressure shelter would be completely useless. Then the micro fabric of quartz c-axes in the vein would have shown a symmetry roughly similar to that of the deformed pebble in the case of coaxial deformation (see section V17B of Figure 28). And the development of columnar forms of the constituent minerals in the vein would also be impossible.

Discussion of recrystallization mechanisms of quartz seems to be presently speculative. However, regardless of the actual deformation mechanism, the quartz axial fabric of deformed pebbles seems to show a consistent symmetry which can be compared to that of the tectonic strain ellipsoid detected from mesoscopic structures such as coaxially deformed pebble, foliation, mineral lineation, etc. Where the mesoscopic structures show a strain ellipsoid of the pancake type ($X_t = Y_t \gg Z_t$, or $X_t \gg Z_t$), the quartz c-axes of deformed pebbles would likely form double small-circle girdles around the Z_t -axis — the direction of maximum tectonic shortening (see section P14 of Figure 28). As the elongation in the X_t -axis of the tectonic strain ellipsoid develops; i.e., the strain ellipsoid becomes the flattening type ($X_t > Y_t \gg Z_t$, or $X_t \gg Z_t$), the double girdles of quartz c-axes

around the Z_t -axis would become elliptical in shape with its minor axis lying in the $X_t Z_t$ plane (sections P13A and P13B of Figure 28).

CHAPTER X

CONCLUSION

Previous controversies of the Couthiching problem arose mainly from different judgements by various workers of the rocks exposed along the shore of Shoal Lake. In this study the present writer has uncovered numerous new field data, mostly previously overlooked or previously inaccessible, which warrant a new interpretation of the stratigraphic sequence. The term Couthiching series may be retained for those sedimentary rocks and local greenstones within them, which underlie the thick sequence of greenstones known as the Keewatin series. The local greenstones within the Couthiching series thus defined, previously have been regarded as Keewatin and so the relative position between the Couthiching and the Keewatin often has been confused.

Several improved methods of analyzing deformed pebbles are introduced, which under certain circumstances enable one to determine the tectonic strain ellipsoid and the original orientation and shape of deformed pebbles, from the final pebble-fabric. To determine the

original orientation and shape of deformed pebbles, it is necessary to have some ideas of the general fabric of the undeformed conglomerate. If the original pebbles had a random orientation and the final deformed pebbles are extractable, then we can determine the original pebble shape and the tectonic strain ellipsoid from certain coaxially deformed pebbles. On the other hand, if the extractable, final, deformed pebbles had an original planar fabric, we may be able to determine the original shape and orientation of the deformed pebbles by finding two sections at one outcrop, one parallel and the other perpendicular, to the original planar fabric. If either of these two sections is not parallel to two principal strain axes, we can use the method developed in Chapter IV of this thesis to determine the tectonic strain ellipsoid from two apparent strain-axial-ratios computed from the measurements of deformed pebbles on these two sections. In the case of unextractable deformed pebbles, determination of both the final shape and the original shape and orientation of the deformed pebbles, as well as their tectonic strain ellipsoid, requires some mental acrobatics. The procedure given in Chapter VI of this thesis presents an approximation method to solve this difficult problem. The result has turned out to be quite conformable with what has been calculated from a special section on which coaxially deformed pebbles were measured.

In the map area, the tectonic strain ellipsoid belongs to the flattening type with three principal axes of $X_t > Y_t \gg Z_t$, where the $(\ln(X_t/Y_t))/(\ln(Y_t/Z_t))$ ratio, K , has a calculated value of 0.274. Except for the eastern part of the area where the strains generally are greater than those to the west, the variations in shortening strain and average shape of the final deformed pebbles of the same lithology at different localities are found to have no systematic change with respect to their geographical position.

Assuming that pebbles of a single lithology have an identical, average, original shape at different localities and that local variation of the stresses responsible for the pebble deformation is negligible, the variation in the final orientation and shape of the deformed pebbles is attributed to the controls of original orientation before plastic deformation and ductility difference. By comparing the average shape of the final deformed pebbles at one outcrop with their calculated original shape in the common direction of coaxial superposition of the strain ellipsoid upon the pebbles, we can compute the strain percentages of the deformed pebbles in that particular direction. Furthermore, variation in strain in the same direction with respect to different pebble lithologies provides the contrast of ductility between different rock types for the conditions under which deformation took place.

Selective cross-veins in the granitic pebbles are found to have developed mainly in extensional fractures and partly in shear fractures with continuous dilation accompanying crystallization of vein minerals after fracturing. The vein quartz of columnar form probably grew in pace with the dilation of fracture through a process of diffusion of soluble quartz supplied from the immediate neighbourhood of the fractured pebble. In the case of the nearly pancake-type deformation ($X_t = Y_t \gg Z_t$) at some localities of the map area, double small-circle girdles of the quartz c-axes around the direction of maximum tectonic shortening at angles of 30° and 60° are reported for the first time in deformed quartzite pebbles. The double girdles shrink in the $X_t Z_t$ plane as the elongation in the X_t -direction develops.

Griggs et al. (1960) have shown that at 5-kilobar confining pressure and 500°C temperature, granitic rock remains elastic up to a differential longitudinal stress of more than 10 kilobars. In other words, the maximum pressure required to deform permanently a granitic rock under such a condition must exceed 15 kilobars. In the map area, the predominant mineral assemblage of quartz-albite-chlorite can hardly be assigned to a grade higher than the middle greenschist facies (Turner and Verhoogen, 1960, pp. 533-537). In fact, no garnet or any mineral assemblage indicating a higher grade than the biotite zone has been observed. So it is assumed that 400°C and 5 kilobars

are the temperature and pressure maxima* (Turner and Verhoogen, 1960, p. 534) having prevailed in the map area. Considering the result of Griggs et al., we cannot expect the granitic pebbles to be deformed plastically in the laboratory under conditions of 5-kilobar pressure and 400°C temperature. It follows that the only plausible explanation for the ductile deformation of the granitic pebbles is a very low strain rate. If we assume the episode of deformation accompanying a regional metamorphism to be the order of 2 to 10 million years in length (Sutton, 1965, p. 42), then the strain rate for the volcanic pebbles of average 60% shortening is $(1 \text{ to } 0.2) \times 10^{-14}$ /sec.; for the quartzose pebbles of average 37% shortening is $(6 \text{ to } 1.2) \times 10^{-15}$ /sec.; and for the granitic pebbles of average 7% shortening is $(1 \text{ to } 0.2) \times 10^{-15}$ /sec.

In view of the fact that both pebble size and gross thickness of the conglomerate beds are much greater in the north limb of the Seine River anticline than those in the south limb, and that the cross-lamination preserved in the arenites underlying the conglomerate sequence indicates a regional flow direction of the paleocurrents towards the present south, a northern source of the Archean sediments in the map area can be inferred. Moreover, the appearance of both turbidites and

* Here the maximum pressure refers to the load pressure augmented by an increment of tectonic overpressure (Turner, 1968, p. 60).

subsequent thick conglomerate beds after a prolonged period of the deposition of the thick Coutchiching fine-grained sediments, might imply some uplifting movements in the source area to the north and subsidence at the deposition site. These movements probably were the first signs of the orogeny occurring around the time of 2.75 b. y. ago; during the orogeny, both the Coutchiching and the Keewatin rocks in the map area were first folded and the pebbles in the conglomerate beds were then deformed by subsequent, continuous compression.

BIBLIOGRAPHY

- Cailleux, A. et Tricart, J. (1965): Initiation a l'étude des sables et des galets, v. 3, 202 p. Centre de Documentation Universitaire, Paris.
- Carstens, H. (1966): Deformation in vein genesis. Norsk Geol. Tidsskr., 46:299-307.
- Cloos, E. (1947): Oolite deformation in the South Mountain fold, Maryland. Geol. Soc. Am., Bull., 58:843-918.
- Donath, F.A. (1963): Fundamental problems in dynamic structural geology, pp. 83-103 in Donnelly, T.W. (editor): The earth science - problems and progress in current research; Univ. Chicago Press, Chicago, 195 p.
- Dott, R.H., Jr. (1963): Dynamics of subaqueous gravity depositional processes. Am. Assoc. Petrol. Geol., Bull., 47:104-128.
- Drucker, D.C. (1966): The continuum theory of plasticity on the macro-scale and the microscale. Jour. Materials, 1:873-910.
- Dunnet, D. (1969): A technique of finite strain analysis using elliptical particles. Tectonophysics, 7:117-136.

- Flinn, D. (1956): On the deformation of the Funzie conglomerate, Fetlar, Shetland. *Jour. Geol.*, 64:480-505.
- _____ (1962): On folding during three-dimensional progressive deformation. *Quart. Jour. Geol. Soc. Lond.*, 68:385-433.
- Gay, N.C. (1968): Pure shear and simple shear deformation of inhomogeneous viscous fluids. *Tectonophysics*, 5:211-234 and 295-302.
- _____ (1969): The analysis of strain in the Barberton Mountain land, Eastern Transvaal, using deformed pebbles. *Jour. Geol.*, 77:377-396.
- Griggs, D. T., Turner, F. J., and Heard, H. (1960): Deformation of rocks at 500° to 800°C. *Geol. Soc. Am., Mem.* 79, pp. 41-48.
- Hart, S.R. and G. L. Davis (1969): Zircon U-Pb and whole rock Rb-Sr ages and early crustal development near Rainy Lake, Ontario. *Geol. Soc. Am., Bull.*, 80:595-616.
- Haughton, S. (1856): On slaty cleavage and the distortion of fossils. *Phil. Mag.*, 12:409-421.
- Johansson, C.E. (1965): Structural studies of sedimentary deposits. *Geologiska Föreningens i Stockholm Förhandlingar*, 87:3-61.
- Lindsay, J. F. (1966): Carboniferous subaqueous mass-movement in the Manning-Macleay Basin, Kempsey, New South Wales. *Jour. Sed. Petrology*, 36:719-732.

- Lindsay, J. F. (1968): The development of clast fabric in mudflows.
Jour. Sed. Petrology, 38:1242-1253.
- _____, Summerson, C. H., and Barrett, P. J. (1970): A long-axis
clast fabric comparison of the Squantum "tillite", Massa-
chusetts and the Gowganda formation, Ontario. Jour. Sed.
Petrology, 40:475-479.
- Lawson, A. C. (1888): Report of the geology of the Rainy Lake region.
Geol. & Nat. Hist. Surv. Can., 190 p.
- _____, (1913): The Archaean geology of Rainy Lake, restudied.
Geol. Surv. Can., Mem. 40, 115 p.
- Merritt, P. L. (1934): Seine-Coutchiching problem. Geol. Soc. Am.,
Bull., 45:333-374.
- Nadai, A. (1950): Theory of flow and fracture of solids. McGraw-Hill,
New York, 572 p.
- Pettijohn, F. J. (1957): Sedimentary rocks, 2nd ed. Harper &
Brothers, New York, 718 p.
- Ramberg, H. (1961): A study of veins in Caledonian rocks around
Trondheimfjord, Norway. Norsk Geol. Tidsskr., 24:
1-43.

- Ramsay, J.G. (1964): Progressive deformation in tectonic processes.
Am. Geophys. Union, Trans., 45:106.
- _____ (1967): Folding and fracturing of rocks. McGraw-Hill,
New York, 568 p.
- Rector, R.J. (1970): An experimental investigation into the influence
of environmental and fabric parameters on the deformational
behaviour of sandstones. Unpublished Ph.D. thesis, Mc-
Master University, 190 p.
- Roberts, D. (1969): Preferential veining in a conglomerate from the
Trondheim region, central Norway. Geol. Rundschau,
Band 58, pp. 862-866.
- Sorby, H.C. (1853): On the origin of slaty cleavage. Edinb. Phil.
Jour., 55:137-148.
- Stauffer, M.R. (1970): Deformation textures in tectonites. Can. Jour.
Earth Sci., 7:498-511.
- Sutton, J. (1965): Some recent advances in our understanding of the
controls of metamorphism, pp. 22-45 in Pitcher, W.D.
and Flinn, G.W. (ed.): Controls of metamorphism.
Oliver & Boyd, Edinburgh, 368 p.
- Turner, F.J. (1968): Metamorphic Petrology. McGraw-Hill, New
York, 403 p.

- Turner, F.J. and Verhoogen, J. (1960): Igneous and metamorphic petrology, 2nd ed. McGraw-Hill, New York, 694 p.
- Van Hise, C.R., Adams, F.D., Bell, R., Lane, A.C., Leith, C.K., and Miller, W.G. (1905): Report of the special committee for the Lake Superior region. Jour. Geol., 13:89-104.
- Zingg, T. (1935): Beitrag zur Schotteranalyse. Schweiz. Mineral. Petrog. Mitt., 15:39-140.

APPENDIX

A. Derivation of Equations Representing the Contours of

$$X_f/d, Y_f/d, \text{ and } Z_f/d$$

By definition (see p. 34), we have

$$d = (X_f Y_f Z_f)^{1/3}$$

which can be transformed into the following relationships:

$$d^{-1} = (X_f Y_f Z_f)^{-1/3}$$

$$\text{or } d^{-3} = (X_f Y_f Z_f)^{-1} \quad (\text{A-1})$$

Multiplying by X_f^3 , Y_f^3 , and Z_f^3 , respectively, with both sides of Equation (A-1), we get

$$(X_f/d)^3 = X_f^3 / (X_f Y_f Z_f) \quad (\text{A-2})$$

$$(Y_f/d)^3 = Y_f^3 / (X_f Y_f Z_f) \quad (\text{A-3})$$

$$\text{and } (Z_f/d)^3 = Z_f^3 / (X_f Y_f Z_f) \quad (\text{A-4})$$

From Equation (A-2),

$$X_f^2/Y_f^2 = (Z_f/Y_f)(X_f/d)^3$$

$$\text{or } a_f^2 = b_f^{-1} (X_f/d)^3$$

$$\text{so } 2 \ln a_f = -\ln b_f + 3 \ln (X_f/d)$$

$$\text{or } \ln a_f = -\frac{1}{2} \ln b_f + \frac{3}{2} \ln \frac{X_f}{d} \quad (3-6)$$

From Equation (A-3),

$$X_f/Y_f = (Y_f/Z_f)(Y_f/d)^{-3}$$

$$\text{or } a_f = b_f (Y_f/d)^{-3}$$

$$\text{so } \ln a_f = \ln b_f - 3 \ln (Y_f/d) \quad (3-7)$$

From Equation (A-4),

$$X_f/Y_f = (Z_f^2/Y_f^2)(Z_f/d)^{-3}$$

$$\text{or } a_f = b_f^{-2} (Z_f/d)^{-3}$$

$$\text{so } \ln a_f = -2 \ln b_f - 3 \ln (Z_f/d) \quad (3-5)$$

B. Proof of Identical Shape for Parallel Cross-Sections through an Ellipsoid

First of all, let us establish an xyz-coordinate system with one axis, say, the z-axis, perpendicular to the parallel sections. The general equation of an ellipsoid in this system is

$$Ax^2 + By^2 + Cz^2 + Dxy + Eyz + Fzx + Gx + Hy + Kz + L = 0 \quad (\text{B-1})$$

Suppose we have two sections cut through this ellipsoid:

$$z = M \quad (\text{B-2})$$

$$z = N \quad (\text{B-3})$$

Substituting Equations (B-2) and (B-3), respectively, in Equation (B-1),

we obtain

$$Ax^2 + Dxy + By^2 + (G+FM)x + (H+EM)y + (L+CM^2+KM) = 0 \quad (\text{B-4})$$

and $Ax^2 + Dxy + By^2 + (G+FN)x + (H+EN)y + (L+CN^2+KN) = 0 \quad (\text{B-5})$

These are two general equations of the second degree, which represent the two elliptical cross-sections of the ellipsoid in the xy-coordinate system.

In order to reduce the general equations to the standard form of ellipses, we can first rotate the coordinate axes to remove the xy-term and second, complete the squares of the transformed equations. Let the rotation angle between the x-axis and the new x'-axis be θ so that the angle between the x'-axis and the y-axis is $(90^\circ - \theta)$ but not $(90^\circ + \theta)$ and that

$$\tan 2\theta = D/(A-B) \quad (\text{B-6})$$

$$\text{Set } \tan \theta = \frac{S}{Q} \text{ and } (Q^2 + S^2)^{1/2} = R$$

where S can be any value.

$$\text{Hence } \sin \theta = S/R$$

$$\cos \theta = Q/R$$

$$\text{and } \tan 2\theta = \frac{2 \tan \theta}{1 - \tan^2 \theta} = \frac{2 S/Q}{1 - S^2/Q^2}$$

$$\text{or } \tan 2\theta = 2QS/(Q^2 - S^2) \quad (\text{B-7})$$

The equations of the transformation, thus, become

$$\begin{cases} x = \frac{1}{R} (Qx' - Sy') \\ y = \frac{1}{R} (Sx' + Qy') \end{cases} \quad (\text{B-8})$$

From Equations (B-6) and (B-7), we know

$$D = \frac{2QS(A-B)}{Q^2 - S^2} \quad (\text{B-9})$$

Substituting Equations (B-8) and (B-9) in Equations (B-4) and (B-5),

respectively, we obtain

$$A'x'^2 + B'y'^2 + G'_1x' + H'_1y' + L'_1 = 0 \quad (\text{B-10})$$

$$A'x'^2 + B'y'^2 + G'_2x' + H'_2y' + L'_2 = 0 \quad (\text{B-11})$$

where

$$A' = \frac{1}{R^2} \left[Q^2 A + S^2 B + \frac{2Q^2 S^2}{Q^2 - S^2} (A-B) \right]$$

$$= (Q^2 A - S^2 B) / (Q^2 - S^2)$$

$$B' = \frac{1}{R^2} \left[S^2 A + Q^2 B - \frac{2Q^2 S^2}{Q^2 - S^2} (A-B) \right]$$

$$= (Q^2 B - S^2 A) / (Q^2 - S^2)$$

and so on.

Equations (B-10) and (B-11) represent the two elliptical cross-sections of the ellipsoid with reference to the new $x'y'$ -system, in which there is no $x'y'$ -term indicating that the principal axes of the ellipses are parallel to the new coordinate axes. On completing the squares in Equations (B-10) and (B-11), we get

$$A'(x'+V_1)^2 + B'(y'+W_1)^2 = U_1$$

and $A'(x'+V_2)^2 + B'(y'+W_2)^2 = U_2$

which can be reduced to the standard form as

$$\frac{(x'+V_1)^2}{U_1/A'} + \frac{(y'+W_1)^2}{U_1/B'} = 1 \quad (B-12)$$

$$\text{and } \frac{(x'+V_2)^2}{U_2/A'} + \frac{(y'+W_2)^2}{U_2/B'} = 1 \quad (\text{B-13})$$

The above two equations represent the two elliptical cross-sections of the ellipsoid in the standard form. Both have the same axial ratio of $(B'/A')^{1/2}$.

In a special case, such as the parallel sections perpendicular to one axis, say, the C-semiaxis, of an ellipsoid with three principal axes of $2A > 2B > 2C$, the equation in the standard form of this ellipsoid is

$$\frac{x^2}{A^2} + \frac{y^2}{B^2} + \frac{z^2}{C^2} = 1$$

The cross-section by the plane $z = M$ (any section perpendicular to the C-semiaxis) is the ellipse

$$\frac{x^2}{A^2} + \frac{y^2}{B^2} = 1 - \frac{M^2}{C^2}$$

which can be reduced to the standard form as

$$\frac{x^2}{A^2(1-M^2/C^2)} + \frac{y^2}{B^2(1-M^2/C^2)} = 1$$

whose axial ratio, $\frac{A(1-M^2/C^2)^{1/2}}{B(1-M^2/C^2)^{1/2}} = \frac{A}{B}$, is equal to that

of the two principal axes parallel to this section.

C. Calculation of a_o , b_o , a_t , and b_t
for the Granitic and Quartzose Pebbles

Unlike the volcanic pebbles, the granitic and quartzose pebbles were not observed at fold hinges. Coaxially deformed pebbles, which can be found in fold limbs, belong to the coaxial superposition of $Z_f || Z_t || Z_o$. It follows that there will not be enough simultaneous equations which can be used to solve the problem (pp. 87-92 and p.103). Therefore, let us assume that the granitic and quartzose pebbles have undergone the same deformation path (actually the same K-value) as the volcanic pebbles within the same stress system. The deformation path, line $V_o V_m$ in Figure 25, of the volcanic pebbles has a slope of $K=0.274$ and can be represented by

$$\ln a_f = 0.274 \ln b_f + 0.265 \quad (6-37)$$

(I) Granitic Pebbles

In Figure 25, let us draw two lines parallel to line $V_o V_m$ and touching the circumscribing polygon of the granitic pebbles. One line which passes through point 413G and almost coincides with line $V_o V_m$, is simply represented by line $V_o V_m$. The other line which passes through point 274G(0.833, -0.329) can be shown as

$$\ln a_f - (-0.329) = 0.274(\ln b_f - 0.833)$$

$$\text{or } \ln a_f = 0.274 \ln b_f - 0.557 \quad (\text{C-1})$$

On the other hand, draw two lines parallel to the Z_f/d contours and touching the same polygon at points 264G and 303G. The line passing through point 264G(0.793, 0.191) is given by

$$\ln a_f - 0.191 = -2 (\ln b_f - 0.793) \quad (\text{C-2})$$

where -2 is the slope of any Z_f/d contour in a logarithmic deformation plot (see pp. 34-35). Equation (C-2) can be written as

$$\ln a_f = -2 \ln b_f + 1.777 \quad (\text{C-3})$$

The line passing through point 303G(0.385, 0.215) is

$$\ln a_f - 0.215 = -2 (\ln b_f - 0.385)$$

$$\text{or } \ln a_f = -2 \ln b_f + 0.985 \quad (\text{C-4})$$

Solving the simultaneous Equations (6-37) and (C-3), we get $\ln b_f = 0.665$ and $\ln a_f = 0.447$. Coordinates (0.665, 0.447) are plotted as point G_m in Figure 25. Similarly, solving the simultaneous Equations (C-1) and (C-3), we obtain $\ln b_f = 1.026$ and $\ln a_f = 0.275$. Coordinates (1.026, -0.275) are plotted as point G_i . Hence the line of Equation (C-3) represent the lowest Z_f/d contour of the granitic pebbles, which has suffered the highest shortening strain among all the granitic

pebbles. And point G_m is assumed to represent the final deformed ellipsoid resulting from coaxial superposition of $X_t \parallel X_o$ and $Y_t \parallel Y_o$, whereas point G_i represents the one from coaxial superposition of $X_t \parallel Y_o$ and $Y_t \parallel X_o$.

From the coordinates of points G_m and G_i together with $K = 0.274$, we have five separate equations (see Equations (6-7) and (6-8b)) as follows:

$$G_m \quad \begin{cases} (\ln a_{og} + \ln a_{tgm} = 0.447 \\ (\ln b_{og} + \ln b_{tgm} = 0.665 \end{cases} \quad \begin{matrix} \text{(C-5)} \\ \text{(C-6)} \end{matrix}$$

$$G_i \quad \begin{cases} (\ln a_{tgm} - \ln a_{og} = -0.275 \\ (\ln a_{og} + \ln b_{og} + \ln b_{tgm} = 1.026 \end{cases} \quad \begin{matrix} \text{(C-7)} \\ \text{(C-8)} \end{matrix}$$

$$K = \frac{\ln a_{tgm}}{\ln b_{tgm}} = 0.274 \quad \text{(C-9)}$$

Solving the above equations, we can get

$$\begin{cases} (\ln a_{tgm} = 0.086 \\ (\ln b_{tgm} = 0.314 \end{cases}$$

and

$$\begin{cases} (\ln a_{og} = 0.361 \\ (\ln b_{og} = 0.351 \end{cases}$$

$$\text{or } \begin{cases} (a_{og} = 1.43 \\ (b_{og} = 1.42 \end{cases}$$

(II) Quartzose Pebbles

Using the same approach to calculate the axial ratios a_o , b_o , a_t , and b_t , we draw two lines parallel to line $V_o V_m$ and touching the circumscribing polygon of the quartzose pebbles in Figure 25. One line passing through point 273Q(1.141, 0.482) is represented by

$$\ln a_f - 0.482 = 0.274 (\ln b_f - 1.141)$$

$$\text{or } \ln a_f = 0.274 \ln b_f + 0.169 \quad (\text{C-10})$$

The other line which passes the point 264Q(1.520, -0.186), is given by

$$\ln a_f - (-0.186) = 0.274 (\ln b_f - 1.520)$$

$$\text{or } \ln a_f = 0.274 \ln b_f - 0.602 \quad (\text{C-11})$$

On the other hand, we draw two lines to parallel the Z_f/d contour and to touch the same polygon at points 263Q and 265Q. The line passing through point 263Q(1.477, 0.425) is

$$\ln a_f - 0.425 = -2 (\ln b_f - 1.477)$$

$$\text{or } \ln a_f = -2 \ln b_f + 3.379 \quad (\text{C-12})$$

The line passing through point 265Q(1.264, 0.039) is

$$\ln a_f - 0.039 = -2 (\ln b_f - 1.264)$$

$$\text{or } \ln a_f = -2 \ln b_f + 2.567 \quad (\text{C-13})$$

From simultaneous Equations (C-10) and (C-12), we get $\ln b_f = 1.412$ and $\ln a_f = 0.556$. Coordinates (1.412, 0.556) are then plotted as point Q_m in Figure 25. Solving simultaneous Equations (C-10) and (C-13), we obtain $\ln b_f = 1.055$ and $\ln a_f = 0.458$. Point Q_n (Figure 25) represents the coordinates (1.055, 0.458). Similarly, from Equations (C-11) and (C-13), we have $\ln b_f = 1.394$ and $\ln a_f = -0.220$. Coordinates (1.394, -0.220) are shown by point Q_j . Here, the line of Equation (C-12) represents the lowest Z_f/d contour (the highest shortening strain) while that of Equation (C-13) the highest Z_f/d contour (the lowest shortening strain) of all the quartzose pebbles. And points Q_m and Q_n are assumed to represent the final ellipsoids resulting from coaxial superposition of $X_t \parallel X_o$ and $Y_t \parallel Y_o$, whereas point Q_j from coaxial superposition of $X_t \parallel Y_o$ and $Y_t \parallel X_o$.

From $K = 0.274$ and the coordinates of points Q_n and Q_j , we have the following equations (see Equations (6-7) and (6-8b)):

$$Q_n \quad (\ln a_{oq} + \ln a_{tqn} = 0.458) \quad (C-14)$$

$$Q_n \quad (\ln b_{oq} + \ln b_{tqn} = 1.055) \quad (C-15)$$

$$Q_j \quad (\ln a_{tqn} - \ln a_{oq} = -0.220) \quad (C-16)$$

$$Q_j \quad (\ln a_{oq} + \ln b_{oq} + \ln b_{tqn} = 1.394) \quad (C-17)$$

$$K = \frac{\ln a_{tqn}}{\ln b_{tqn}} = 0.274 \quad (C-18)$$

Subtracting Equation (C-17) with Equation (C-15), we get

$$\ln a_{oq} = 0.339$$

From Equation (C-14), we have

$$\ln a_{tqn} = 0.458 - \ln a_{oq} = 0.119$$

$$\text{Thus } \ln b_{tqn} = \frac{\ln a_{tqn}}{0.274} = \frac{0.119}{0.274} = 0.434$$

From Equation (C-15), we obtain

$$\ln b_{oq} = 1.055 - \ln b_{tqn}$$

$$= 0.621$$

So $a_{oq} = 1.40$ and $b_{oq} = 1.86$.